ELECTRICAL TRANSMISSION COMPONENTS FOR A LARGE AEROSPACE ENVIRONMENTAL CHAMBER

Francis J. Clauss
Materials Sciences Laboratory
Lockheed Missiles and Space Company
Palo Alto, California

February 1965

ARNOLD ENGINEERING DEVELOPMENT CENTER

AIR FORCE SYSTEMS COMMAND

ARNOLD AIR FORCE STATION, TENNESSEE

NOTICES

ELECTRICAL TRANSMISSION COMPONENTS FOR
A LARGE AEROSPACE ENVIRONMENTAL CHAMBER

· Francis J. Clauss

Materials Sciences Laboratory

Lockheed Missiles and Space Company

Palo Alto, California

FOREWORD

The work reported herein was done for the Arnold Engineering Development Center (AEDC), Air Force Systems Command (AFSC), under Program Element 62405334/8952, Task 895211.

The theoretical and experimental results were obtained by the Materials Sciences Laboratory, Lockheed Missiles and Space Co., Palo Alto, California, under Contract AF 40(600)-1070. This report is also identified as Report 2-68-64-1. The reproducibles used in the reproduction of this report were supplied by the authors.

This program was conducted with Dr. Francis J. Clauss, Senior Staff Scientist in the Materials Sciences Laboratory, as program director. Personnel who supported the program included Mr. S. Elster of the Information Technology Department (experimental instrumentation and data analysis), Mr. W. O. Kassebaum of the Materials Sciences Laboratory (experimental equipment and operation), Messrs. R. Rolling and J. Douglas of the Aerospace Sciences Laboratory (secondary radiation simulation), Mr. L. Haas of the Engineering Staff (power distribution), and Dr. H. Lavendel and Messrs. E. Bruce and R. Pasternak of the Materials Sciences Laboratory (preparation of brush contact materials).

This technical report has been reviewed and is approved.

Marshall Kingery   Donald D. Carlson
Project Engineer   Colonel, USAF
DCS/Plans and Technology   DCS/Plans and Technology

ABSTRACT

Secondary radiation in a large aerospace systems environmental chamber can be adequately simulated by an array of tungsten filament lamps mounted on a cage that surrounds the test vehicle. For conditions specified in this study, a total of 2528 lamps are required, arranged on 68 circuits (36 to 40 lamps per circuit) that are individually controlled for the purpose of simulating orbital fluctuations. Peak input to each of the circuits is approximately 75 A at 430 V, and peak total input is 0.818 MW.

· The simulator should be mounted so that it can tumble with the vehicle about the vehicle's pitch axis. Variations in intensity of secondary radiation around the circumference of the vehicle can be programmed electrically so that the simulator need not rotate about the roll axis of the test vehicle. Sliding electrical contacts are preferred to flexible cables or rotary transformers for transmitting power to the simulator, and separate slip rings can be provided for each of the circuits.

Self-lubricating powder metallurgy composites of silver, copper, and molybdenum disulfide have demonstrated satisfactory performance in ultrahigh vacuum for use on slip rings providing power to the secondary radiation simulator. Optimum composition is from 82.5 to 85% silver, 2.5% copper, and 12.5 to 15% molybdenum disulfide. Experimental measurements indicate that brushes of such materials can be operated against silver or gold rings in ultrahigh vacuum (10^{-9} Torr) with negligible wear (approximately 0.015 in.) and low noise (on the order of a few millivolts) over a period of 700 to 850 hr at sliding velocities up to 424 in./min while carrying current densities up to 300 A/in.^{2}. It is probable that the brushes could also be operated at significantly higher current densities without difficulty.

CONTENTS

ILLUSTRATIONS

TABLES

SECTION 1
INTRODUCTION

The objective of this program was to develop design criteria, manufacturing techniques, and operational guides which can be used to produce and operate reliable components for transmission of electric power and signals across moving interfaces in a space chamber.

The requirements for the electrical transmission components were set by the secondary radiation simulator. Large electrical power loads must be transmitted across a sliding interface to the secondary radiation sources, which are mounted on a cage that surrounds the space vehicle. The space vehicle is on a gimbal mount with two degrees of freedom for roll and pitch. The sources will be turned on and off, or operated at intermediate intensities, in pre-programmed fashion to simulate the effect of orbiting the earth. Requirements for electrical signal transmission are primarily a need for command and data channels to control the simulator and to gather data.

Specific considerations that were involved in the contractual specifications of the electrical transmission system included the following:

- The environmental tests of a space vehicle may be continuous for periods of 6 months or more, during which time the spacecraft will be exposed to solar and secondary radiations, simulated space heat sink, and pressures as low as 1×10^{-8} Torr.

- The simulator should accomodate a maximum vehicle envelope size of 50 ft in diameter by 100 ft in length and should be capable of operating at vehicle roll and pitch rates up to 15 rpm.

- The radiation sources should be able to be controlled individually or in small groups in order to simulate orbital fluctuations in the secondary

1

radiation. The sources could be operated in series-parallel combinations, but the number of individual lamps in any one group should be limited so that the cycling flexibility of the simulator is not severely compromised.

● The power transmission components should be able to work over a wide range of currents and voltages to provide for variable lamp intensities.

● Consideration should be given to making all power distribution on the rotating vehicle cage inside the last gimbal. Three-phase alternating current should be considered in order to reduce the number and physical size of circuit components such as conductors and other rotating interface components.

● An effort should be made to define any compatibility problems which might arise as a result of operating power and signal-type components close together in a space environment.

● Transmission component serviceability and reliability problems associated with friction, wear, and electrical characteristics of the construction materials are prime considerations.

Since the requirements for the electrical transmission components were set by the secondary radiation simulator, the first step in this study was to define the simulator configuration and its operating characteristics. This work is reported in Section 2. It involved selecting sources and arranging them in an optimum configuration so that the secondary radiation could be adequately simulated for the range of vehicle and orbital conditions indicated above.

Sources of secondary radiation that were considered included the following general types: tungsten filament lamps, resistance heating rods, and compact arc lamps. Characteristics considered in selecting sources for simulating secondary radiation included the following: operating voltage, current, spectral distribution of output, intensity and its directional distribution, efficiency, type of electrical load, ability to be combined in series and/or parallel circuits, stability of electrical operating characteristics and radiation output with time, size, simplicity of

2

installation, advisability of using with reflectors, cooling requirements, variability and controllability of the intensity and spectral distribution of output, compatibility with power and data systems (e. g., noise interference), cost, availability, reliability, useful lifetime, simplicity of maintenance, and reproducibility.

Factors considered in arranging the selected sources in an optimum combination or configuration and in evaluating alternate procedures for switching and transmitting power and control inputs to the sources included the following: uniformity of radiation on the test device, number of sources required, arrangement of sources in zones or groups, response of the sources to on/off signals and to variation in power input, additional thermal loads imposed on the chamber cold walls, blockage of simulator for direct solar insolation, overall power and cooling requirements, and requirements imposed upon the electrical transmission system.

Once the requirements of the electrical transmission system were defined, the next step was to analyze alternate means for transmitting this power to the rotating secondary radiation simulator across a sliding interface. This work is reported in Section 3. Slip rings were shown to be preferable to flexible cables and rotary transformers provided that satisfactory contact materials could be provided for operating in ultrahigh vacuum.

Section 4 discusses the experimental program that was conducted to develop and evaluate contact materials for use in ultrahigh vacuum. Evaluation tests were conducted both in the Research Laboratories of the Lockheed Missiles & Space Company (LMSC) and in the 7-ft Aerospace Research Chamber at the Arnold Engineering Development Center (AEDC), and a satisfactory material was found.

Section 5 summarizes the conclusions and indicates design criteria, manufacturing techniques, and operational guides for producing and operating reliable components for transmitting electrical power and signals across moving interfaces in a space chamber.

SECTION 2

SECONDARY RADIATION SIMULATION

SECONDARY RADIATION

Secondary radiation includes the following two types of radiation:

- Albedo radiation – solar radiation that is reflected or scattered by a planet's atmosphere back out into space
- Planet and atmospheric emission – solar radiation that is absorbed by the atmosphere or reaches the planet and is then reradiated.

The solar radiant energy reflected or backscattered by the earth is, on the average, 36% of the total incident energy. This value is based upon an upper limit of 56% for completely overcast skies and a lower limit of 16% for clear skies (Ref. 1). The spectral distribution of this energy is similar to that of solar radiation and is primarily located between 0.3 and 3.2 μ. The exact nature of the directional behavior of the albedo is still a matter of speculation even though it is generally agreed that it is not purely diffuse. Presently contemplated flight experiments may provide more information on this characteristic. For this study, the earth albedo has been taken to be a diffuse source having a maximum slightly in excess of one-third the solar constant.

Earth emission can be directly attributed to the radiant equilibrium between absorbed solar energy and emitted energy of the earth's surface and atmosphere. With respect to the total incident solar energy, 17% is radiated from the earth's surface with a spectral distribution approximating that of a blackbody at 288°K, and 47% is radiated from the stratosphere with a spectral distribution approximating that of a blackbody at 218°K (Ref. 2). The combined effect produces a radiant spectrum approximating a blackbody at 250°K and provides diffuse energy approximately

4

equal to two-thirds the total earth incident solar energy. Thus, the energy from albedo and earth emission is contained in the spectral range from 0.3 to 50 μ and is distributed in such a manner that complete spectral simulation would be difficult and expensive.

Table 1 illustrates the manner in which the average intensities of earth albedo and earth-atmosphere emission vary with the altitude and orientation of a satellite surface. Note that in addition to the variations in absolute values, the relative amounts of albedo and emission also vary with the altitude and orientation.

The angle of incidence at which albedo radiation impinges upon a satellite surface can cover the range of angles subtended by the illuminated portion of the earth. For earth-atmosphere emission, the angle of incidence covers the range of angles subtended by the earth, whether directly illuminated by the sun or not. Consequently, the angles of incidence vary with altitude and, in the case of albedo, also with the satellite's position with respect to the earth-sun line.
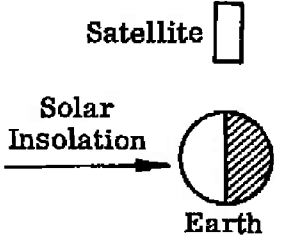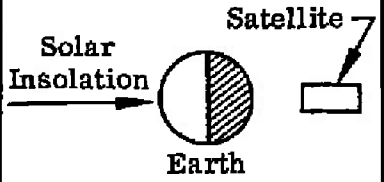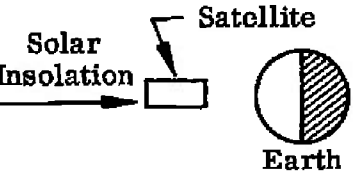
SIMULATION TECHNIQUES

In theory, several approaches can be taken for simulating secondary radiation in a space chamber. In practice, compromises must be made between the degree of simulation desired and that which can be obtained at reasonable cost. The following general approaches must be considered:

- Separate sources are provided for simulating albedo radiation and earth-planet emission, and the outputs of the different types of sources are combined to reproduce the spectral distribution, intensity, and angle of incidence of the secondary radiation on the test device.

- A single type of source is used to approximate the combined spectral distribution and intensity of earth albedo and earth-planet emission and to reproduce their combined absorbed flux and angle of incidence.

- A single type of source, such as an infrared heater, is used that, although it may not offer a good approximation of the spectral distribution and intensity of earth albedo and earth-planet emission, can be

TABLE 1

VARIATIONS OF INTENSITY OF EARTH ALBEDO AND EARTH-ATMOSPHERE EMISSION WITH ALTITUDE AND ORIENTATION

Altitude (sm)	Type of Radiation	Average Intensity (Btu/hr-ft^2)					
		Sides	End	Sides	End	Sides	End
100	Albedo	< 2.5	< 1.25	0	0	76	160
	Emission	31	65	31	65	31	65
500	Albedo	< 4.7	< 2.4	0	0	54	133
	Emission	22	54	22	54	22	54
1000	Albedo	< 5.1	< 2.5	0	0	46	108
	Emission	19	44	19	44	19	44
2300	Albedo	< 5	< 2.5	0	0	27	74
	Emission	11	30	11	30	11	30

operated at such an intensity that the total radiant energy absorbed by the test device equals the energy of secondary radiation that the test device would absorb in orbit.

In view of the obvious difficulties associated with precise simulation of both the intensity and spectrum of earth emission and albedo, it is necessary to consider the simulation accuracy required for satisfactory thermal tests. The tests conducted in the Mark II chamber require secondary simulation primarily for studies of thermal performance of the entire vehicle, and the secondary radiation spectrum is not a major source of surface degradation. Therefore, a simulator which provides the desired thermal effects without a spectral match would be satisfactory for the anticipated task.

The temperature dependence of the vehicle on the spectrum of incident energy is also an important consideration. The thermal control surfaces used on vehicle skins are chosen for their desirable optical properties in the solar and/or infrared portion of the heat transfer spectrum. Four general types of such surfaces are presently in use: these are termed solar reflectors, solar absorbers, flat reflectors and flat absorbers, depending upon their reflecting or absorbing spectral properties. When energy having a spectral distribution which differs from the sun is incident upon a solar absorbing or reflecting surface, the amount absorbed is not equal to that absorbed when the surface is exposed to the solar spectrum. This obviously results in a different thermal behavior of that surface. In many cases, it is possible to vary the intensity of incident energy to provide the same thermal effects even though the spectrum is not well simulated. This technique is commonly termed simulation of absorbed thermal radiation. For vehicle designs using one type of thermal control surface, this technique may be entirely satisfactory. However, care must be exercised when it is used on vehicles which consist of large stripes or patches of varied thermal control materials. Vehicle design and mission must be considered in specifying the required accuracy of source spectral distribution simulation. The final decision on specifying the required simulation accuracy for intensity and spectral distribution should be made in conjunction with prior analytical predictions of expected vehicle thermal behavior. It will be found that each vehicle and mission results in different tolerances.

SOURCES FOR SIMULATING SECONDARY RADIATION

The necessity for full-scale performance tests on space vehicles has resulted in the construction of a number of space chambers using solar or infrared sources for absorbed radiation simulation. The development of these facilities has generated increased efforts by various manufacturers in the production of more satisfactory sources for accomplishing the thermal simulation requirement. These activities, by both the manufacturer and user, have produced literature in increasing amounts outlining the operational characteristics of various sources. This information was sought during a literature search and was the primary basis of final source selection for this program. The literature search included all listings available to the LMSC Technical Information Center, the Armed Services Technical Information Agency (ASTIA), the technical information available from major manufacturers, and reports supplied by AEDC in support of this program. References 3 through 13 were found most useful. In order to insure continuity with previous AEDC programs, the values for the intensity of secondary radiation that are used in the computations in this section were taken from Ref. 3. These values are slightly lower than the values indicated in Table 1.

The source selection was made in terms of the lamp characteristics as applied to a rotating cage type simulator. The anticipated 15 rpm rotation rate of the cage-vehicle combination requires sources which are light weight, intense, and stable, yet have high resistance to mechanical forces, rapid on-off characteristics, and provide a minimum of cold wall blockage. Voltage and amperage characteristics must also be considered in terms of the required power transmission system. Table 2 presents a comparison of these characteristics for arc lamps, tungsten filament lamps, and resistance heating rods. These three sources are considered to be the most probable sources for use on a cage type simulator and have all been utilized previously in space simulation applications.

The compact arc lamps are generally considered to be the best source where a close spectral match to the solar spectrum is required. Filtered mercury-xenon lamps can achieve this goal to a considerable degree. Further advantages are that

TABLE 2

TYPICAL CHARACTERISTICS OF SOURCES FOR SECONDARY RADIATION SIMULATION

COMPARED AT 1000-W INPUT

Characteristic	Compact Arc Lamp	Tungsten Filament Lamp	Infrared Heating Rod
Spectral distribution	Continuous from approximately 0.2 to 5 μ, with superimposed line spectra in the case of Hg-Xe lamps and similar types; rich in ultraviolet radiation	Continuous; typically approximates a 2450°K blackbody with peak intensity at 1.2 μ, but can be operated at higher or lower temperatures with corresponding shifts in spectral distribution	Continuous; typically approximates a 1060°K blackbody with peak intensity at 2.8 μ but can be operated at higher or lower temperatures with corresponding shifts in spectral distribution
Type of operating current	Either ac or dc; dc gives approximately 3 times longer lifetime, is easier starting, and gives steadier operation (i.e., less arc wander); ac gives better uniformity of arc brightness.	Either ac or dc, but ac is preferred because of slower recrystallization of filament and correspondingly longer lifetime; ac types are also easier to obtain	Either ac or dc
Efficiency (radiant output to power input)	About 48% from 0.2 to 1.4 μ	About 80 to 100%	About 80 to 100%
Control on intensity	Small changes in voltage or current cause little appreciable fluctuation in brightness, but large changes will usually extinguish the arc.	Power input can be varied continuously over a wide range to control intensity, but spectral distribution also changes with intensity	Power input can be varied continuously over a wide range to control intensity, but spectral distribution also changes with intensity
Lifetime	Typically, 200 to 500 hr	Typically, 1000 hr or more; operating at high intensity reduces lifetime; low intensity increases lifetime	More than 1000 hr, depending upon operating intensity
Stability	Fair to good	Excellent	Excellent
Arrangement in series and/or parallel	Not recommended	Possible	Permissible
Response to on/off signals and rapid modulation	Poor	Excellent	Fair

they are available in configurations which are compact, light weight, rugged and closely approximate an intense point source. All of these are desirable features. However, a number of their operational characteristics would present severe difficulties. They are not yet capable of extended operation beyond 500 hr. This alone would seriously restrict their use where continuous tests are to be performed for several thousand hours. Additionally, compact arc lamps cannot be controlled in intensity over any practical limits, they are relatively unstable due to arc wander (approximately 5% in intensity), response to on-off signals is poor due to a required high frequency start, and their radiant efficiency is only about 48%. The requirement of providing a special starting circuit with large current surges and possibly a lamp coolant would further complicate the use of these arc lamps.

Several of these characteristics are not objectionable except in cases where the lamps are inaccessable for the full duration of a long-term test. Since the lamps are isolated and cannot be serviced during a test in the Mark II chamber, all of the undesirable characteristics must be considered as detrimental in terms of this application. Therefore, compact arcs were rejected as a possible source for this study.

Tungsten filament lamps and infrared heating rods are both resistance type sources and as such have a number of similar operating characteristics. Their power requirements, radiant efficiency, steady state intensity control and stability, operating life, and size are all approximately equivalent. There are several important characteristics which differentiate the sources and may be used to select the most desirable type.

Infrared heating rods are manufactured using a high-temperature resistance wire which is contained inside a stainless steel (or other high-temperature metal) sheath. The heater element is insulated from the sheath with powdered magnesium oxide. This construction results in a rod with considerable mass (compared to that of a tungsten filament with the same power rating) and slow response time to a step increase in applied voltage. Response to a step increase is typically 20 sec for a 1000-W rod. The overall weight of these rods also presents a problem since they tend to sag appreciably (on the order of 0.05 in./in.) when operated horizontally

with end supports at elevated temperatures. Both of these physical characteristics make infrared rods undesirable for flux simulation on a rapidly rotating cage.

Quartz-enclosed tungsten filament lamps do not suffer from deleterious weight effects since the filament is surrounded by a thin transparent quartz cylinder. The step response of these lamps is on the order of 1 sec which is compatible with the 2-sec requirement for proper simulation with 15 rpm tumbling. The sagging problem is avoided by light construction, relatively low operating temperature of the quartz envelope, and sufficient supporting disks attached to the filament itself.

The tungsten filament lamps do have the disadvantages of a spectral mismatch in terms of secondary radiation simulation. The spectral energy from the lamp is distributed in approximately the same manner as that from a blackbody at the filament temperature. However, at wavelengths beyond 3.5 μ the distribution is modified to some extent due to absorption and re-emission by the quartz envelope. Maximum filament temperatures under full voltage are on the order of 2500°K which provides a peak spectral radiance at 1.15 μ. In view of the previously stated spectral distribution of secondary radiation, the tungsten sources must be used to provide proper levels of absorbed rather than incident flux.

The above characteristics of compact arc lamps, infrared heating rods, and tungsten filament lamps, when evaluated in terms of use on a large rotating cage for secondary radiation simulation, lead to a final selection of tungsten filament lamps as the most desirable source for simulating secondary radiation.

Tungsten filament lamps are available in a number of configurations over a wide range of power and voltage ratings. They may also be used with or without reflectors which provide different distributions of energy in half space normal to the lamp. These variables necessarily enter into the detailed design of a simulation cage.

Selection of lamps in terms of maximum power ratings is based upon the requirement of providing a minimum number of lamps for satisfactory simulation of the highest anticipated flux levels. This results in the fewest number of sources and a minimum cold wall blockage. However, consideration must also be given to the voltage and current carrying capacity of the power transmission system.

A combination of high voltage and low current is desirable in order to minimize power losses. The maximum voltage is limited by arcing and insulation breakdown. Arcing to ground at the mounting lugs of tungsten filament lamps is likely at potentials above 280 V*. Therefore, to provide a system compatible with all of these considerations, lamps rated at 240 V were selected for use in the simulator.

SIMULATOR CONFIGURATION AND OPERATING CHARACTERISTICS

Simulator configurations and operating characteristics were analyzed for tungsten-filament lamps used both with and without reflectors. The required number of lamps and their arrangements on cages about the vehicle were determined, as well as their operating voltages and currents.

Simulator Without Reflectors

Figure 1 indicates the geometrical relations for a single bare lamp located at a distance D from a point directly below it on the vehicle's surface and with the axis of the lamp parallel to the axis of the vehicle. The energy from the lamp is radiated into 4π space and is distributed as though the filament were diffuse. The energy striking any particular area, dA_s, may be determined by solution of the defining equation

$$i = \frac{dq}{dA \, d\omega} \tag{2.1}$$

where

$\quad i \quad = \quad$ intensity (Btu/hr-ft^2-sr)

$\quad dq \quad = \quad$ radiant power (Btu/hr)

$\quad dA \quad = \quad$ projected area of source (ft^2)

$\quad d\omega \quad = \quad$ solid angle from receiver to source (sr)

From Eq. (2.1), the energy falling on the vehicle surface is

$$dq = i dA \, d\omega$$

---

*Private communication from Research Inc., Minneapolis, Minnesota

12
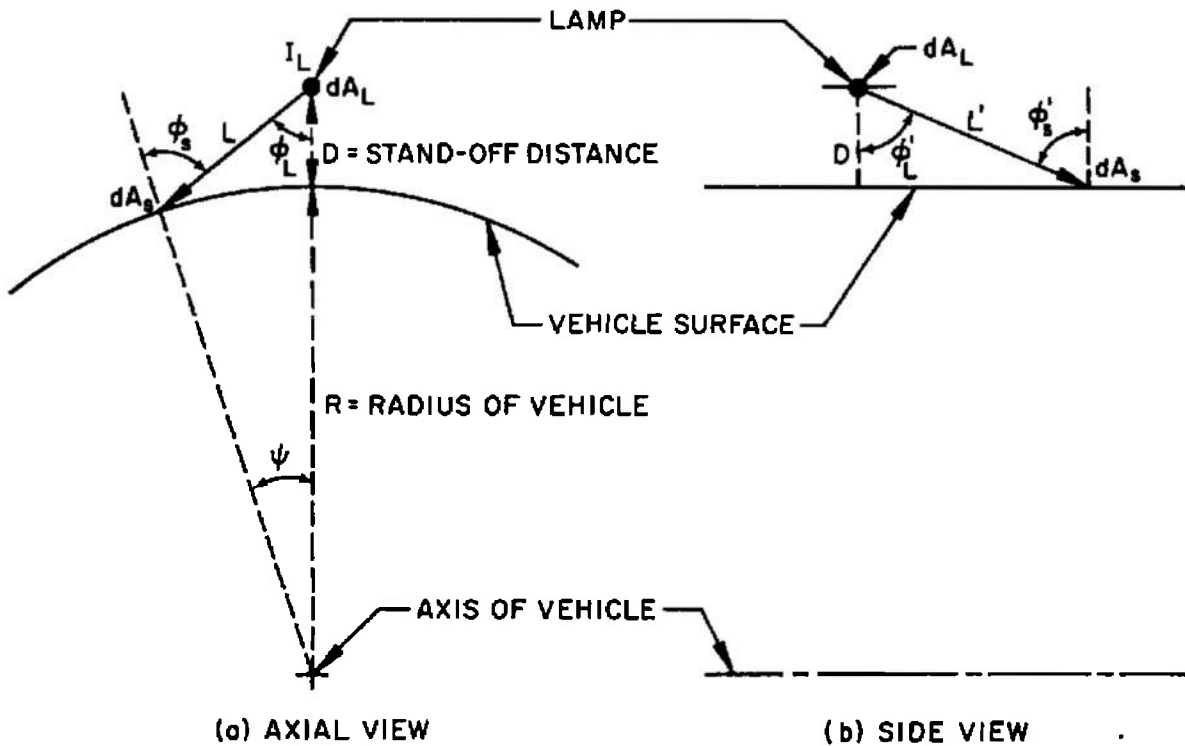
Fig. 1 Geometrical Relations for Bare Lamp and Vehicle Surface

For the incremental surface area dA_s, the solid angle to the source is given by

$$\frac{dA_s \cos \phi_s}{L^2}$$

The radiant flux on dA_s is then given by

$$dq = \frac{i_L \, dA_L \cos \phi_s \, dA_s}{L^2} \tag{2.2}$$

Integration of this equation over all dA_L and dA_s gives the required relation for computing flux distribution on the vehicle. For a short line source and a curved vehicle the integration becomes formidable in view of the geometry involved.

However, a number of approximations can be used for simplification which do not seriously affect the utility of the result in establishing the overall power requirement. The first simplification is to assume that instead of a finite line source, the total energy is incident from an incremental line source of area A_L at the center of the lamp. In view of the small lamp length (10 in.), and probable stand-off distances greater than four lamp lengths, this assumption is adequate for initial design. The second approximation calls for separate solutions of the circumferential and axial directions. These are then combined for the complete solution. For the incremental source this is a valid procedure.

Returning now to Fig. 1a, and utilizing the incremental source approach, we find the distribution of energy in the circumferential direction is given by

$$q_L = i_L \, da_L \, d\omega = \frac{i_L \, dA_L \, \cos \phi_s \, dA_s}{L^2}$$

For a cylindrical filament the projected area dA_L and intensity i_L are constant with ϕ_L. At a point directly under the lamp where $\phi_s = 0$, the energy is given by

$$q_D = \frac{i_L \, dA_L \, dA_s}{D^2}$$

where D is the lamp stand-off distance.

The ratios of energy at L and D are

$$\frac{q_L}{q_D} = \frac{D^2 \, \cos \phi_s}{L^2} \qquad (2.3)$$

This may be placed in a form which is more amenable to computation by including the geometrical relationships between D, L, ϕ_S, ϕ_L, and R. The final result is

$$\frac{q_L}{q_D} = \frac{D^2 \cos(\phi_L + \psi)}{(R+D)^2 + R^2 - 2(R+D)R \cos \psi} \tag{2.4}$$

For the axial distribution (Fig. 1b) the intensity from the incremental cylinder is once again constant. Therefore, at distance L'

$$q_{L'} = \frac{i_{L'} \cos \phi_{L'} \cos \phi_{S'} dA_{S'} dA_{L'}}{(L')^2} \tag{2.5}$$

For this configuration $\phi_{L'} = \phi_{S'}$ and

$$q_{L'} = \frac{i_{L'} (\cos \phi_{S'})^2 dA_{S'} dA_{L'}}{(L')^2} \tag{2.6}$$

Equations (2.3) and (2.5) provide the basic relationships for generating distribution curves over the vehicle surface, with lamp spacing and stand-off distance as the controlling parameters. The distribution from a single lamp is combined with that from adjacent lamps to produce a simulator geometry which meets the prescribed uniformity requirements. Figures 2 and 3 present typical distribution curves derived from the results of Eqs. (2.3) and (2.5).

The distribution curves are used as a guide for specifying the stand-off distances and lamp spacing. In addition, the spacing must also provide sufficient energy on the vehicle for adequate secondary radiation simulation. These criteria are met in the bare lamp case by using high-power lamps (i. e., 360 W/in.) as widely spaced as possible. The final configuration results in a design using a 4-ft spacing between lamps at a 7.5-ft stand-off distance. With a 4-ft spacing the cage has
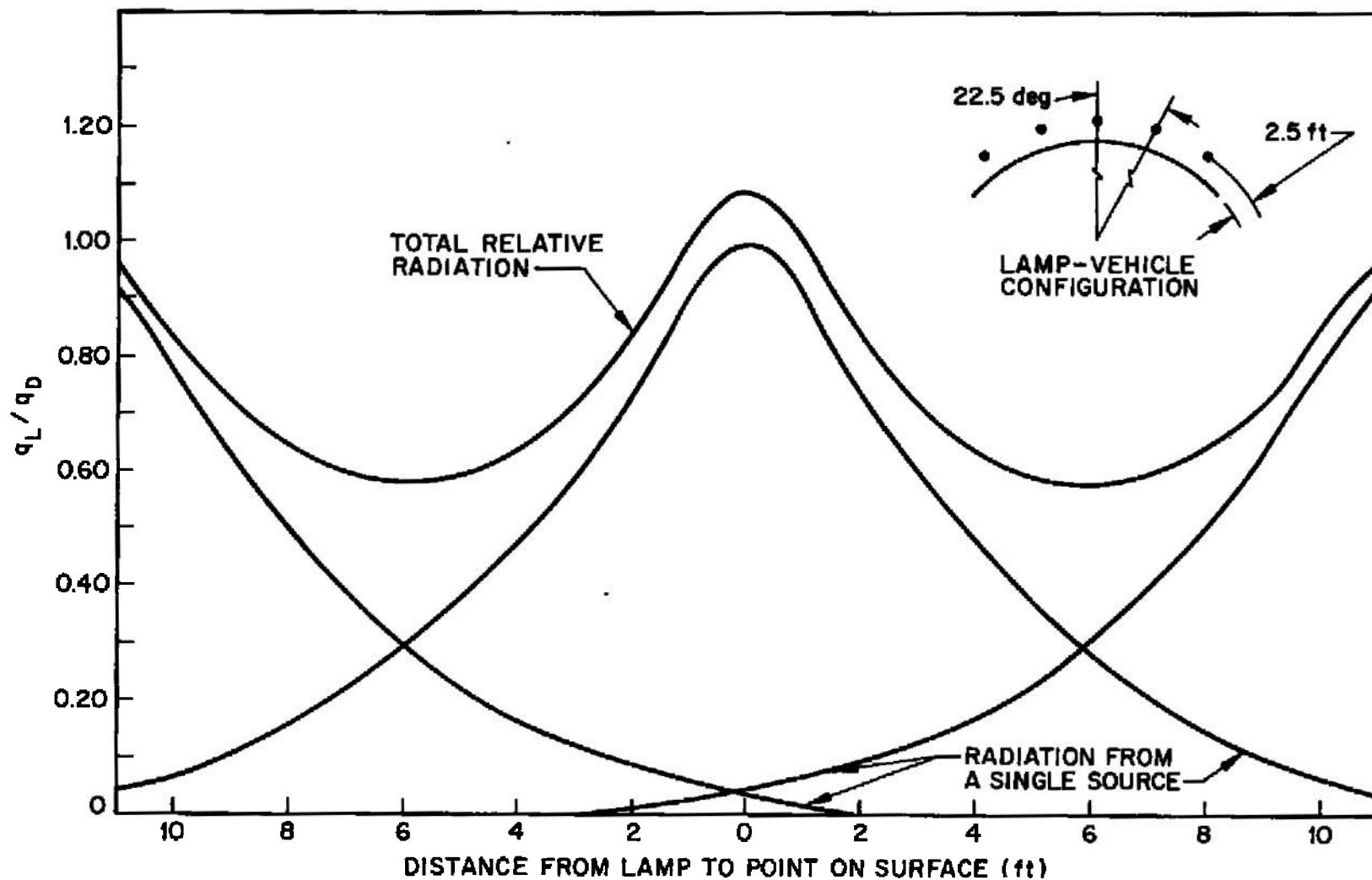
Fig. 2 Normalized Circumferential Radiation Distribution from Bore Lamps

Fig. 3 Normalized Axial Radiation Distribution from Bare Lamps

45 circumferential banks, each consisting of 25 lamps spaced axially along the vehicle. Each end requires 164 lamps of the eage is a flat ended cylinder.

Under conditions of peak intensity, the power drawn by a circumferential bank of lamps would be 90,000 W (i.e., 3600 W per lamp × 25 lamps). If this were supplied at 240 V, the corresponding current would be 375A.

Simulator With Reflectors

A search for commercial vendors producing reflectors for use with the T-3 lamp indicated that Research Inc., Minneapolis, Minnesota, produces several reflector assembly models especially designed for use in space simulation chambers. The Series 5236 solar heating reflector assemblies combine extreme lightweight (~0.6 lb with lamp included) with slender profile (12.0 in. by 0.75 in. by 0.75 in.). The geometry facilitates mounting in any orientation and minimizes blockage of cryogenic panels. The reflector is a wide-angle type (~145 deg) with an overall efficiency of ~80% (Fig. 4).
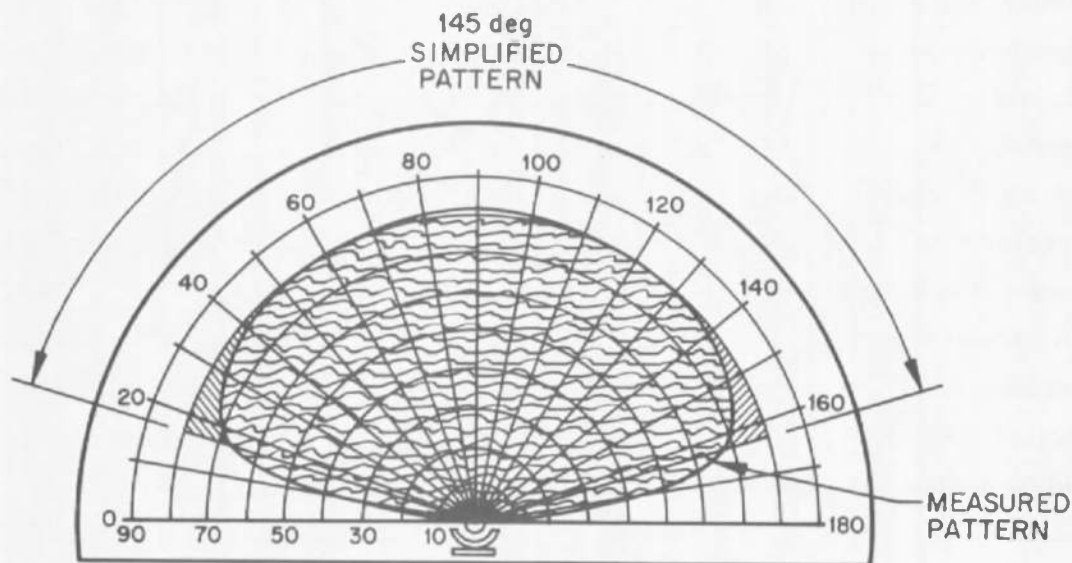
Fig. 4 Distribution of Radiation From T-3 Lamp With Reflector

The basic reflector material is Type 303 stainless steel plated with gold (Cerragold) capable of withstanding a surface temperature of 1100° F. To avoid deterioration of the reflector surface, it is recommended that low dissipation rate type T-3 1000 W lamps (100 W/in.) with an overall length of 11 15/16 in. and 0.345 to 0.422 in. diameter be used. It is also suggested that lamps with high temperature end seals be used under vacuum conditions since a coolant is not utilized.

Reflector surface degradation tests have been performed by Research Inc. (Ref. 5) with Model 5250 modular radiant heating units (similar to Model 5236 except for mounting unit) in a vacuum (5×10^{-4} Torr) without a cryopanel.

These tests are still in progress so that final results cannot be stated in this report. The studies are being performed by measurement of temperature at the back of the reflector geometric center. This point was previously shown to be the hottest location during operation in vacuum. The lamp being used is a 500 W (80 W/in.) 120 V, 6.25 in. long and is in front of a standard reflector. At rated conditions, the reflector temperature has been measured at 795° F with no observable reflector degradation after 1180 hr of continual operation.

Extrapolation of the Research Inc. observations for a 10-in. lamp running at the same capacity suggests a probable reflector temperature of 870° F for the higher dissipation rate. It is also noted that the tests were conducted in a chamber without a cold wall. Therefore, the measured temperatures may be slightly higher than are anticipated. The information available from Research Inc. indicates that the lamps can be operated for long times. However, due to the limited number of observations and lamp ratings used, it is advisable to perform further investigations on lamp reflector stability.

A second important consideration is the effect on filament life of increased G-forces distributed on the lamp assembly. In order to minimize these G-forces on the heated tungsten filament during 15 rpm tumbling, the lamp-reflector units should be positioned perpendicular to the vehicle axis.

A study of the mechanics involved shows that a parallel orientation could encourage the tantalum supporting discs to oscillate and eventually flip over upon rapid vehicle tumbling. The force on a filament element when oriented parallel to the vehicle axis is in the order of 0.02 lb. If it is assumed that this entire force

19

is carried by a section between the end support and first tantalum support discs, then a deflection on the order of 0.004 in could result. Forces sufficient to cause deflections of this magnitude could induce flipping of the tantalum spacers or filament contact within the quartz envelope. Here again, there is insufficient information to provide definite predictions of lamp life on a tumbling simulator cage.

Finally, the radiant spectrum from the lamps should be considered. LMSC data on the spectral and total radiosity of bare T-3 lamps were used, since no data were available on reflector-backed lamps.

A continuous line of lamps around the periphery of the vehicle was selected for the following reasons:

● This geometry permits a larger row spacing in the axial direction where surface irradiation is proportional to the inverse of the distance. A noncontinuous line of lamps gives a surface irradiance which varies approximately as the inverse-square of spacing and requires a closer axial spacing. Lamp-reflector unit support structures are also minimized by larger axial spacing.

● Simulated energy distribution for secondary radiation in a given orbit around the curved surface of a vehicle is more closely matched with a greater number of circumferentially positioned lamps.

The incident radiation at a point is again a function of the stand-off distance and the relative radiation pattern of the lamp-reflector system. The wide angle pattern provided by the selected reflector can be approximated by a 145-deg sector (Fig. 4). The lamp-reflector system is assumed to place 80% of the total energy dissipated, as radiant energy into this region. The radiation pattern from the reflector ends was considered to be the same as from a line emitter, since information concerning the distribution in a direction parallel to the lamp axis was unavailable. It is noted that the continuous line source postulated is actually a series of discrete 10-in. lighted lengths separated by 3-in. spacings (Fig. 5).

The distribution of energy on the vehicle surface can be established exactly by integration of the equation, $dq = i\, dA\, d\omega$ over the entire vehicle and lamp surface. However, this complete solution is not necessary for initial specification of a satisfactory system. Consider a vehicle segment (Fig. 6) to be completely

20
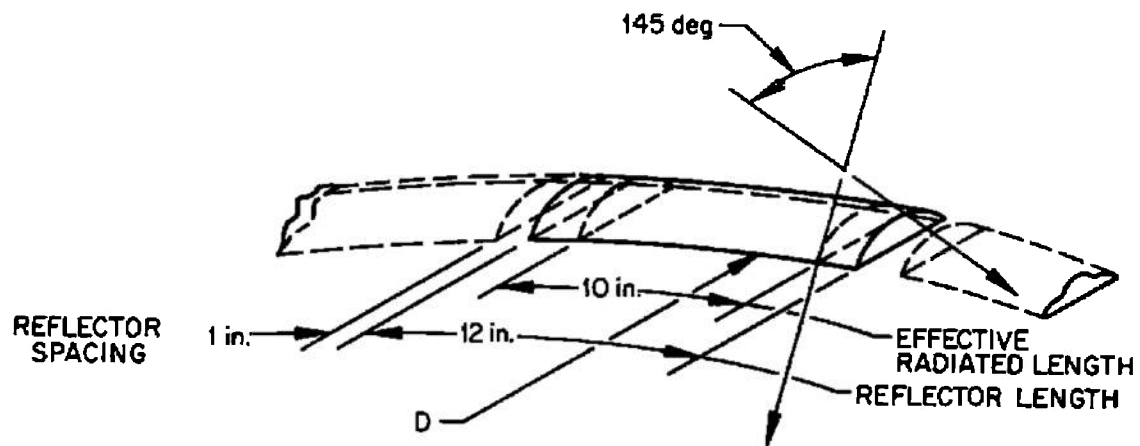
Fig. 5 Effective Radiation Sector
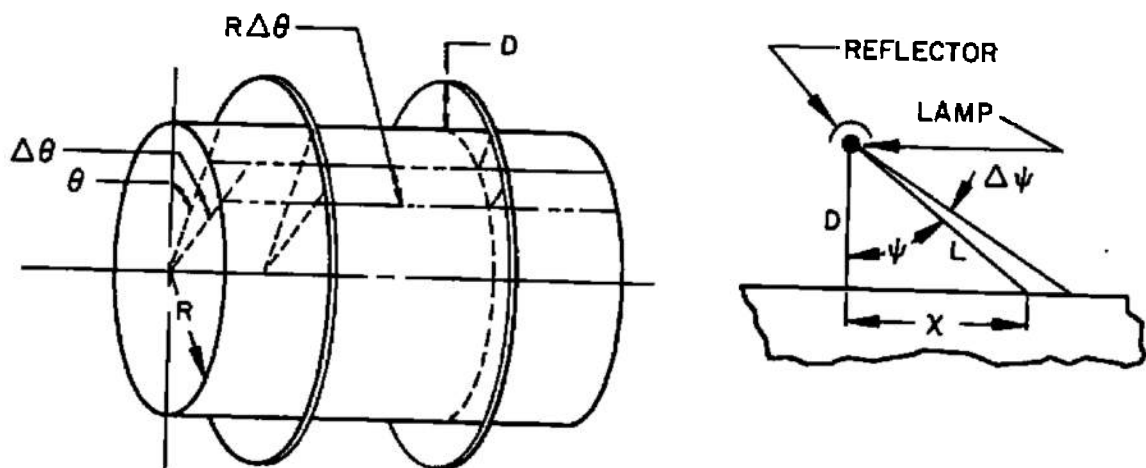
Fig. 6 Geometrical Relations for Energy Distribution From Lamp-Reflector System

21

enclosed by a continuous cylindrical line source. It is obvious that energy will be uniformly incident circumferentially and will vary only in the axial direction. The determination of variation in the axial direction can be established by considering a segment $R\Delta\theta$ of the vehicle shown and the portion of lamp enclosed by that segment. It may be assumed that this vehicle segment is illuminated only by the portion of lamp enclosed by $(R+D)\Delta\theta$, since all adjacent lamp segments' contributions exactly make up the losses of the lamp segment studied. The radiant energy distribution from the lamp is uniformly distributed over a 145-deg sector (Fig. 4) and amounts to 80% of the total lamp dissipation.

The following terms are used to establish the distribution:

W = radiant power of lamp per unit length per unit angle ψ in the 145-deg illuminated sector Btu/hr-ft-radian

ψ = radial angle on lamp from surface normal (radians)

θ = radial angle in vehicle (radians)

D = stand-off distance (ft)

G = irradiation (Btu/hr-ft^2)

The total irradiation at point x on the vehicle surface due to a single lamp row is given by

$$W(R+D)\Delta\theta\,\Delta\psi = G\,\frac{L\Delta\psi}{\cos\psi}\,R\Delta\theta \tag{2.7}$$

and since $L = \dfrac{D}{\cos\psi}$

$$G = \frac{W(1+D/R)\cos^2\psi}{D}$$

$$G = W\left(\frac{1}{D} + \frac{1}{R}\right)\cos^2\psi \tag{2.8}$$

Equation (2.8) shows that the distribution of energy on the surface is inversely proportional to the stand-off distance for a continuous line source. However, in

the actual application the source will not be entirely continuous due to the lamp mounting devices and finite filament lengths (Fig. 5). Equation (2.8) may still be used for the solution if it is assumed that the energy from the sources is sufficiently distributed to apply the line source approximation.

Figure 7 presents a number of curves showing the axial distribution of energy for various stand-off distances using a single line source. These must then be combined with the distribution from adjacent line sources with stand-off distance and row spacing as parameters. This procedure results in an infinite number of possible solutions where required absolute intensity and ±5% uniformity can be achieved.

A guide toward selection of an optimum configuration is obtained by plotting results in the form used for Fig. 8. This figure presents the absolute surface irradiation at a point directly under a lamp row and a point half way between rows for various spacings and stand-off distances. The zone of useful solutions is seen to be $D > 7$ ft and 10 ft $\leq S \leq 13$ ft.

The cold wall shadowing or blockage may be approximately determined by considering the ratio of blocked area on an imaginary cylinder containing the lamps to the total area of that cylinder.

$$B = \frac{2\pi(R+D)(K+a\sin\theta_n)N}{2\pi(R+D)L_c} \qquad (2.9)$$

where

B = blockage or shadowing
N = number of lamp rows in cylinder length $L_c(N+L_c/S)$
S = row spacing between lamp rings
K = reflector width
a = reflector depth

The $(K+a\sin\theta_n)$ term is the effective reflector width since it takes into account the reflector depth of the nth lamp and for a rough approximation can be taken as

23
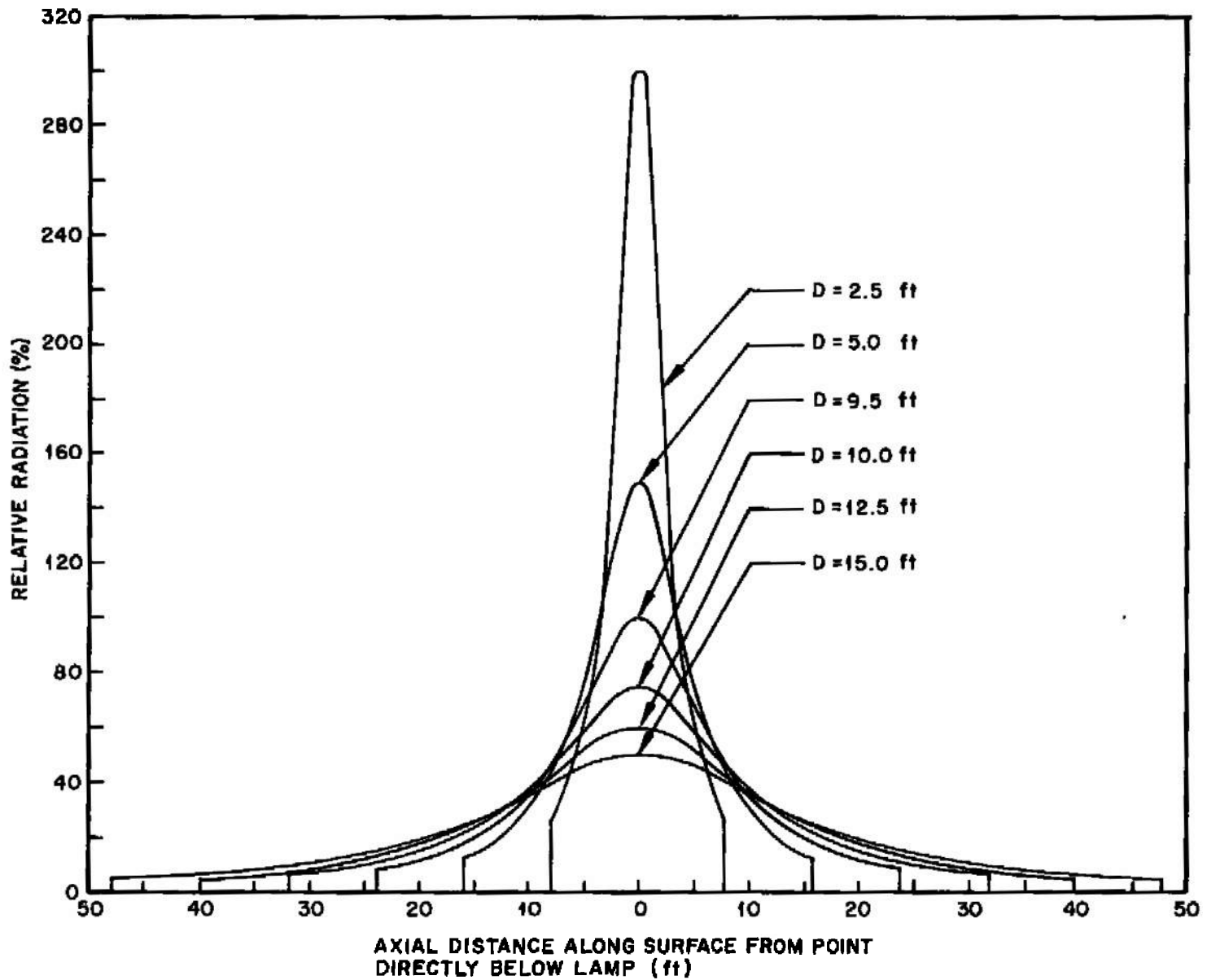
Fig. 7 Relative Axial Distribution of Radiation Incident on the Surface of a Cylindrical Test Vehicle From a Row of Circumferentially Positioned Line Sources at Various Stand-off Distances
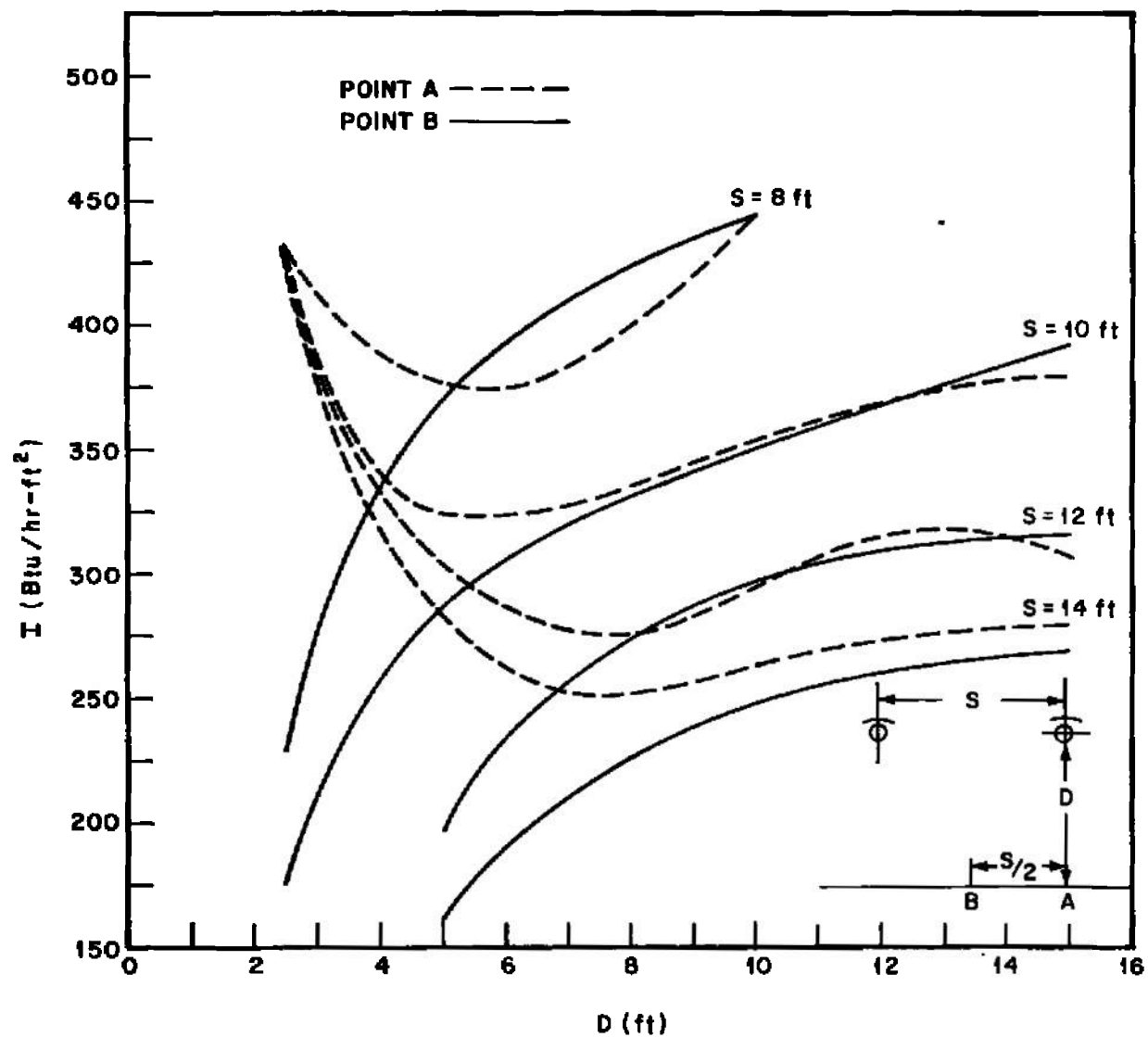
Fig. 8 Incident Radiation on Vehicle Surface From Circumferential Rows of Lamps

an average of a/2 over n lamps. Therefore,

$$B = \frac{K + a/2}{S} \qquad (2.10)$$

Figure 9 plots the shadowing due to lamp spacing for various groups of lamp banks where a single row of sources may contain several lamps immediately adjacent to each other.

The results plotted on Figs. 7, 8, and 9, present the basic information required to optimize a given simulator. The optimization must not only be guided by energy considerations but also by the total number of lamps required, number of control zones, switching, reliability, and the complexity of the cage itself. In view of all of these governing criteria a final selection was made with a stand-off distance of 7. 5 ft and a spacing between rows of 12 ft. This requires 9 circumferential rows each containing 192 lamps, or a total of 1728 lamps around the circumference of the cylinder.

Establishment of the final geometry permits a more detailed analysis of shadowing by lamps of the chamber cold wall and primary solar radiation simulation. An exact solution was performed using a shape factor analysis for cold-wall blockage and projected areas for solar energy shadowing. The result showed cold-wall blockage to be 1% and primary blockage of collimated energy to be 1.3% for this arrangement of lamps. These computations do not include blockage due to structural members which hold the sources, but include only the geometry of the lamp-reflector units.

A graph of the maximum secondary irradiation on a cylindrical vehicle in an 100-sm orbit in the earth-sun line was prepared from information in Ref. 3. The energy variation on the vehicle surface is dependent upon the angular position β, as shown in Fig. 10. The step function in Fig. 10 indicates the power levels at which the banks of lamps would be operated to simulate the circumferential variations in intensity around the test vehicle.
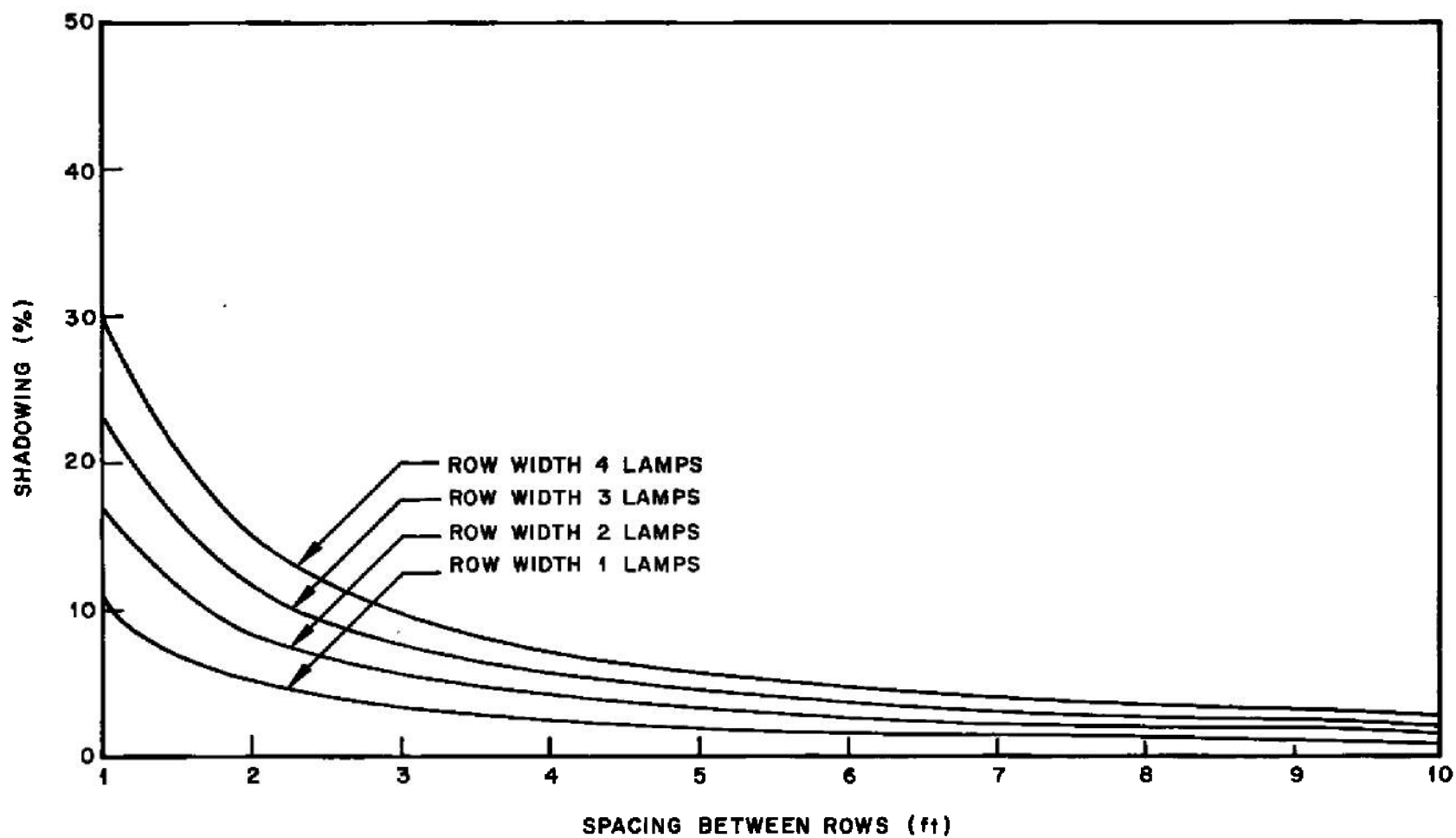
Fig. 9 Shadowing due to Spacing of Lamp Rows
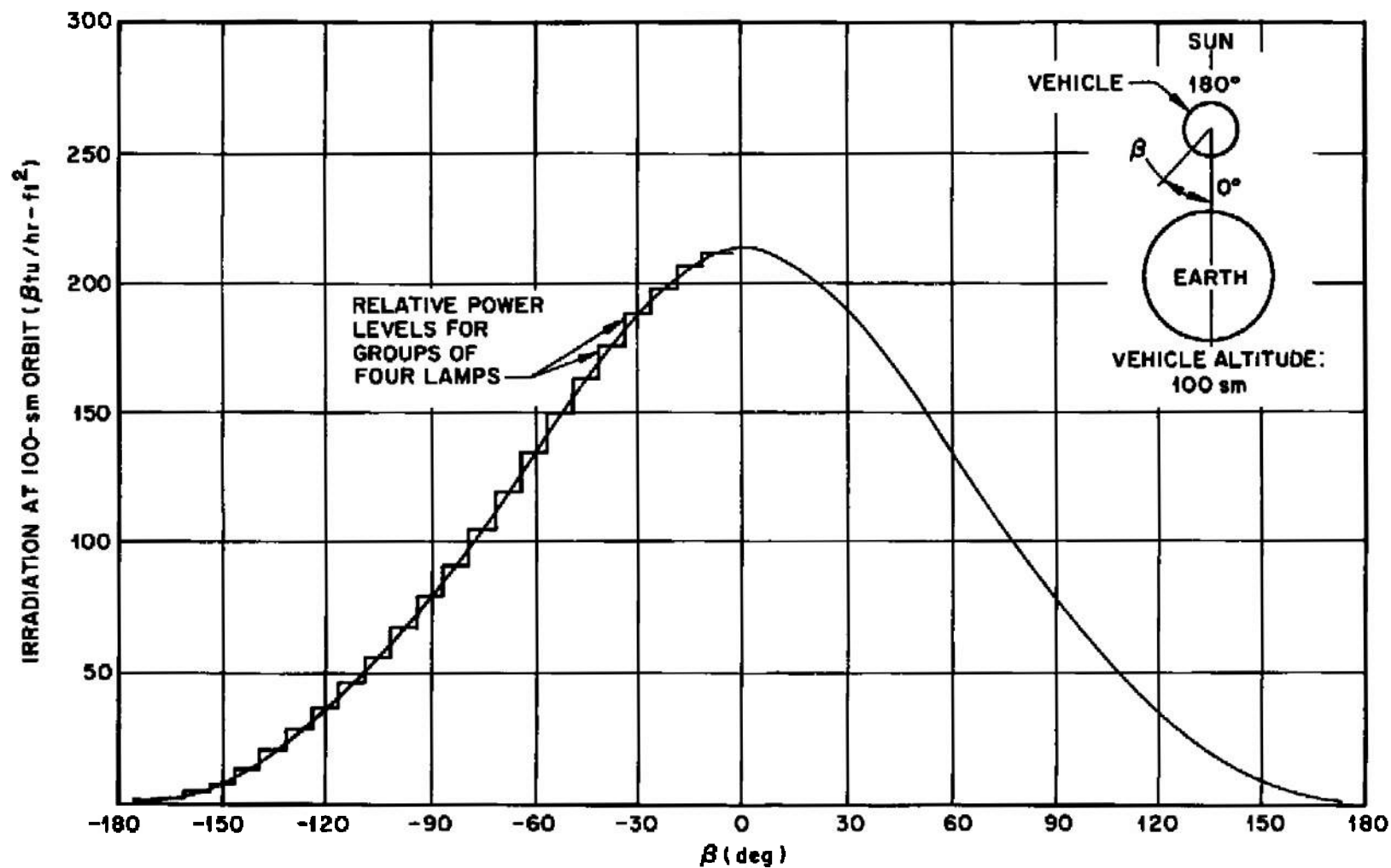
Fig. 10 Maximum Secondary Radiation Condition When Axis of Vehicle is Perpendicular to Earth-Sun Axis

Design of the simulator configuration for irradiation the flat ends follows the same techniques as those used for the sides of the cylinder with the simplification that the irradiated surface is flat. Several geometrical arrangements are satisfactory from a thermal point of view. An arrangement of lamps along concentric circles was selected because it provides a simple mechanical layout and allows the intensity of the lamps to be programmed around the end caps to match the variations in intensity on vehicles that do not have flat ends (e. g. , vehicles with conical or spherical nose caps), as well as provides satisfactory simulation on vehicles with flat ends. A total of 400 lamps is required for each end cap of the simulator, and the lamps can be arranged in groups of 20, 70, 130, and 180 lamps around concentric circles with diameters of 9, 27, 45, and 63 ft, respectively. Stand-off distance is 7.5 ft, the same as for the circumferential belts of lamps.

Adding the 400 lamps required on each of the two end caps of the simulator to the 1728 lamps required for the circumferential belts of lamps gives a total of 2528 lamps. Operating the lamps at 100% of their full-rated power produces a maximum total radiant flux at the vehicle surface of 265 Btu/hr-ft^2. As Fig. 10 indicates, the required maximum value for simulating secondary radiation is only 215 Btu/hr-ft^2. As a result, the maximum power level that the lamps must be operated at is only 81% of their rated power, which level extends their operating lifetime and increases their reliability. Under these conditions, lamp lifetime is expected to be on the order of 5 yr, provided that the end seals do not leak and there are no adverse effects either from the gravitational forces set up during cage rotation and tumbling or from cycling the power to the lamps. These effects should be clarified experimentally prior to constructing the simulator.

A summation of the operating power levels around the circumference, according to the step function shown in Fig. 10, requires 602 kW (excluding the end plates). If the vehicle is in this position, then the end plate areas are assumed to be at $\beta = \pm 90°$, giving an end plate power of 216 kW. Thus, for a vehicle in an 100-sm orbit in the earth-sun line, a total power of 0.818 MW is required for satisfactory secondary radiation simulation.

The spectral distribution of the T-3 lamps as compared to that of the secondary radiation can influence the effective absorption of energy on the vehicle skin. Many

thermal control surfaces are strong ultraviolet absorbers and low visible and infrared absorbers, so that in some cases a correction factor changing the magnitude if incident energy should be applied in order to allow for the spectral shift. For example, a vehicle with an aluminum skin could require the input power to be raised by a factor as high as 2.2 times the values specified in this report. This could be accomplished by doubling the lamp banks.

SUMMARY

The configuration and power requirements of a secondary radiation simulator for use under the conditions specified in Section 1 are met by the following:

- Sources — Type T-3 tungsten filament lamps, reflector-backed, 1000-W rating; 2528 lamps required; maximum operating power required is 81% of rated capacity

- Circumferential configuration — The 1728 lamps required for irradiating the circumferential area are arranged in 48 circumferential banks of lamps (36 lamps per bank) spaced at 7.5-deg intervals around the circumference as shown in Fig. 11. Within each bank, the lamps are arranged in 9 groups spaced at 12-ft intervals in the axial direction (4 lamps per group). Each of the 48 circumferential banks of lamps can be operated independently of the other circumferential banks in order to simulate orbital fluctuations in secondary radiation. Stand-off distance (distance from vehicle surface to center of lamps) is 7.5 ft.

- End cap configuration — Each of the two end caps requires 400 lamps at a stand-off distance of 7.5 ft. The lamps are arranged in groups of 20, 70, 130, and 180 lamps around concentric circles with diameters of 9, 27, 45, and 63 ft, respectively.

- Maximum power — Maximum power drawn by the simulator is 0.818 MW

7.5 deg (48 BANKS, 7.5 deg APART.
36 LAMPS PER BANK)

65 ft

7.5 ft STAND-OFF
DISTANCE

12 ft

VEHICLE ENVELOPE
50 ft DIAMETER BY
100 ft LONG

END CAP
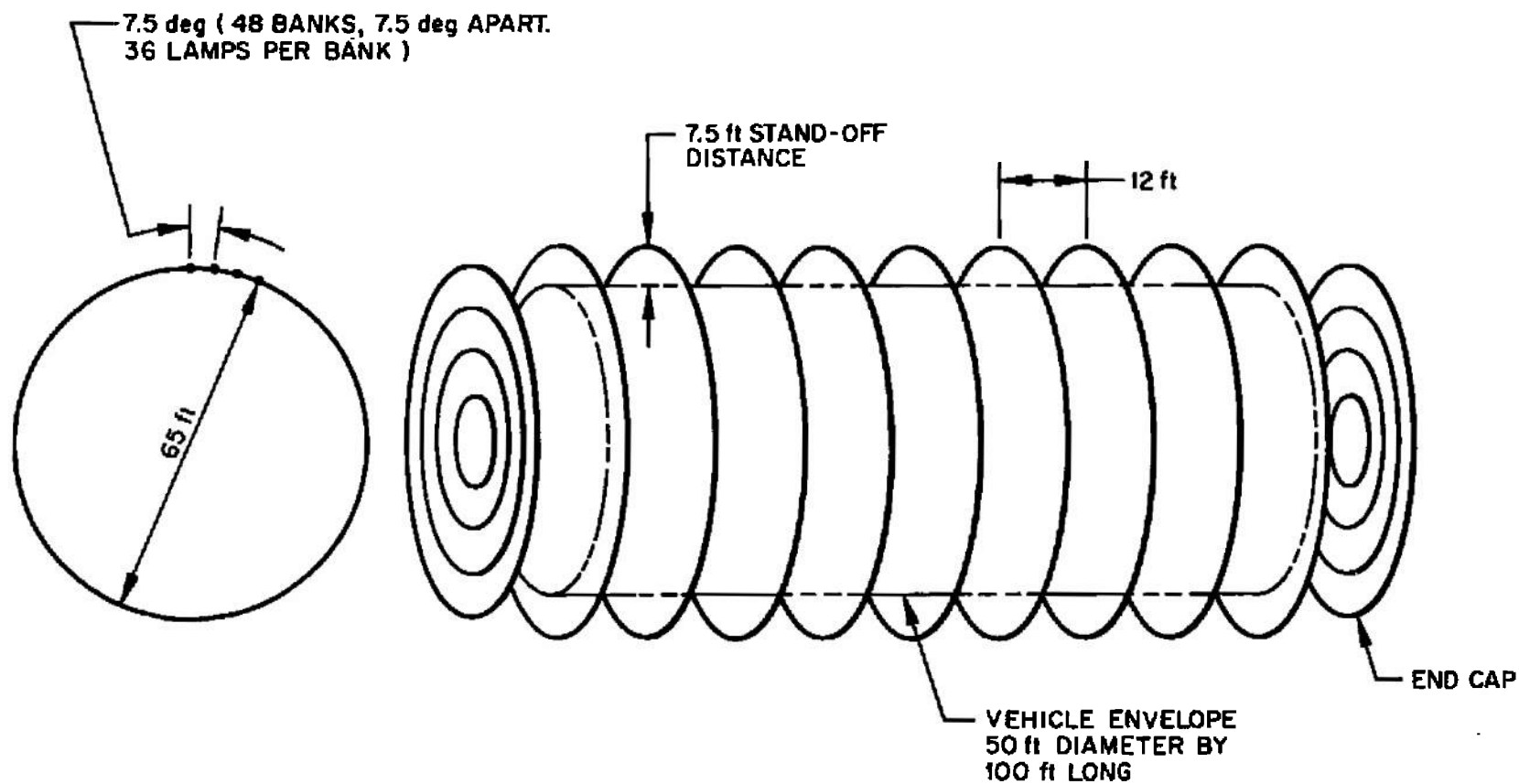
Fig. 11 Secondary Radiation Simulator Configuration

SECTION 3

POWER TRANSMISSION SYSTEM

The two tasks performed in this section are an analysis of the means by which electrical power could be transmitted from a source to the rotating simulator in vacuum and a determination of the operating characteristics of the power transmission system.

TRANSMISSION OF ELECTRICAL POWER

The analysis of the means for transmitting electrical power to the simulator was based on transmitting 1 MW of power, since this is the level required for simulating secondary radiation (see Section 2), and the other specifications indicated in Section 1.

The three means of transmission analyzed were flexible cables, rotary transformers, and sliding contacts.

Flexible Cables

Two basic problems with flexible cables for this application are providing sufficient length and flexibility to permit windup of the conductors during the test and limiting the current density within the conductors to values that will allow the I^2R losses to be dissipated without overheating and damaging the insulation.

In order to estimate the length of conductor required, it will be assumed that the mean length of turn of the coil when wound about a spindle is 12.5 ft ($\sim$ 4 ft mean diameter). For a 1-hr portion of a test in which the test vehicle is tumbling or rolling at 5 rpm (maximum rotational speed specified is 15 rpm and maximum test duration is 6 months), the length of each conductor required would be

$$5 \text{ rpm} \times 12.5 \text{ ft/r} \times 1 \text{ hr} \times 60 \text{ min/hr} = 3750 \text{ ft}$$

Half of this length can be saved by using a wind-up/wind-out spool arrangement in which the conductor is first played out in one direction from the rotating test bed to a storage spool and then wound up in the opposite direction on the rotating test bed for the second half of the operation. For a 3-phase circuit, current in the neutral line will be zero under conditions of perfect balancing and will be quite small under nearly balanced conditions and full power dissipation.

For the simulator configuration indicated in Section 2, total current drawn by the simulator is on the order of 2000 A. Since the conductors will be operating in vacuum, normal cooling by air convection will be absent and the current carrying capacity of the conductors must be reduced to prevent overheating and damage to the insulation. If one can operate at a current density of 500 A/in.^{2}, the required cross-sectional area of the conductors is 4 in.^{2} for the three line conductors of a 3-phase system. Increasing the cross-sectional area will reduce the transmission losses and reduce the heat load radiated from the conductors, but it will also make the cables heavier and more difficult to wind and unwind, and the storage spools and associated cable handling apparatus will be larger.

Power losses for 1875 ft of conductor 4 in.^{2} cross-sectional area carrying 2000 A will be

$$I^2R = (2000)^2 \times 1.71 \times 10^{-6} \times \frac{1875 \times 12}{4 \times 2.54} = 15,150 \text{ W}$$

where $1.71 \times 10^{-6} \mu\Omega$-cm is the resistivity of copper conductors at 20° C. The percentage loss in transmitting power through the conductor is therefore approximately 1.5%. A rough, order-of-magnitude estimate of the size required for a system using continuous conductors can be made for comparative purposes by assuming that the cables are wound on spools 2 ft in diameter by 5 ft long. If the required 4 in.^{2} (see calculations above) of conductor cross-sectional area is lumped into a single cable and an allowance is made for the neutral conductor and insulation, the cable diameter will be approximately 3 in. For the 1-hr portion of a test in which the test vehicle is tumbling or rolling at 5 rpm, the number of revolutions will be 60 min × 5 rpm = 300.

If two spools and a wind/unwind technique are used on each conductor to minimize the conductor length, each spool will handle 150 loops of cable. Each spool will accommodate 19 loops of cable along its 5-ft length $\left(\frac{5 \times 12}{3}\right.$ less allowance for packing and for end plates$\Big)$, so that $\frac{150}{19}$ = 8 rows of cable will be wound on each spool and the mean diameter of the cable coils will be $\left(24 + \frac{8}{2} \times 6\right)$ in. = 48 in. or 4 ft. Total length of cable will be (150 loops $\times$ 4 π ft/loop) = 1885 ft. Each of the four spools when half-full will occupy a volume of 5 ft $\times$ (4. ft)^2 $\frac{\pi}{4}$ = 62. 8 ft^3, so that the total volume of the system, including the four spools and auxiliary winding equipment (e.g., drives, guides, etc.) will be greater than 260 ft^3.

Rotary Transformers

The preliminary evaluation of rotary transformers for this application is based on the fact that a wound-rotor induction motor acts as a transformer when its rotor is locked. By treating the rotary transformer as a wound-rotor induction motor with a fixed (or very slowly rotating) rotor, it is possible to estimate size, weight, efficiency and other operating parameters.

The size of the rotary transformer can be estimated from the following equations (Ref. 14):

$$W = en\,E_{ph}\,I_{ph}\,\cos\theta \tag{3.1}$$

where

$\quad$ W $\quad$ = $\quad$ power output (W)

$\quad$ e $\quad$ = $\quad$ efficiency

$\quad$ n $\quad$ = $\quad$ number of phases

$\quad$ I_{ph} $\quad$ = $\quad$ current per phase

$\quad$ θ $\quad$ = $\quad$ phase angle

and E_{ph} is given by

$$E_{ph} = 2.22\,f\phi d\,Z \times 10^{-8} \tag{3.2}$$

where

f = frequency (cps)

ϕ = lines of magnetic flux (Mx)

d = winding factor

Z = number of active conductors per phase

The lines of magnetic flux, ϕ, is given by

$$\phi = B_g \pi D L_a \tag{3.3}$$

where

B_g = flux density in the air gap lines per square inch

D = diameter of air gap (in.)

L_a = active length of conductor (in.)

Substituting Eq. (3.3) into Eq. (3.2), one obtains:

$$E_{ph} = 2.22 \, f B_g \pi D L_a d Z \times 10^{-8} \tag{3.4}$$

By definition,

$$q = \frac{n I_c Z}{\pi D} \tag{3.5}$$

where

q = specific loading, ampere-conductors per inch of armature periphery

I_c = current per conductor

and the other symbols have the same meanings as before.

Rearrangement of Eq. (3.5) gives

$$I_c = \frac{q \pi D}{nZ} \tag{3.6}$$

For a single conductor per phase, $I_c = I_{ph}$, whence

$$I_{ph} = \frac{q \pi D}{nZ} \tag{3.7}$$

Substituting Eqs. (3.4) and (3.7) into Eq. (3.1) and setting $\cos \theta = 1.0$ (since the load is essentially a pure resistive load), one obtains

$$W = 2.22 \, e f B_g dq \pi^2 D^2 L_a \times 10^{-8} \tag{3.8}$$

whence

$$D^2 L_a = \frac{W \times 10^8}{2.22 \, e f B_g dq \pi^2} \tag{3.9}$$

and

$$\text{Rotor volume} = \frac{\pi}{4} D^2 L_a = \frac{W \times 10^8}{8.88 \, e f B_g dq \pi} \tag{3.10}$$

As a first approximation, the volume of the stator will equal the volume of the rotor, so that

$$\text{Rotary transformer volume} = \frac{W \times 10^8}{4.44 \, e f B_g dq \pi} \tag{3.11}$$

The design of an induction motor begins with an estimate of the flux density in the air gap, B_g, and the specific loading, q. Estimates of these two quantities are based on judgment from previous experience, the materials available, losses that can be accepted, and economics. Large values of these two parameters favor small size but result in poor efficiency and high electrical losses. Small values improve the efficiency and reduce the losses, but result in large size, heavy weight, and high equipment cost. For 60 cps, 1-MW equipment, values of B_g and q generally lie in the ranges 60,000 to 65,000 lines/in.^{2} and 800 to 900 A-conductors/in., respectively.

Varying the flux density in the air gap has two opposing effects on losses; increasing this factor reduces the total weight of iron in the magnetic structure but increases the power lost per unit weight of iron due to eddy currents and hysteresis (commonly combined into core loss).

The effects of varying the specific loading are harder to analyze. Increasing the loading makes it more difficult to remove heat generated by electrical losses because of the more compact design coils.

Optimum design involves balancing the current density and the mean length of turns with the rotor diameter for the required value of D^2L_a, which in turn depends upon the specific loading and the flux density in the air gap. Because of the interdependence of these variables and the length and non-linearity of the calculations, computers are used to perform the design iterations until the desired performance is obtained. Both analysis and synthesis techniques are used (Refs. 15 and 16). In the analytical method, the desired parameters are programmed along with designs that are known to give the approximate performance desired. The output is a group of changes to the existing designs which are necessary to meet the new requirements. Synthesis is used when designs are required that cannot be based on existing equipment. This is the type of program that would be used to optimize the design of a rotary coupler.

In the preliminary calculations that follow, the size and feasibility of a rotary coupler are estimated for values of B_g and q of 60,000 and 850, respectively, corresponding to conventional practice. Calculations are also made with B_g and q assigned values of 40,000 and 700, respectively, to indicate the increase in size that would be involved in going to a higher efficiency design.

Raising the frequency at which the rotary transformer operates will reduce its size but will have the disadvantage of increasing the losses. Lowering the frequency has the opposite effects. In the preliminary calculations that follow, the frequency is taken as 60 cps.

The efficiency of a unit of this output operating without windage losses should be about 96%. This can be seen from the extrapolation of the curve in Fig. 12, which is based on data for induction motors varying in size from 1 to 700 hp and operating at speeds from 500 to 3600 rpm. The efficiency from the curve at 1 MW (1341 hp) is 94%, and it should be 2% higher since there would be no windage losses.

An approximate value of 0.95 for the winding factor is assumed in the preliminary calculations.

Inserting the values selected above into Eq. (3.11), one finds that the volume of the rotary transformer will be on the order of the following:

	$B_g = 40,000$		$B_g = 60,000$	
	$q = 700$	$q = 850$	$q = 700$	$q = 850$
Volume (ft^3)	2.7	2.1	1.8	1.5

Sliding Contacts

Sliding contacts are commonly used for transmitting electrical power across moving elements of machinery, and they are an efficient method for doing so under normal conditions.

Preliminary estimates during the course of the investigation indicated that slip rings were preferable to flexible cables and rotary transformers. As a result, a scaled-up model was fabricated for actual evaluation at AEDC, and it is therefore possible to indicate the characteristics and performance of a slip ring for use in the secondary radiation simulator on the basis of actual data.
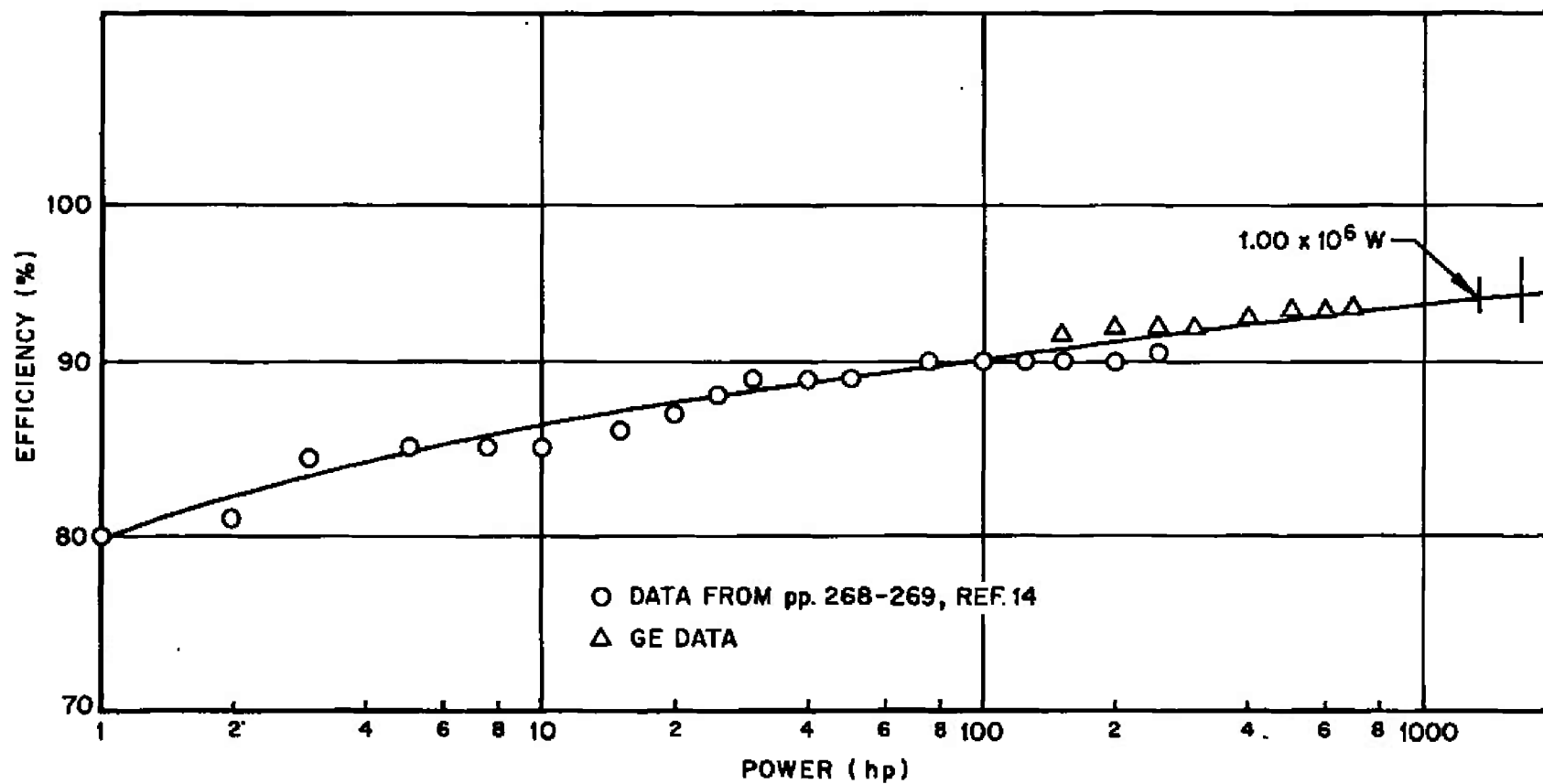
Fig. 12 Variation of Efficiency With Motor Output

The following three types of losses occur in operating a slip ring assembly:

- I^2R losses in the conducting members that compose the sliding contacts
- Contact resistance losses at the sliding interface
- Friction losses at the sliding interface

Experimental measurements (see Section 4) indicated that the total resistance involved in the first two items would be less than 1 mΩ for each slip ring involved in the power distribution system (see Section 3), and the total loss through the slip rings operating under peak conditions would be less than 100 W. Torque measurements on the 8-ring scaled-up unit gave a value of 119 in-lb (see Section 4), which indicates that the power required to rotate the slip ring assembly at a maximum speed of 15 rpm would be less than 250 W. Total losses would therefore be less than 350 W, which is less than 0.1% of the transmitted power of 1×10^6 W. (Preliminary estimates had placed the total losses at not more than 0.5%.)

Extending the size of the 8-ring scaled-up unit to accommodate 76 rings for use in the secondary radiation simulator indicates the final volume would be about 6 ft^3.

Comparative Merits of Alternative Systems

Table 3 compares the merits of the three alternate systems. In comparing the values in this table, one should bear in mind that the estimated efficiencies and sizes for the continuous conductor and rotary transformer systems are based on one lumped circuit and on simplifying assumptions that have been weighted in favor of these systems, whereas these factors have been measured in the case of the slip ring and are for a system that provides 76 separate circuits (one to each of the lamp banks). Despite this, the slip ring assembly is obviously superior to the other two systems.

POWER DISTRIBUTION SYSTEM

In order to reduce the current in the distribution system as much as possible, thereby minimizing losses and reducing conductor cross sections, power should be transmitted at as high a voltage as practical. The maximum practical voltage is limited by insulation and surface flashover characteristics, and voltages are therefore kept below 500 V in order to use standard insulation practices.

TABLE 3

COMPARISON OF ALTERNATE TRANSMISSION SYSTEMS

	Continuous Conductor	Rotary Transformer	Slip Ring
Electrical efficiency	~ 98% (estimated)[a]	~ 96% (estimated)[a]	> 99% (measured)
Size	> 260 ft^3 (estimated)[a]	~ 3 ft^3 (estimated)[a]	~ 6 ft^3
Ease of heat removal	Poor	Fair	Good
Relative equipment cost	Low	High	Low
Ease of repair	Good	Poor	Good
Feasibility	Components available and techniques well established	Requires development	Demonstrated to be feasible.
Stability in vacuum	Outgassing from cable insulation will increase pumping load and con-taminate vacuum.	Entrapped gases in windings will contribute to pumping load.	Demonstrated to be satisfactory.
Limitations on test flexibility	Useful if the number of revolutions in one direction is limited; unsatisfactory for unlimited rotation.	None	None

(a) These estimates are based on one lumped circuit, whereas the values for the slip ring system is for one that provides 76 separate circuits (one to each lamp bank).

By connecting two of the T-3 tungsten-filament lamps (rated at 1000 W at 240 V) in series, the simulator arrays can be operated with an input voltage below 500 V. For operation at 800 W, the effective voltage across each lamp will be 215 V (i. e., 240 V $\times \sqrt{800/1000}$).

Figure 13 is a circuit diagram for distributing power to one of the circumferential banks of lamps. There are 48 such circuits in the secondary radiation simulator, and each must be able to be operated independently of the other. Each group of 4 lamps is arranged in 2 series-connected pairs, and equalizer bus bars are used between the pairs of lamps to eliminate the loss of two lamps due to the failure of one lamp in a series pair. Since each lamp operates at 80% of its nominal rating under peak intensity conditions, three lamps on one side of the equalizer bus would have to fail before the input to one of the remaining lamps would exceed its nominal rating. The requirement for independent operation of the lamp banks is met by using a separate slip ring to provide the input power (28,800 W at 430 V) to each lamp bank. The slip rings are located on the pitch axis of the spacecraft vehicle undergoing test.

Figure 14 shows the distribution system for supplying power from a 3-phase source to 12 circumferential banks of lamps. The power loads on the lamp banks are well balanced so that all 12 of the lamp banks can be connected in common to a single neutral return line, and the neutral line then carries only the unbalanced current.

The largest current that would be carried by the neutral line from the circumferential banks of lamps occurs when the simulator is operating under the conditions shown in Fig. 10 and all of the 12 banks of lamps are on one side of the axis of symmetry in this figure. For a 3-phase system, the maximum currents in the three phase are as follows:

Phase	x-Component	y-Component
A	$1.00\ I_A$	0
B	$-0.50\ I_B$	$+0.866\ I_B$
C	$-0.50\ I_C$	$-0.866\ I_C$

430 V, MAX

9 SETS OF 4 LAMPS EACH,
SPACED 12 ft APART

⋀⋀⋀ = TUNGSTEN FILAMENT LAMP, NOMINALLY RATED AT 1 kW AT 240 V
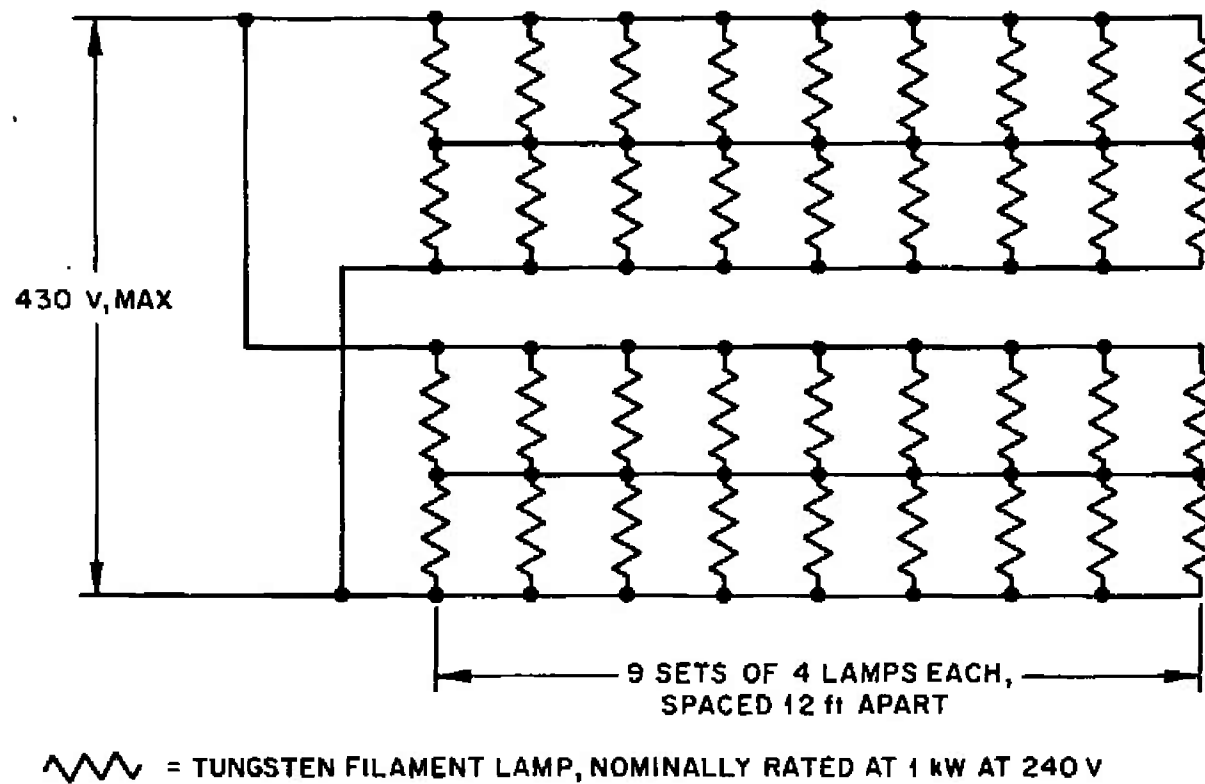
Fig. 13 Circuit Diagram for Power Distribution to One of the Circumferential Banks of Lamps

BANK OF LAMPS
(SEE FIG 13 FOR DETAILS)

SLIP RINGS
(MOUNTED ON PITCH AXIS)

CHAMBER WALL

CONTROLLERS

3-PHASE
440-V
a-c POWER
PHASE A
PHASE B
PHASE C
NEUTRAL
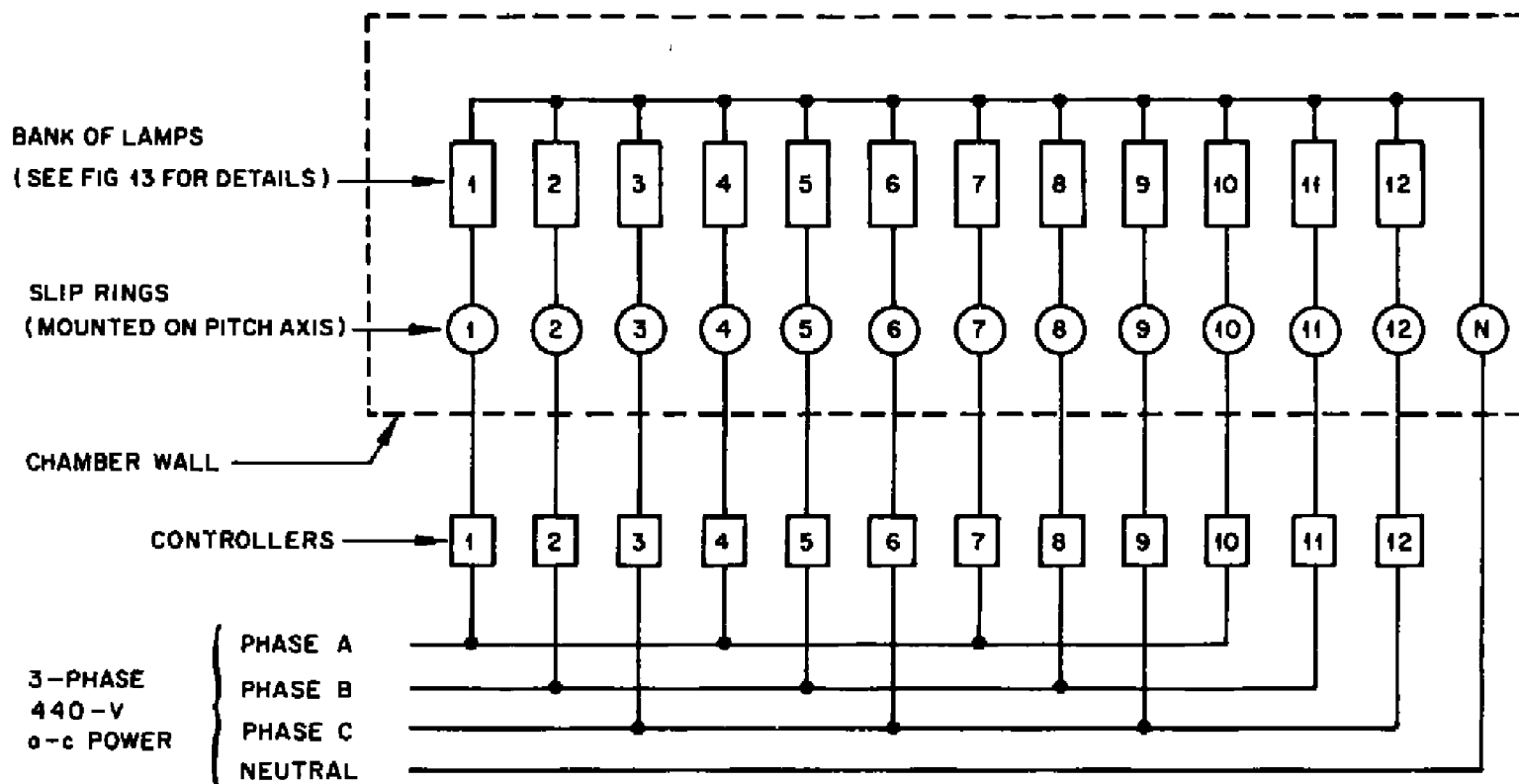
Fig. 14 Schematic of Power Distribution System to 12 Circumferential Banks of Lamps

and the absolute value of the current is given by

$$I = \sqrt{x^2 + y^2}$$

Since the power drawn by a bank of lamps is proportional to its intensity, the currents in the 12 banks of lamps shown in Fig. 14 for the condition of worst unbalance vary as follows:

Bank	Phase	Current (%)	x-Component (%) +	-	y-Component (%) +	-
1	A	100	100			
2	B	99.4		49.7	86.0	
3	C	97.8		48.9		84.7
4	A	95.9	95.9			
5	B	93.3		46.7	81.0	
6	C	90.0		45.0		77.9
7	A	87.2	87.2			
8	B	83.5		41.8	72.3	
9	C	79.8		39.9		69.1
10	A	74.6	74.6			
11	B	70.0		35.0	60.7	
12	C	64.6		32.3		55.9
			+357.7	339.3	+300.0	287.6
			-339.3		-287.6	
			+18.4		+12.4	

The current conducted by the common neutral is $18.4^2 + 12.4^2 = 22.2\%$ of the current in Bank 1.

Four common neutrals are sufficient for handling current to the 48 circumferential banks of lamps, so that the total number of slip rings for supplying power to the circumferential bank of lamps is 52.

Power distribution to the end caps would be similar to that for the circumferential banks. In the case of the end caps, the 400 lamps in each cap would be divided into 10 banks of 40 lamps each, so that the circuit for each of the end banks would be similar to that for each of the circumferential banks. shown in Fig. 13, except that there would be 40 lamps instead of 36. This means the requirements of the distribution lines and slip rings or the two types of lamp banks are within 10% of one another and the same sizes can be used throughout. The banks of lamps on the end caps can also be balanced, so that, at most, 2 common neutrals are needed on each end cap.

The current carried to each of the 48 circumferential banks of lamps (each bank consisting of 36 lamps connected as shown in Fig. 13) will be a maximum of

$$\frac{36}{2} \times \frac{1600}{430} = 67.0 \text{ A}$$

For the banks in the end caps, each of which contains 40 lamps in a similar circuit, the maximum current will be 74.4 A. A value of 75 A is used for selecting conductor sizes and designing the slip rings.

Since the electrical distribution system will operate in vacuum, however, there will be no heat dissipation by the normal means of air convection. As a result, the current carrying capacity of insulated wires must be reduced in order to avoid overheating and insulation damage. Normal design practice would permit No. 8 insulated wire to carry 73 A if the wire were freely ventilated. Derating should be on the order of 50%. No. 4 insulated wire should be satisfactory. Characteristics of No. 4 insulated wire per MIL-W-5086 are as follows:

Maximum resistance = 0.274 Ω per 1000 ft at 20° C

Diameter of finished wire = 0.370 in.

Weight = 176 lb per 1000 ft

Losses in No. 4 cable would be $75^2 \times 0.274 = 1542$ W per 1000 ft or 1.542 W/ft, and voltage drop would be $75 \times 0.274 = 20.55$ V per 1000 ft or 0.02055 V/ft under maximum loading conditions.

For cooling by radiation alone (i. e., no conduction to the supporting structure), the approximate operating temperature of the wire can be computed from the basic radiation formula

$$Q = 0.173 \, A_1 e_1 F_{12} \left[\left(\frac{T_1}{100} \right)^4 - \left(\frac{T_2}{100} \right)^4 \right]$$

where

$\qquad Q \quad = \quad$ heat transfer (Btu/hr)

$\qquad A_1 \quad = \quad$ area (ft^2)

$\qquad e_1 \quad = \quad$ emissivity

$\qquad F_{12} \quad = \quad$ form factor

$\qquad T_1 \quad = \quad$ temperature of wire (°R)

$\qquad T_2 \quad = \quad$ temperature of sink (°R)

For a 1-ft length of No. 8 insulated wire carrying a current of 75 A the following values are obtained:

$\qquad Q \quad = \quad 1.542 \, W \times \dfrac{3.41 \, Btu/hr}{1 \, W} = 5.26 \, Btu/hr$

$\qquad A_1 \quad = \quad 3.1416 \times \dfrac{0.370}{12} = 0.0969 \, ft^2$

$\qquad e_1 \quad = \quad 0.80$ (estimated)

$\qquad F_{12} \quad = \quad 0.50$ (assuming that one-half the wire will see the cold wall and one half will see the frame holding the lamps or the back of the reflectors which are further assumed to be at the temperature of the wire insulation)

$\qquad T_2 \quad = \quad 150°\,R$ (estimated)

Solving for T_1 by substitution of the above values into the basic radiation formula, one obtains

$$T_1 = 100 \left[\frac{5.26}{0.173 \times 0.0969 \times 0.80 \times 0.50} + 1.5^4 \right]^{1/4} = 100 \left[784 + 5 \right]^{1/4}$$

$$= 531 \, °R \text{ or } 71°\,F$$

47

Further refinement of this calculation requires a detailed layout of the simulator structure. However, the estimated wire temperature calculated above indicates that No. 4 insulated wire can be used safely.

SECTION 4

SLIDING CONTACT MATERIALS

An investigation of sliding contact materials was undertaken since sliding contacts were shown to be preferable to other techniques for transmitting electrical power to the secondary radiation simulator (Section 3) and since the only forseeable drawbacks to their use were the lack of suitable contact materials and information on their performance in ultrahigh vacuum.

MATERIALS

Three types of brush materials were evaluated; viz., silver-graphite (Ag-graphite), silver-copper-molybdenum disulfide (Ag-Cu-MoS$_2$), and silver-molybdenum-molybdenum disulfide (Ag-Mo-MoS$_2$). These were operated against rings of either electrodeposited silver or electrodeposited gold.

Silver-graphite brushes have been commercially available for some time, and they were evaluated as a basis for comparison with the other two types of brush materials. The specific compositions tested were 90% silver − 10% graphite (90 Ag − 10 graphite) and 80% silver − 20% graphite (80 Ag − 20 graphite).

Silver was selected as the base metal in the two types of developmental materials in order to provide good electrical conductivity. Molybdenum disulfide was selected to provide lubricity during sliding in vacuum. Earlier work at LMSC (Ref. 17) indicated that silver brushes lubricated with molybdenum disulfide did, in fact, operate with less wear and noise in vacuum than silver brushes lubricated with graphite, but that further improvement in wear resistance was desirable. Copper and molybdenum were therefore added in order to study their effect on hardening the silver and reducing brush wear.

The general procedure for preparing compacts started with mixing the powders in the proper proportions with a porcelain mortar and pestle. The mixed powders were then cold-pressed in closed steel dies, following which they were sintered in vacuum. The samples were maintained under a vacuum of 10^{-5} Torr during both heating and cooling in the furnace.

The composites tested at LMSC (Test Runs 1 through 4) were prepared in the form of discs, 0.5 in. in diameter by approximately 0.2 in. thick in the direction of pressing, from which brushes were then machined. Composites tested at AEDC (Test Run 5) were prepared in the form of larger discs, 1.25 in. in diameter by approximately 0.5 in. thick. Brushes were machined from these compacts so that the brush thickness was in the same direction as the direction of pressing.

Some of the $Ag-Cu-MoS_2$ composites evaluated in Test Run 5 were repressed (coined) and resintered in order to increase their density and hardness. Hot-pressing in vacuum was also considered, and equipment was assembled for fabricating brushes by this technique, but this effort was terminated before any specimens could be produced for evaluation.

EVALUATION EQUIPMENT AND PROCEDURE

Brush and ring material combinations were evaluated by operating them in ultrahigh vacuum in an actual slip ring assembly and measuring their resistance, noise, temperature, and wear characteristics. Equipment and procedures used at AEDC and LMSC were essentially similar; differences in the slip ring assemblies and operating conditions are noted in the following sections.

Equipment

Figure 15 shows schematically the test circuitry and equipment. The equipment is divided into the following four subsystems for ease of discussion:
- Slip ring assembly
- Vacuum system including rotational drive
- Power supply
- Measuring instrumentation
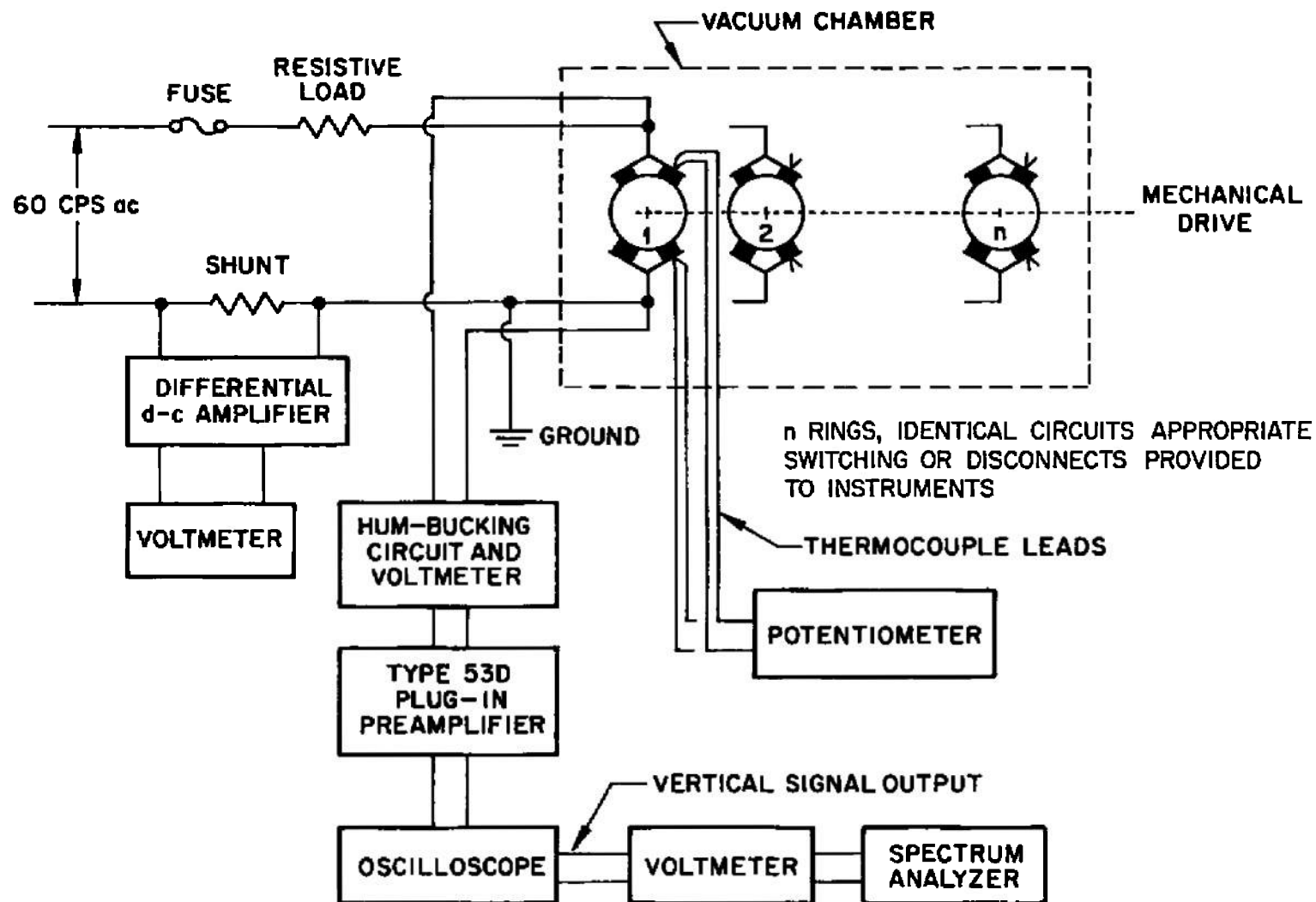
Fig. 15 Schematic of Test Circuit

Slip ring assembly. The slip ring assembly used in Test Runs 1 through 4 conducted at LMSC is shown in Fig. 16. This assembly had 24 rings measuring 2.25 in. in diameter by 0.1875 in. wide. Ring materials were either electro-deposited fine silver or gold. Each ring was contacted by two identical brushes, so that power could be brought in and out on the same ring. The brushes were in the form of buttons that were soldered to a beryllium-copper arm. The contacting faces of the brushes were 0.090 (± 0.005) in. wide by 0.150 (± 0.005) in. long, giving a projected contact area of 0.0135 in.^{2} and were contoured to mate with the ring radius. Both brushes rode on the same track on the ring. Brush materials were Ag-graphite, Ag-Cu-MoS$_2$, and Ag-Mo-MoS$_2$ with varying concentrations of the constituents, as discussed in the section on materials.

Most of the tests with this slip ring assembly were conducted with the standard type of brush holder, shown schematically in Fig. 17a. In this type of holder, the beryllium-copper arm served both as a conductor and as a cantilever spring for pressing the contact button against the ring, and the amount of brush contact force was set by the deflection of the spring. The advantage of this type of holder is its simplicity, whereas its disadvantages for research are the difficulty in setting the brush contact force precisely and maintaining the contact force constant when the brushes wear badly. Figure 17b shows a second type of brush holder that was used on 12 rings tested in Test Run 4 and on the 8 rings, Test Run 5. In this type of holder, the beryllium-copper arm again serves as a conductor, but the contact force is set and maintained by a compression spring pushing against the top of the arm, immediately above the point of contact.

One brush on each ring had an iron-constantan thermocouple spot-welded to the top of the beryllium-copper leaf spring, directly above the center of the brush button on the opposite side.

The scaled-up slip ring assembly tested at AEDC in Test Run 5 was a larger unit, with rings measuring 6.75 in. in diameter by 0.500 in. wide (Fig. 18). This unit had only 8 rings, 6 of them being electrodeposited silver and 2 electrodeposited gold. Each ring was contacted by four identical brushes, connected in pairs, so
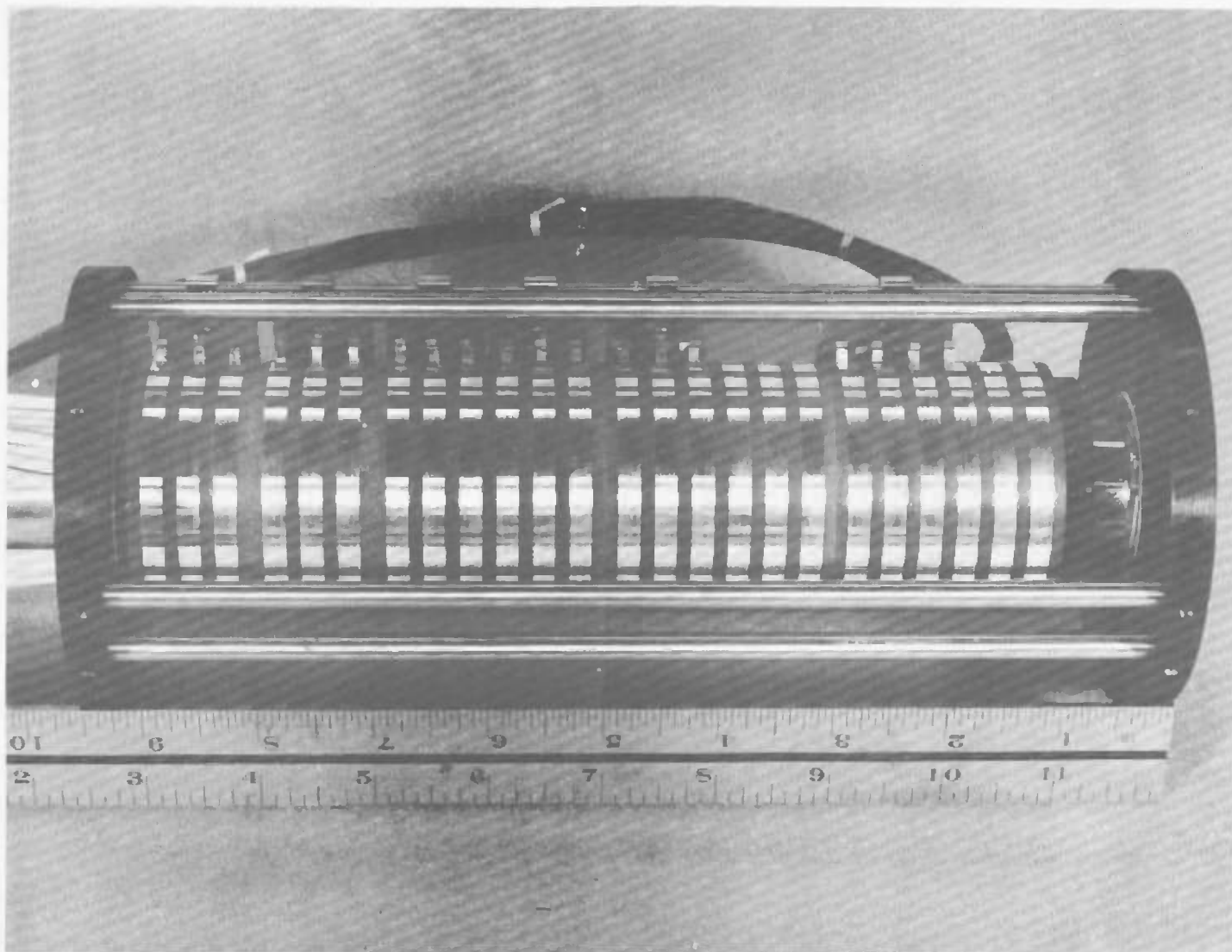
Fig. 16 Slip Ring Assembly 1 Before Testing
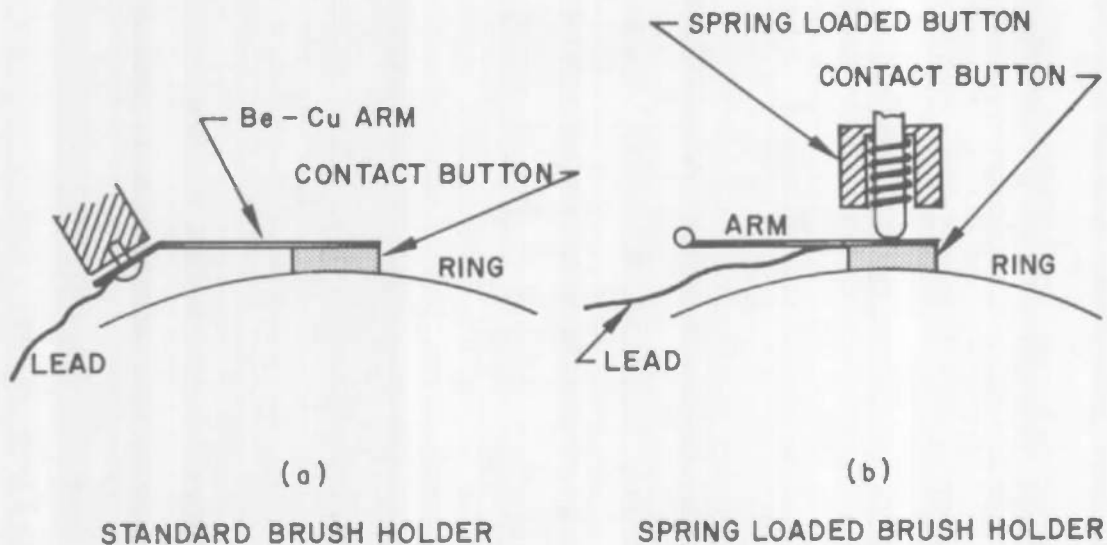
Fig. 17 Schematic of Brush Holders

that power could be brought in and out on the same ring. The brushes were in the form of buttons that were soldered to copper arms, as shown in Fig. 17b. Current was carried from the terminals to the brushes by flexible pig tails. The contacting faces of the brushes were 0.437 in. wide by 0.750 in. long, giving projected contact areas of 0.328 in.^{2}, and were contoured to mate with the ring radius. All four brushes rode on the same track on the ring. Brush materials were Ag-graphite and Ag-Cu-MoS$_2$

One brush of each pair had a copper-constantan thermocouple spot-welded to its top, directly above the center of the brush button on the opposite side.
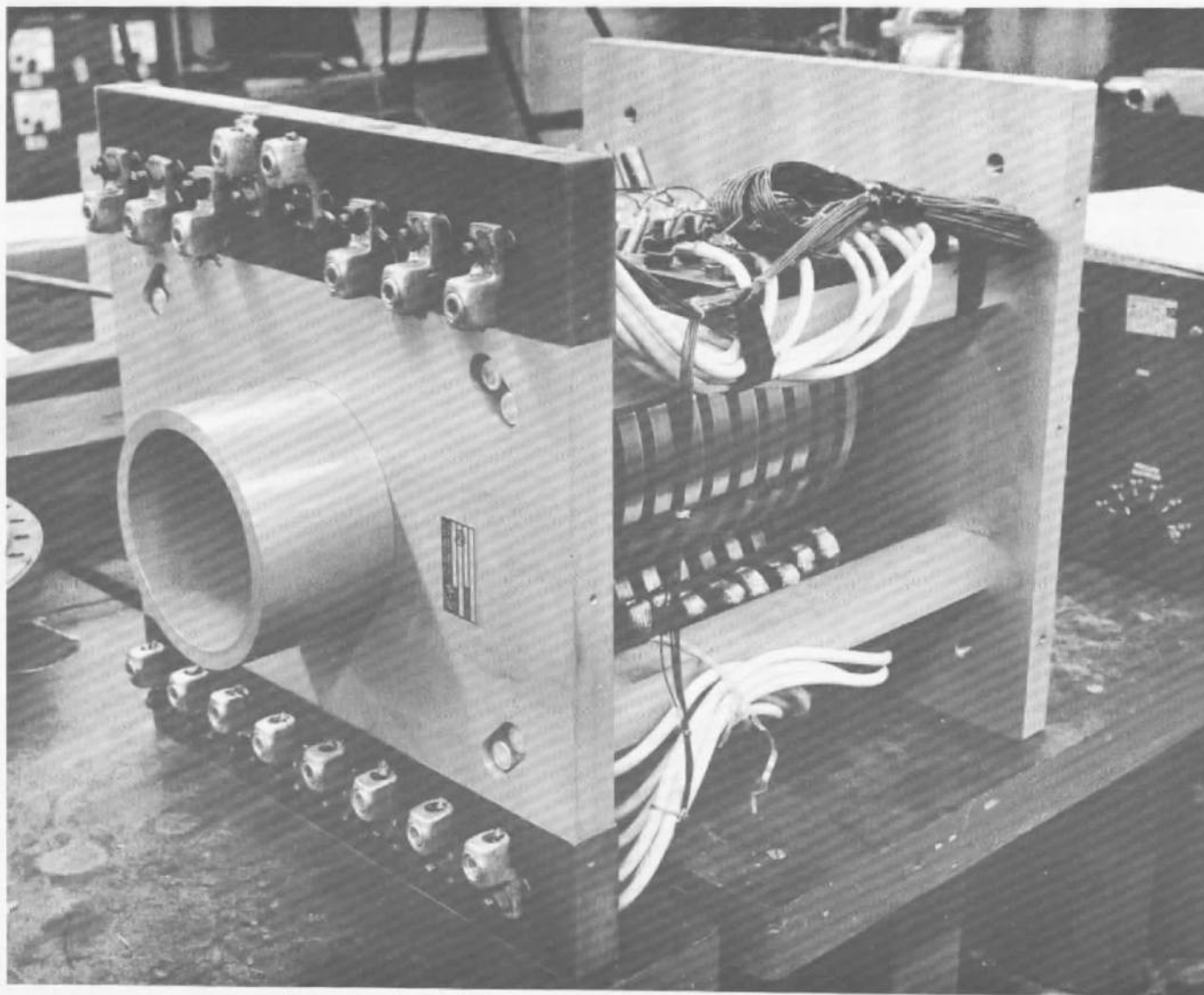
Fig. 18 8-Ring Scaled-up Slip Ring Assembly After Testing at AEDC

Vacuum System. Figure 19 shows schematically the vacuum system used in Test Runs 1 through 4 at LMSC, and Fig. 20 shows the chamber and associated equipment.

The vacuum chamber is a stainless steel cylinder measuring 12 in. diameter by 22 in. long and was pumped by a 360 liter/sec ion pump (Ultek Model 336) through a 6-in. diameter leg. The chamber was provided with a valve (Veeco R-50-PSS) for initially evacuating it to a pressure low enough for the ion pump to be energized. Initial roughing was by means of a mechanical pump provided with a liquid nitrogen finger for trapping oil vapors and preventing contamination of the vacuum system. After the ion pump had been put into operation, the roughing valve was closed and the roughing pump removed from the system.

Power to the ion pump came from the 60 cps, 115-V a-c house supply through an ion pump power supply (Ultek Model PS-1000). The pump was mounted in the vertical position on a rigid frame.

The slip ring assembly was mounted on a 12-in. diameter flange that contained hermetically sealed feed-throughs for making all electrical connections. The axis of the slip ring assembly was horizontal. The slip ring was rotated by a hermetically sealed magnetic drive which was attached to the 12-in. diameter flange by means of a smaller flange. All attachments and checkouts were made to the 12-in. diameter flange before it was mounted to the chamber. All flanges were sealed with copper metal crush gaskets to eliminate contamination by outgassing from elastomeric seals.

The magnetic drive was operated by a d-c motor through a pair of pulleys providing the proper speed reduction. Power to the d-c motor came from the 60 cps, 115-V a-c house supply through a rectifier and control circuit, which allowed the speed of the motor to be adjusted to give the exact speed desired on the slip ring shaft. The motor was mounted with vibration damping mounts.

The chamber was provided with an ionization gage (Veeco RG-75-K) for making pressure measurements within the chamber and for serving as a check on pressure measurements made by means of the pump current reading. The ionization gage was connected to an ionization gage control circuit (Veeco RG-31A). Power to the ionization gage control circuit came from the 60 cps, 115-V a-c house supply.
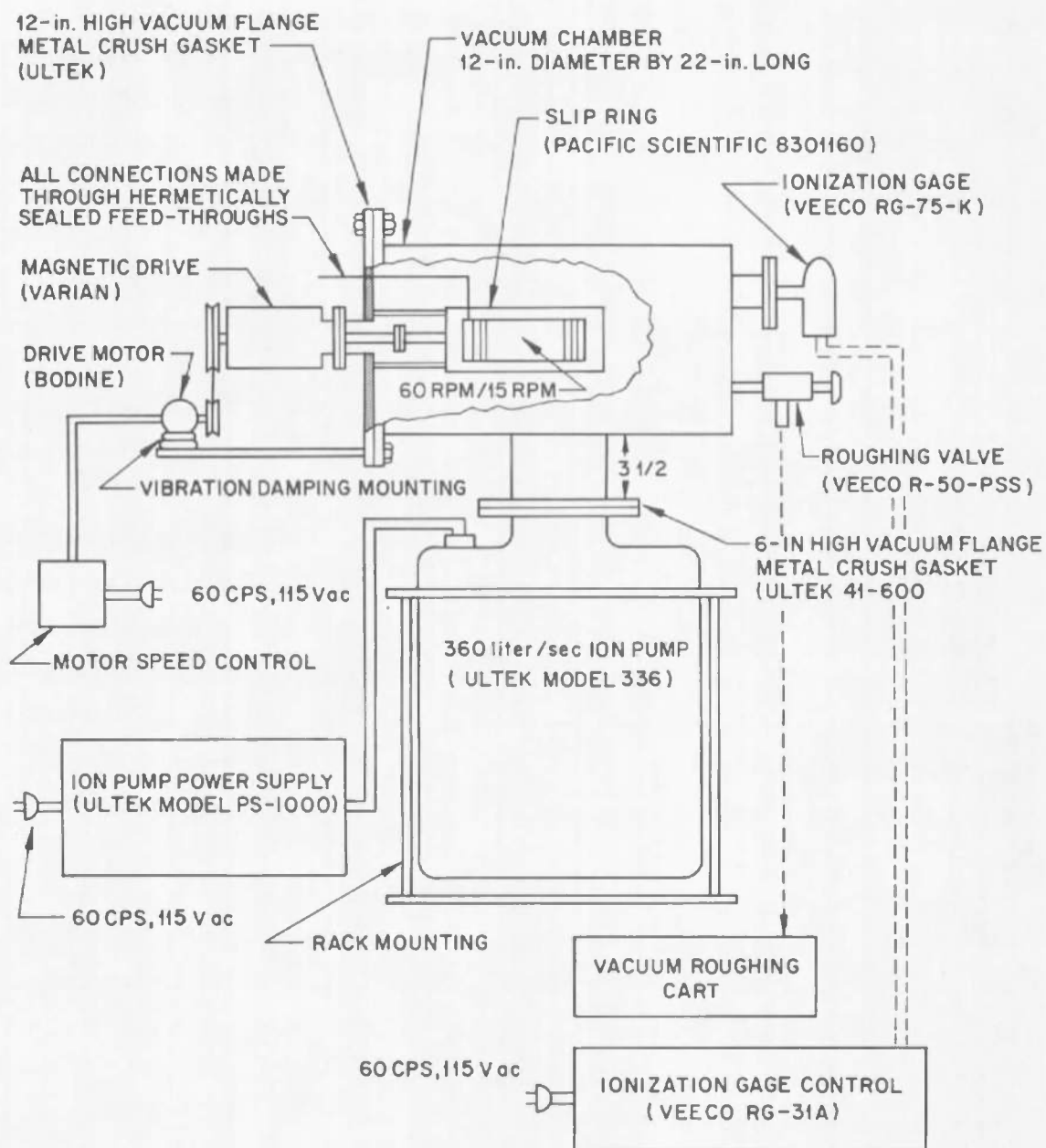
Fig. 19 Vacuum System
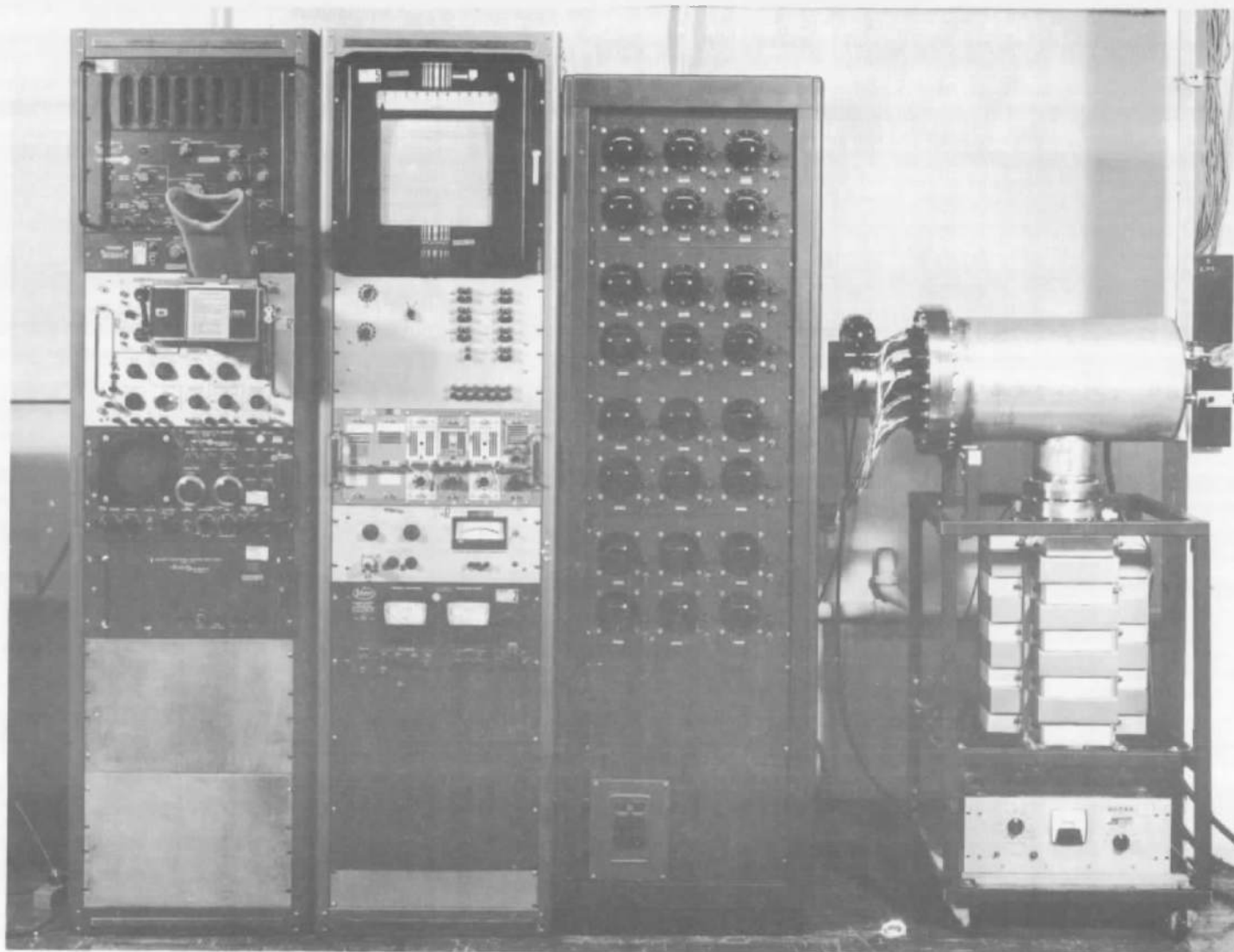
Fig. 20 Vacuum Chamber and Associated Equipment at LMSC

Power supply. Current was adjusted to the desired level by means of a variable autotransformer, a separate transformer being used for each ring and associated pair of brushes. A resistive load having a resistance considerably higher than that of the slip ring and brushes was inserted in series to maintain an essentially constant current, despite minor fluctuations in the resistance of the brush contacts. The amount of current passing through the slip ring was determined from the voltage drop across a calibrated manganin shunt wire placed in series with the slip ring.

Measuring instrumentation. Brush temperatures were measured by means of thermocouples whose hot junctions were spot-welded to one of the brushes on a ring (two brushes in the case of Test Run 5).

Brush resistance and noise were measured by monitoring the potential drop across the brush pairs. An audio frequency microvolter (e.g., Type 548C Audio Frequency Microvolter of General Radio Co.) was used to measure the potential drop across the brushes and to eliminate the 60-cps common mode from the input to the preamplifier (e.g., Type 53D) of the oscilloscope (e.g., Tektronix Model RM 45A). The vertical signal output of the oscilloscope was fed into a voltmeter (e.g., Hewlett Packard Model 400D vacuum-tube voltmeter) and into a spectrum analyzer (e.g., Panoramic Analyzer Model TMI-1 of Panoramic Radio Products). In use, the hum-bucking circuit of the audio frequency microvolter was adjusted to eliminate the 60-cps wave form from the oscilloscope pattern, which in turn minimized the voltmeter reading.

Procedure.

The following independent variables were either held constant or varied from one set of brushes and rings to another to study their effects:

1. Brush material — Brushes were made of Ag-graphite, $Ag-Cu-MoS_2$, and $Ag-Mo-MoS_2$ composites with varying concentrations of the constituents.

2. Ring material — Rings were either electrodeposited silver or electrodeposited gold.

3. Brush geometry — In·Test Runs 1 through 4 at LMSC, brushes were 0.090 in. wide by 0.150 in. long, giving a projected contact area of 0.0135 in.^{2} and were contoured to mate with the 2.25-in. diameter rings. In Test Run 5 at AEDC, brushes were 0.437 in. wide by 0.750 in. long, giving a projected contact area of 0.328 in.^{2}, and were contoured to mate with the 6.75-in. diameter rings.

4. Ring geometry — In Test Runs 1 through 4 at LMSC, rings were 2.25 in. in diameter with 0.1875 in. wide faces. In Test Run 5 at AEDC, rings were 6.75 in. in diameter with 0.500 in. wide faces.

5. Brush contact force — In Test Runs 1 through 4 at LMSC, brush contact forces were either 2.16 oz (61.2 g) or 1.30 oz (36.7 g), giving contact pressures of 10 and 6 psi, respectively. In Test Run 5 at AEDC, brush contact forces were either 3.27 or 1.96 lb, giving contact pressures of 10 and 6 psi, respectively.

6. Current — Test Runs 1 through 4 at LMSC were run with a current of 4.05 A, giving a current density of 300 A/in.^{2} of projected brush contact area. In Test Run 5 at AEDC, current was either 75 or 40 A, giving current densities of 114 and 61 A/in.^{2} when the current was divided equally between the brushes in a pair and 229 and 122 A/in.^{2} when the current was carried by only one brush.

7. Speed — Rotational speed was 60 rpm in Test Runs 1 through 4 at LMSC, giving a peripheral sliding velocity of 424 in./min. Rotational speed was 15 rpm in Test Run 5 at AEDC, giving a peripheral sliding velocity of 318 in./min. At certain times in some of the tests, as noted in the following sections, the speed was reduced or rotation stopped completely in order to determine what effect, if any, there was on noise or contact welding.

8. Temperature — All tests were conducted at room temperature.

9. Atmosphere — All tests were conducted in ultrahigh vacuum (pressure below 10^{-6} Torr).

10. Duration — All tests were conducted for a minimum duration of 500 hr or prior failure.

For each set of brushes and rings, the following dependent variables were measured:

- Contact resistance (static and dynamic)
- Brush temperature
- Noise (average and peak) and noise spectrum
- Wear (decrease in brush thickness and erosion of ring and brush surfaces)

Contact force was measured on each brush as the force required to lift the brush out of contact with the ring. To do this, an ohmmeter was connected across the slip ring and the two brushes. A lifting force was applied to one of the brushes, and the force increased until the resistance increased to at least 10 times the initial value, indicating that the brush has been lifted out of contact.

The brush thickness was measured before and after testing and the difference recorded as the brush wear. The initial brush thickness was measured before final assembly and shipping to AEDC. Evaluations of surface roughness and erosion were made by visual examinations at the conclusions of the tests.

Measurements were made on all ring and thermocouple circuits before the test assembly was placed into the vacuum chamber to insure circuit continuity and to check for loose or broken wires. The following tests were conducted in air.

With all voltage controls set to zero and all switches set to the off position, the slip rings were rotated at 60 (Test Runs 1 through 4) or 15 rpm (Test Run 5). The current in each ring circuit was then increased from zero to the nominal test current. The initial dynamic potential drop across the brush leads was measured in air for each brush-ring-brush combination by connecting them sequentially to the voltmeter and measuring the voltage.

Average and peak noise were measured initially with the oscilloscope, which was connected sequentially to each brush-ring-brush combination at the same time that the voltmeter was connected. Oscilloscope traces were also photographed for each brush-ring-brush combination at this time.

After the above dynamic measurements in air had been completed for all brush-ring-brush combinations, all circuits were de-energized by opening the switches (without disturbing the current settings), rotation was stopped, and the

static potential drop across the brush leads was measured. This was done by energizing each circuit sequentially and connecting them to the voltmeter and measuring the voltage.

After the initial static contact resistance of all brush-ring-brush combinations had been measured, the slip rings were again rotated at test speed. Rotation in air was continued overnight (16 to 20 hr) with the test current in each circuit, following which measurements of dynamic potential drop across the brushes and noise were repeated as before. In addition, the brush temperature of each brush-ring-brush combination was measured by connecting a potentiometer to the thermocouples sequentially through the d-c differential amplifiers. Following this, rotation was stopped and the static contact resistance measured, following the same procedure as before.

After the air run-in and calibration measurements had been completed, all circuits were de-energized and evacuation of the test chamber was begun. Within 2 hr from the time of starting evacuation or when the pressure reached 1×10^{-6} Torr, whichever occured first, rotation was resumed, and all circuits were energized. Measurements of pressure, temperature, dynamic contact resistance, and noise were made in the same manner as before. These measurements were repeated after an additional 1 hr and after approximately 5, 25, 50, 100, 200, and 500 hr of operation in vacuum.

EXPERIMENTAL RESULTS

This section describes the experimental results from five separate runs. Test Runs 1 through 4 were conducted at LMSC; Test Run 5 at AEDC. Since the independent variables in Test Runs 3, 4, and 5 were selected on the basis of preliminary conclusions reached from the results of preceding runs, the results of each run are analyzed separately.

Test Run 1 (LMSC)

Test Run 1 contained 15 pairs of brushes of Ag-Cu-MoS$_2$ composites and 4 pairs of brushes of Ag-graphite. All brushes were operated at 60 rpm against

2.25-in. diameter slip rings of electrodeposited fine silver. Copper content of the Ag-Cu-MoS$_2$ brushes was varied from 0 to 15% and MoS$_2$ content from 2.5 to 15%. Purposes of this test were to compare the general performance in vacuum of Ag-Cu-MoS$_2$ brushes and to determine the approximate amounts of Cu and MoS$_2$ for best performance.

Assembly 1 was run-in for 20 hr in air and then operated for 500 hr in vacuum (2×10^{-5} to 2×10^{-6} Torr). During the first 100-hr of the test run, the following trends were noted:

- All Ag-Cu-MoS$_2$ composites containing only 2.5% MoS$_2$ suffered failures.
- All Ag-Cu-MoS$_2$ composites containing only 10% or more Cu either failed or became very noisy.
- Ag-Cu-MoS$_2$ composites containing 10 and 15% MoS$_2$ and less than 10% Cu operated quietly.
- Both the 90 Ag − 10 graphite and 80 Ag − 20 graphite brush compositions operated with high noise levels and suffered failures.
- Brush failures were preceded by noisy operation.

Figures 21 through 24 show the conditions of the brushes and rings at the conclusion of the 500-hr vacuum run.

One can note in Fig. 21 that Brushes 6, 9, 10, 16, and 19 have been worn or broken from the beryllium-copper leaf springs to which they had been soldered. Brushes 1, 5, 7, and 18 were also dislodged on the back side of the assembly, which is hidden from view in this figure. One can also note that the outrider springs on Brushes 5, 16, 17, and 19 are no longer in contact with the leaf springs, so that they are not performing their function of maintaining the brush contact force. A similar condition exists with the outrider spring on Brush 18 on the back side of the assembly. In Fig. 21, the brush compositions vary from left to right in the following order:

Brush	Composition (% wt)			
	Ag	Cu	MoS_2	Graphite
1	97.5	0	2.5	
2	95	0	5	
3	90	0	10	
4	85	0	15	
5	92.5	5	2.5	
6	87.5	10	2.5	
7	85	10	5	
8	85	5	10	
9	82.5	15	2.5	
10	80	15	5	
11	80	10	10	
12	80	5	15	
13	75	15	10	
14	75	10	15	
15	70	15	15	
16	90			10
17	90			10
18	80			20
19	80			20

Figure 22 shows in detail the conditions of the rings and brushes at Positions 1, 2, 3, and 4. These four brushes contain only silver and MoS_2 (no copper). Brush 1 (97.5 Ag − 2.5 MoS_2) is badly worn; failure of this brush composition occurred within the first 100 hr, due to dislodging of the brush on the back side of the assembly. From this result, and similar results with other brushes containing only 2.5% MoS_2 plus copper (Brushes 5, 6, and 9), one concludes that 2.5% MoS_2 is insufficient for good brush performance, due to excessive brush and ring wear.

Figure 23 shows in detail the conditions at Positions 9, 10, and 11. All three rings are badly worn. Ring 9, which was contacted by a brush of high copper − low MoS_2 content (82.5 Ag − 15 Cu − 2.5 MoS_2) was the worst worn of this group.
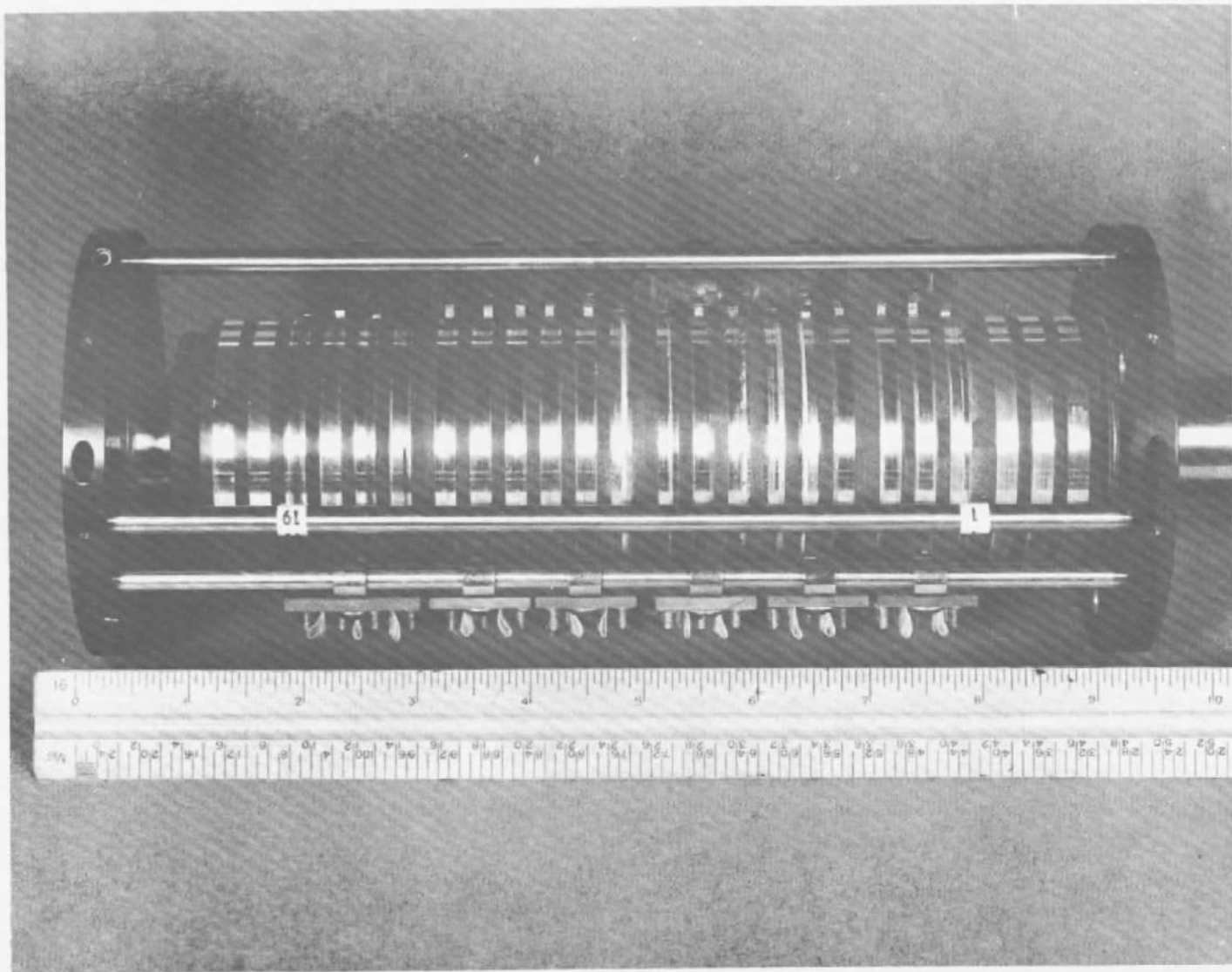
Fig. 21 Slip Ring Assembly 1 After Testing
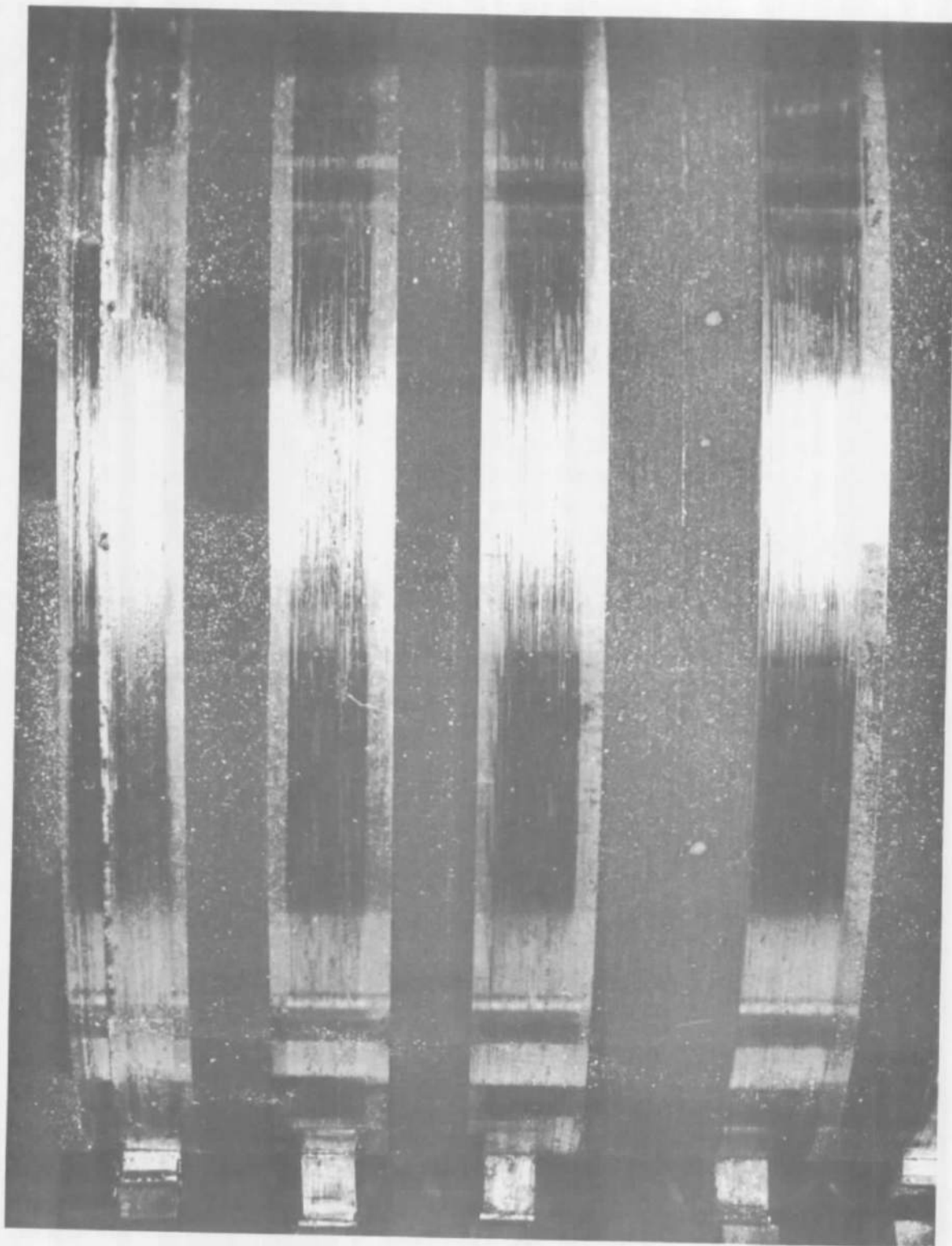
Fig. 22 Detail on Rings 1 to 4 of Assembly 1 After Testing
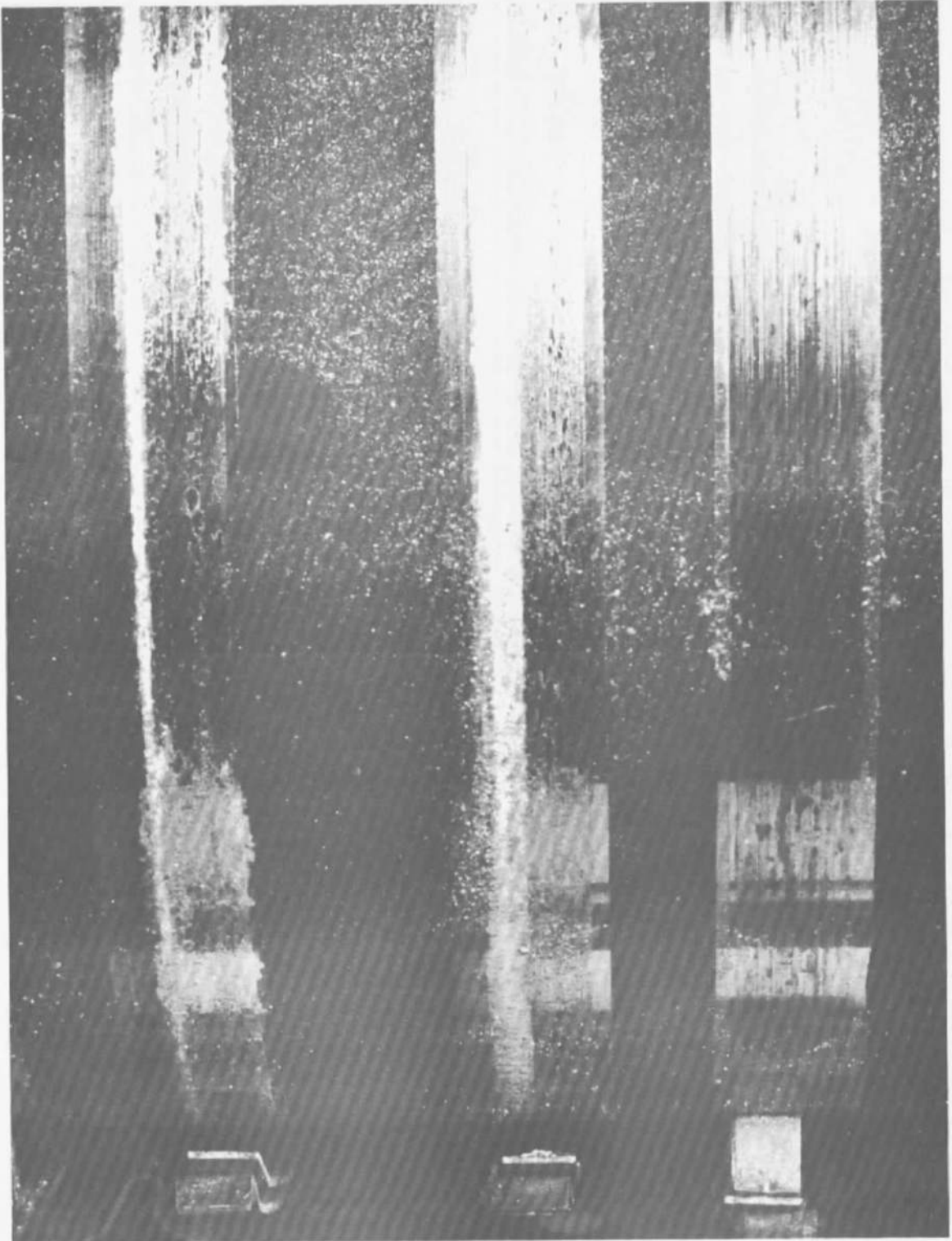
Fig. 23 Detail on Rings 9, 10, and 11 of Assembly 1 After Testing
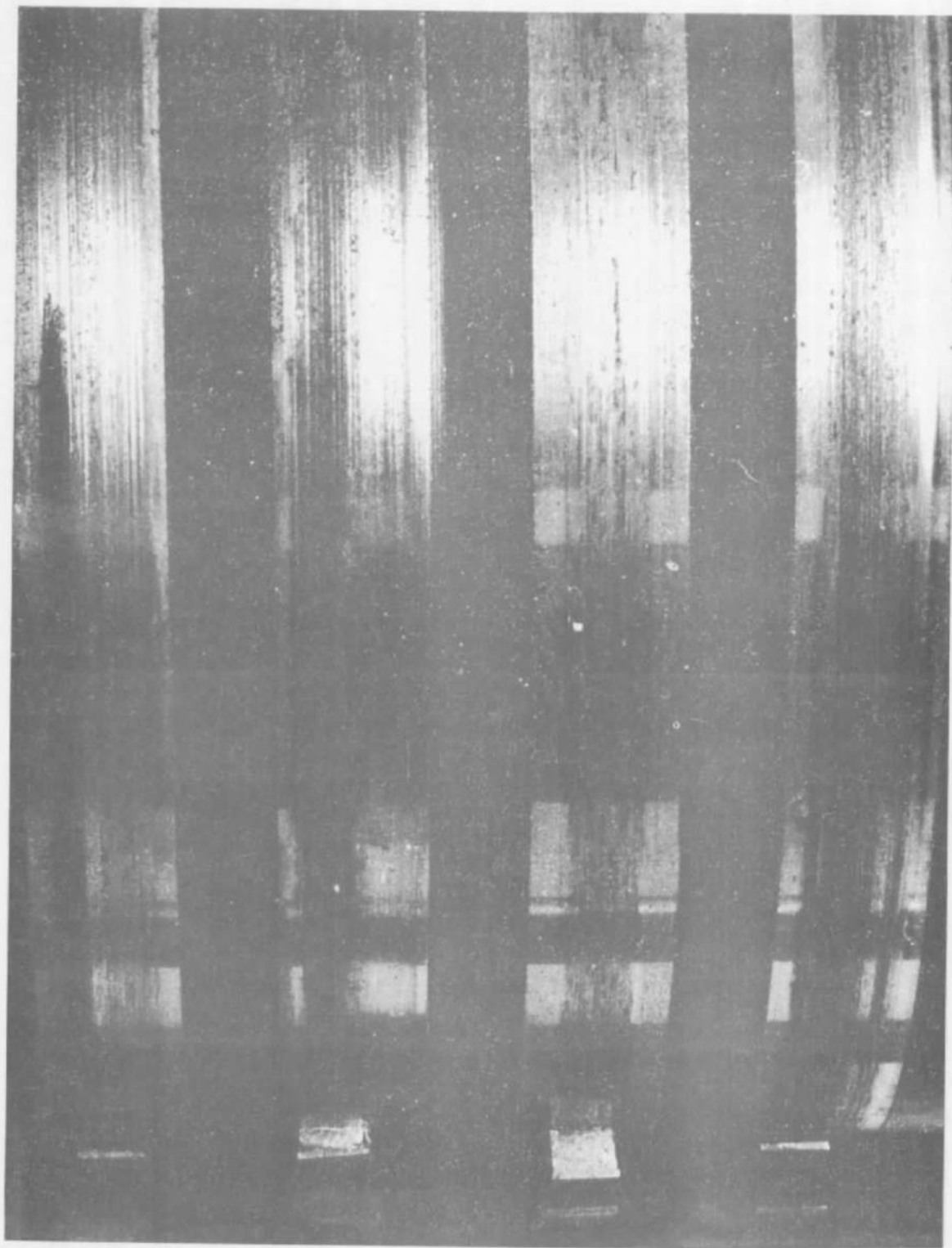
Fig. 24 Detail on Rings 16 to 19 of Assembly 1 After Testing

Brushes with 10 or 15% Cu and 10 or 15% MoS_2 (e.g., Brush 11), did not appear severely worn, although their operation was noisy and ring wear was slightly greater than that provided by the best performers (0 to 5 % Cu with 10 or 15% MoS_2).

Figure 24 shows in detail the conditions at Positions 16, 17, 18, and 19. Brushes at these four positions were commercial silver-graphite brushes. All brushes and rings were badly worn. These results verify results from earlier investigations at LMSC, which indicate that silver-graphite brushes are inadequate for use in vacuum.

Table 4 summarizes the measurements and observations on the wear of the brushes and rings at the conclusion of the test run, and indicates the time at which the brushes failed. The results on brush wear are also plotted in Fig. 25, in which the results for the Ag-CuMoS_2 composites are grouped according to their copper content (0, 5, 10, and 15%) and in each group are arranged in order of increasing MoS_2 content (2.5, 5, 10, and 15%). Final dimensions were measured on both brushes of a given composition in ten cases, although in three of these cases the final measurement was in error and had to be discarded. In nine cases, one of the two brushes broke off the brush holder during the test run, so that the final dimensions were obtained for only one brush. Where brush wear was low, (i.e., 0.015 in. or less), both brushes of a pair survived the complete 500 hr of testing in vacuum, and measurements were fairly consistent. Where brush wear was high, measurements were obtained on only one brush of a pair, and there were anomalies in the trends, probably because (1) current was flowing through the brushes for only a part of the tests and (2) the type of spring loading was unable to maintain a constant pressure on brushes that wore badly.

Figure 25 indicates that MoS_2 contents of 2.5 and 5% generally resulted in high brush wear, whereas MoS_2 contents of 10 and 15% resulted in low brush wear. The higher copper contents also appeared to favor lower brush wear, as expected from the hardening action of copper in silver, although the effect was less than that of MoS_2. On the other hand, the higher copper contents (i.e., 5 and 10% Cu) were undesirable from the standpoint of ring wear and electrical noise (see results on noise).

TABLE 4

BRUSH AND RING WEAR ON SLIP RING ASSEMBLY 1

Brush Position	Composition (% wt)				Thickness (in.)				Wear (in.)			Ring Wear	Time to failure in vacuum (hr)
					Initial		Final						
	Ag	Cu	MoS$_2$	Graphite	Brush 1[a]	Brush 2[b]	Brush 1	Brush 2	Brush 1	Brush 2	Average		
1	97.5	0	2.5	0	0.111	0.118	0.040	M[c]	0.071		0.071	Severe	22
2	95	0	5	0	0.117	0.104	0.108		0.009		0.009	Light	(d)
3	90	0	10	0	0.110	0.085	0.096	0.079	0.004	0.006	0.005	Light	(d)
4	85	0	15	0	0.098	0.094	0.096	0.085	0.002	0.009	0.006	Light	(d)
5	92.5	5	2.5	0	0.119	0.120	0.035	M	0.084		0.084	Severe	22
8	85	5	10	0	0.106	0.110	0.102	0.095	0.004	0.015	0.010	Light	(d)
12	80	5	15	0	0.105	0.107	0.100	0.099	0.005	0.008	0.006	Light to Mod.	(d)
6	87.5	10	2.5	0	0.120	0.122	M	0.075		0.047	0.047	Severe	5
7	85	10	5	0	0.119	0.121	0.070	M	0.049		0.049	Severe	189
11	80	10	10	0	0.108	0.117	0.104	0.115	0.004	0.002	0.003	Moderate	(d)
14	75	10	15	0	0.108	0.102	0.100		0.008		0.008	Moderate	(d)
9	82.5	15	2.5	0	0.119	0.112	M	0.101		0.011	0.011	Severe	1
10	80	15	5	0	0.111	0.120	M	0.065		0.055	0.055	Severe	26
13	75	15	10	0	0.107	0.110	0.103	0.105	0.004	0.005	0.005	Moderate	(d)
15	70	15	15	0	0.105	0.099	0.099		0.006		0.006	Moderate	(d)
16	90	0	0	10	0.109	0.106	M	0.070		0.036	0.036	Severe	67
17	90	0	0	10	0.095	0.106	0.028	0.045	0.067	0.061	0.064	Severe	(d)
18	80	0	0	20	0.068	0.079	0.058	M	0.010		0.010	Severe	0
19	80	0	0	20	0.085	0.076	M	0.040		0.036	0.036	Severe	189

(a) Brush 1 – brush without thermocouple.
(b) Brush 2 – brush with thermocouple attached to leaf spring holding it.

(c) M – missing (broke off during test; no final measurement obtained).
(d) No failure; both brushes operated for full test time.
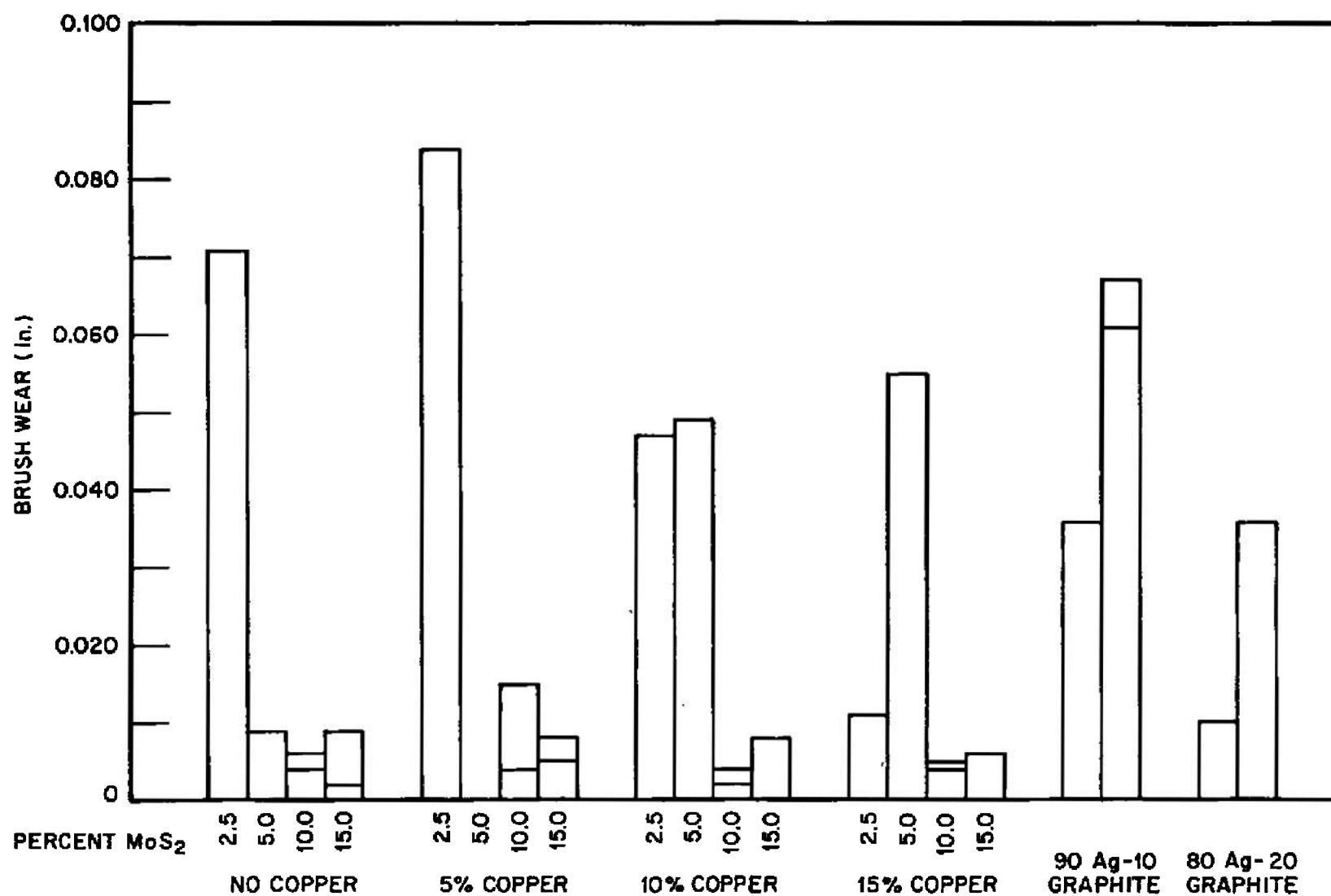
Fig. 25 Brush Wear on Slip Ring Assembly 1

Figure 26 summarizes some of the noise measurements made during the operation of Slip Ring Assembly 1. The noise (in mV rms at 730 cps) is shown for the pre-run condition, after 28.1 hr of operation in vacuum, and after 500 hr of operation in vacuum. These results indicate that the general noise level in vacuum of the better Ag-Cu-MoS$_2$ brush composites is as good as the noise level in air of premium, commercially available brush materials, and that the noise level of the Ag-Cu-MoS$_2$ brush composites increases with increasing copper content.

Table 5 summarizes measurements of brush contact resistance before run-in, shortly after the start of operation in vacuum, and after about 100 and 500 hr of operation in vacuum. The resistance of the leads has been subtracted in these measurements, so that the reported values are essentially the resistance across the two brush-ring interfaces in each case. This resistance is seen to be on the order of 10 mΩ. No significant trends appear in the data, except that the dynamic resistance is usually slightly higher than the static resistance.

Silver-graphite brushes generally suffered excessive wear themselves, caused severe wear to the rings, and operated with high noise levels. The 80 Ag – 20 graphite composition appeared to wear less than the 90 Ag – 10 graphite composition, but its noise was higher, as expected.

Test Run 2 (LMSC).

Test Run 2 contained 20 pairs of brushes with Ag-Mo-MoS$_2$ composites and 2 pairs of brushes of Ag-graphite. All brushes were operated at 60 rpm against 2.25-in. diameter slip rings of electrodeposited silver. The content of metallic molybdenum in the Ag-Mo-MoS$_2$ composites was varied from 5 to 40%, and MoS$_2$ content from 0 to 15%. Purposes of this test were similar to those of Test Run 1, except that molybdenum was substituted for copper as the alloying metal in the silver base. This assembly was run-in for 20 hr in air and then operated for 500 hr in vacuum.
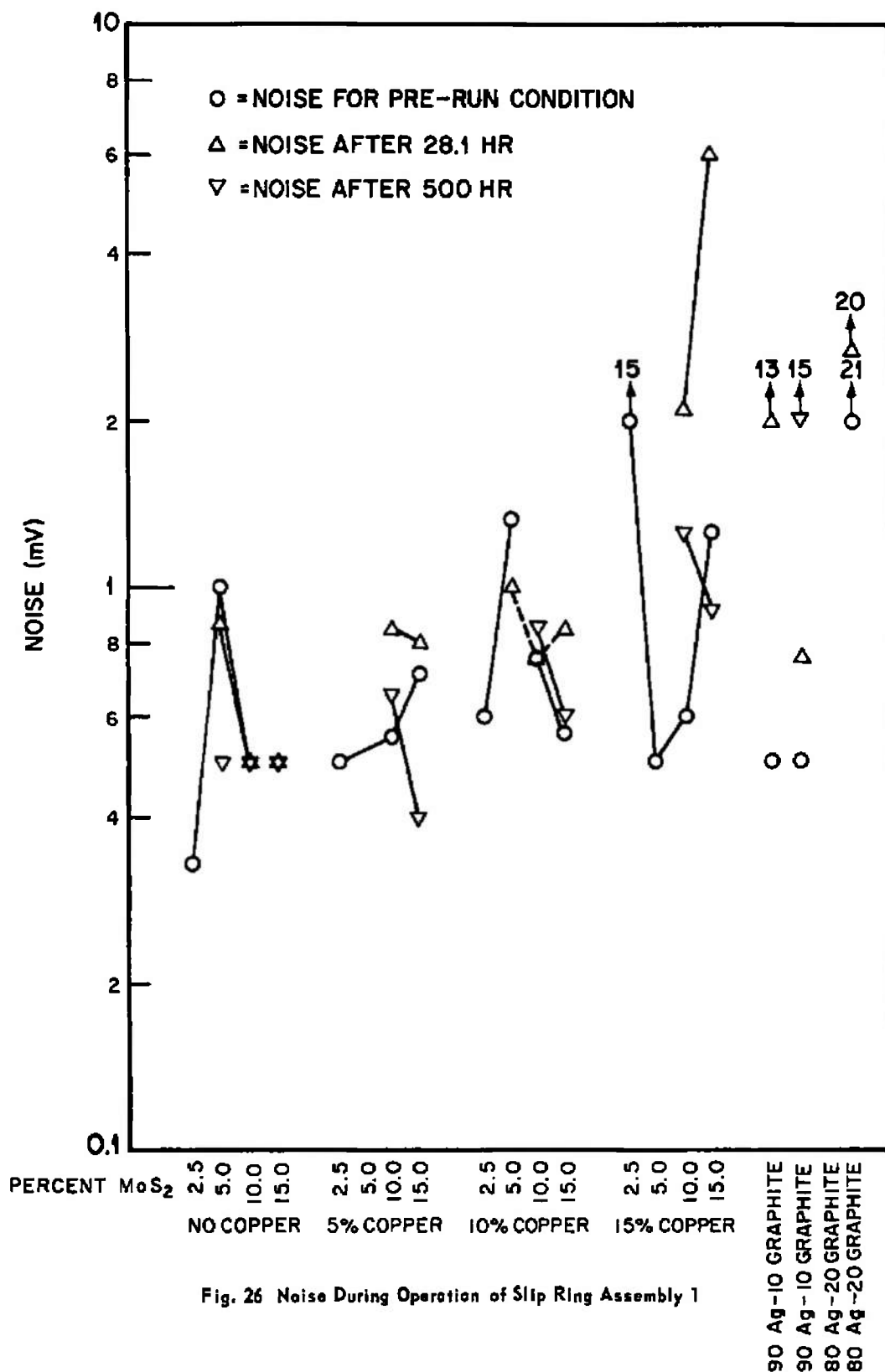
Fig. 26 Noise During Operation of Slip Ring Assembly 1

TABLE 5

CONTACT RESISTANCE FOR SLIP RING ASSEMBLY 1

Brush Position	Composition (% wt)				Contact Resistance (mΩ)							
					Static[a]				Dynamic[a]			
	Ag	Cu	MoS$_2$	Graphite	Pre-run	24 hr	120 hr	520 hr	Pre-run	24 hr	120 hr	520 hr
1	97.5	0	2.5	0	3.8	29.8			7.8	29.8		
2	95	0	5	0	11.2	1.5	4.0	4.5	17.8	1.5	4.5	5.2
3	90	0	10	0	4.5	3.2	4.5	8.2	15.8	3.8	4.5	8.8
4	85	0	15	0	12.8	3.5	5.8	5.0		5.0	6.8	6.2
5	92.5	5	2.5	0	5.2	4.5			6.2	6.0		
8	85	5	10	0	4.2	13.2	9.8	12.0	6.8	13.2	10.2	13.2
12	80	5	15	0	7.0	8.2	4.8	11.0	19.5	11.5	5.8	12.8
6	87.5	10	2.5	0	2.0	4.5		2.0	4.5			
7[b]	85	10	5	0								
11	80	10	10	0	1.8	5.0	7.5	10.8	9.2	6.2	8.8	12.8
14[b]	75	10	15	0								
9	82.5	15	2.5	0	6.2	7.8			8.8	7.8		
10	80	15	5	0	2.2	5.2			4.2	6.0		
13	75	15	10	0	2.5	23.0	21.8	21.5	7.8	25.0	21.2	21.8
15	70	15	15	0	5.0	5.8	13.2	10.0	11.5	6.5	10.0	14.2
16	90	0	0	10	5.5	3.5			8.8	2.0		
17	90	0	0	10	6.8	2.8	6.5	6.5	10.2	2.8	6.5	7.8
18	80	0	0	20								
19	80	0	0	20	5.2	24.2	33.2		23.0	27.5	31.0	

(a) Values are total times (time in vacuum is 20 hr less).
(b) Readings incorrect for this position.

Results from Test Run 2 are summarized in Tables 6 and 7 and in Figs. 27 through 31.

The Ag-graphite compositions tested in Run 2 again behaved poorly, with results the same as those observed in Run 1. With both Ag-graphite compositions the brushes and rings were worn badly, early failures were experienced, and operation was noisy.

Results from the Ag-Mo-MoS$_2$ brush composites are not as consistent as from the Ag-Cu-MoS$_2$ ones, and trends are not as well defined. The most important point demonstrated, however, is that the Ag-Mo-MoS$_2$ composites were generally much noisier than the Ag-Cu-MoS$_2$ composites. The lowest noise obtained with the Ag-Mo-MoS$_2$ composites was, in fact, about 10-times that of the best Ag-Cu-MoS$_2$ brush composites. Some brush arcing was noted, which resulted in greater wear and outgassing loads. The composition 85 Ag $-$ 5 Mo $-$ 10 MoS$_2$ appeared to give the best overall performance, with low wear on both brushes and ring and about the lowest noise obtained with the Ag-Mo-MoS$_2$ composites. The composition 80 Ag $-$ 10 Mo $-$ 10 MoS$_2$ also gave low wear, but one brush broke off during installation so that no data were obtained with current flowing through the brushes. Although Mo contents of 15%, or more, generally resulted in bad ring wear and noisy operation, the composition 58 Ag $-$ 40 Mo $-$ 2 MoS$_2$ appears to be an exception. This composition also appears an exception to the general trend for wear to be high when the MoS$_2$ is 5% or less.

During fabrication of the Ag-Mo-MoS$_2$ composites, it was noted that those with low silver content were chalky and had to be ground to shape rather than machined.

Figure 27 shows Slip Ring Assembly 2 after testing. Twenty-three of the 24 brush/ring combinations were tested. The ring to the left of the one marked 18 in the photograph was not tested, so that the original ring conditions can be seen for comparison.

TABLE 6

RESULTS FOR OPERATION OF SLIP RING ASSEMBLY 2

Brush Composition (% wt)			Results
Ag	Mo	MoS$_2$	
95	5	0	One brush lost during first hour of operation, other brush slightly worn; ring slightly worn
93	5	2	One brush lost after 158 hr, other brush badly worn; ring worn
90	5	5	One brush lost after 181 hr, other brush badly worn; ring worn; operation quiet
85	5	10	Both brushes survived 500 hr operation with little wear; ring wear slight; operation generally quiet (3.5 mV at 15 hr, 2.5 mV at 378 hr and 730 cps)
80	5	15	Arcing occurred during first 0.5 hr of operation; one brush lost, other brush had only slight wear; ring was damaged by arcing
80	10	10	One brush broken during installation, other brush had only slight wear during operation; ring wear slight
85	15	0	Both brushes survived 500 hr operation with little wear; ring was worn; operation was noisy at start and quieted down to 2.2 mV at 378 hr
83	15	2	One brush lost within 100 hr of operation, other brush badly worn; ring badly worn and discolored
80	15	5	One brush lost within 100 hr of operation, other brush worn; ring badly worn
75	15	10	Both brushes survived 500 hr of operation with slight wear; ring worn; operation quiet, increasing during test to 3.3 mV at 378 hr
70	15	15	Both brushes broke off during installation; no data obtained
75	25	0	One brush lost after about 13 hr operation, other worn; ring worn

TABLE 6 (Continued)

Brush Composition (% wt)			Results
Ag	Mo	MoS$_2$	
70	25	5	One brush lost within 157 hr of operation, other brush had very little wear; ring worn
65	25	10	One brush lost during first hour of operation, other brush worn; ring worn
60	25	15	One brush lost within 253 hr of operation, other brush worn; ring worn
60	40	0	Arcing and one brush lost during first 9 hr of operation, other brush had very little wear; ring badly worn
58	40	2	Both brushes survived 500 hr operation with very little wear; ring was slightly worn; operation was generally quiet, with some noisy operation
55	40	5	One brush broken off during installation, other brush had little wear; ring was worn
50	40	10	One brush lost within 157 hr of operation, other brush had little wear; ring had very little wear; operation was very noisy
45	40	15	One brush lost within 157 hr of operation, other brush had little wear; ring slightly worn
90 — 10 graphite			Arcing; current discontinued after 91 hr; both brushes and ring badly worn
80 — 20 graphite			One brush lost after about 85 hr of operation, other brush badly worn; ring worn

TABLE 7
BRUSH AND RING WEAR ON SLIP RING ASSEMBLY 2

| Brush Position | Thickness (in.) | | | | | | | | | | | Ring Wear | Time to failure in vacuum (hr) |
| | Composition (% wt) | | | | Initial | | Final | | Wear (in.) | | | | |
	Ag	Mo	MoS$_2$	Graphite	Brush 1[a]	Brush 2[b]	Brush 1	Brush 2	Brush 1	Brush 2	Average		
16	95	5	0	0	0.109	0.109	M[c]	0.150		0.004	0.004	Light	< 1
17	93	5	2	0	0.104	0.100	M	0.042		0.058	0.058	Moderate	158
19	90	5	5	0	0.094	0.107	M	0.059		0.048	0.048	Moderate	181
20	85	5	10	0	0.095	0.102	0.092	0.100	0.003	0.002	0.002	Light	(d)
22	80	5	15	0	0.102	0.107	M	0.103		0.004	0.004	Arcing	<0.5
2	80	10	10	0	0.111	0.110	0.108	M	0.003		0.003	Light	0
12	85	15	0	0	0.117	0.117	0.116	0.115	0.001	0.002	0.002	Moderate	(d)
3	83	15	2	0	0.108	0.111	M	0.049		0.062	0.062	Severe	<100
4	80	15	5	0	0.113	0.105	M	0.064		0.041	0.041	Severe	<100
7	75	15	10	0	0.095	0.107	0.074	0.083	0.021	0.024	0.022	Moderate	(d)
1	70	15	15	0	0.101	0.104	M	M				Light	0
11	75	25	0	0	0.108	0.115	M	0.055		0.060	0.060	Moderate	13
13	73	25	2	0	0.115	0.111	M	0.049		0.062	0.062	Severe	< 1
14	70	25	5	0	0.110	0.113	M	0.103		0.010	0.010	Moderate	<157
15	65	25	10	0	0.110	0.107	0.045	M	0.065		0.065	Moderate	< 1
10	60	25	15	0	0.107	0.109	M	0.049		0.060	0.060	Moderate	<253
6	60	40	0	0	0.113	0.112	M	0.079		0.033	0.033	Severe	9
21	58	40	2	0	0.112	0.108	0.111	0.104	0.001	0.004	0.002	Light	(d)
5	55	40	5	0	0.117	0.111	0.115	M	0.002		0.002	Moderate	0
8	50	40	10	0	0.097	0.108	M	0.104		0.004	0.004	Light	<157
9	45	40	15	0	0.102	0.099	0.100	M	0.002		0.002	Light	<157
23	90	0	0	10	0.094	0.100	0.023	0.047	0.071	0.053	0.062	Severe	91
24	80	0	0	20	0.090	0.090	0.050	M	0.040		0.040	Severe	85

(a) Brush 1 – brush without thermocouple
(b) Brush 2 – brush with thermocouple attached to leaf spring holding it
(c) M – missing (broke off during test; no final measurement obtained)
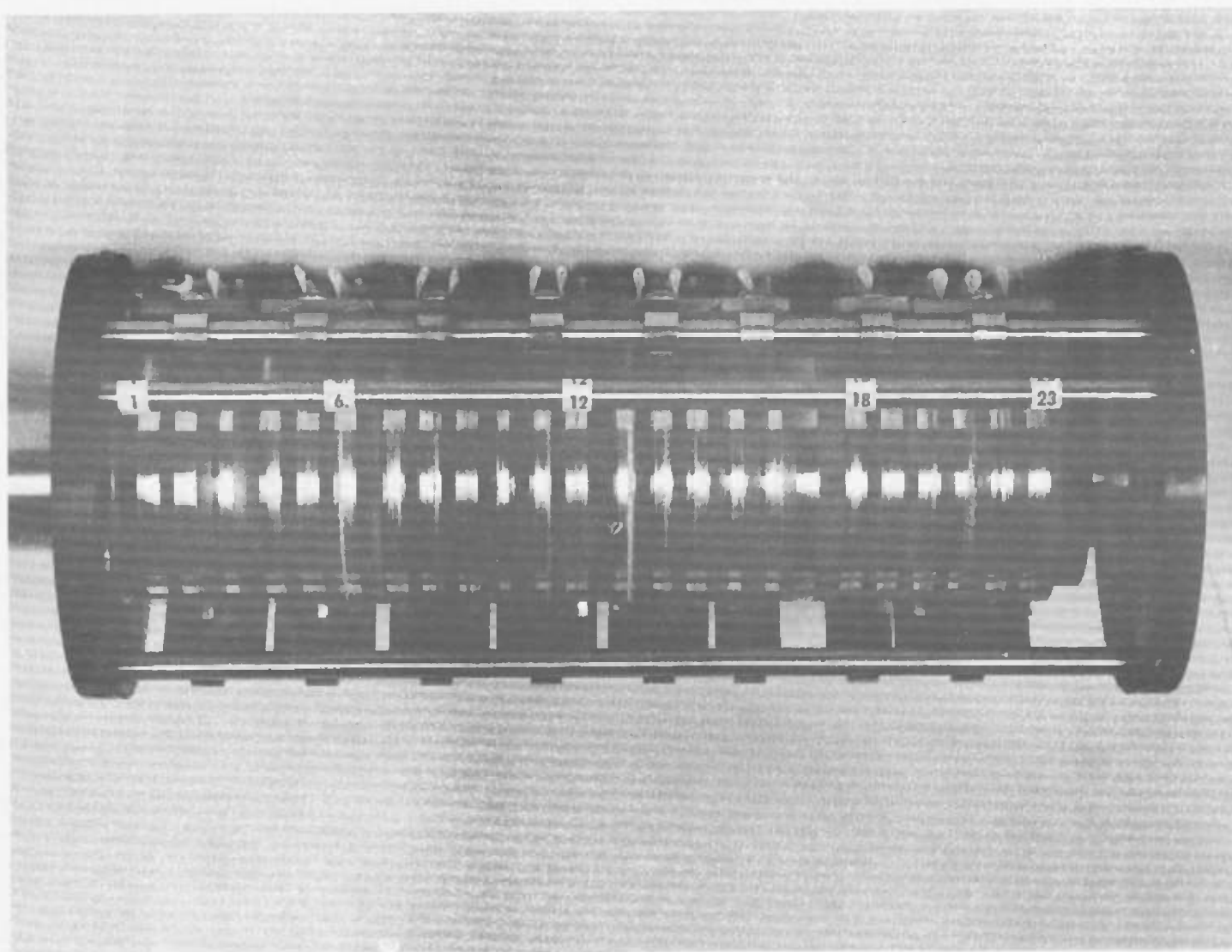(d) No failure; both brushes operated for full test time

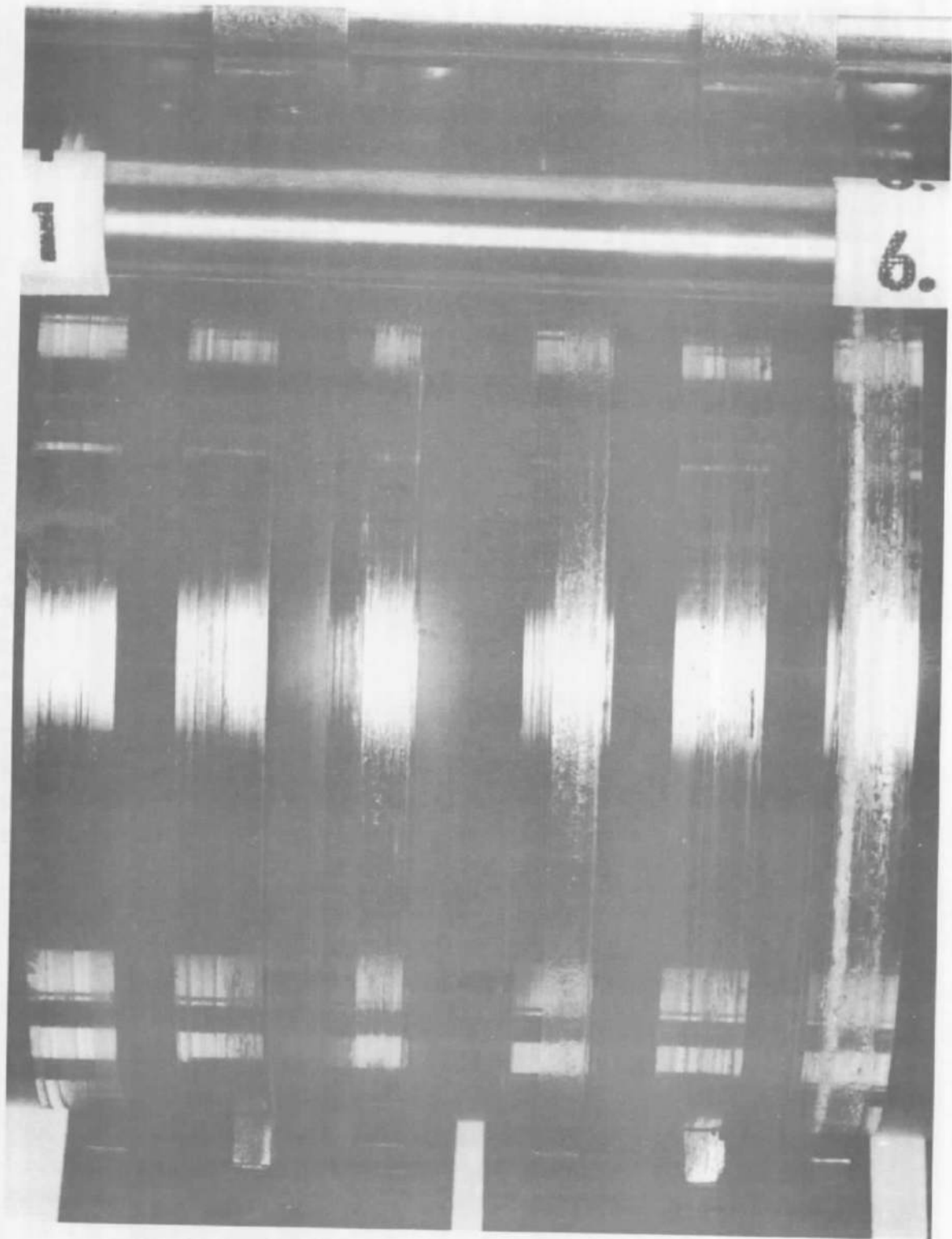Fig. 27 Slip Ring Assembly 2 After Testing

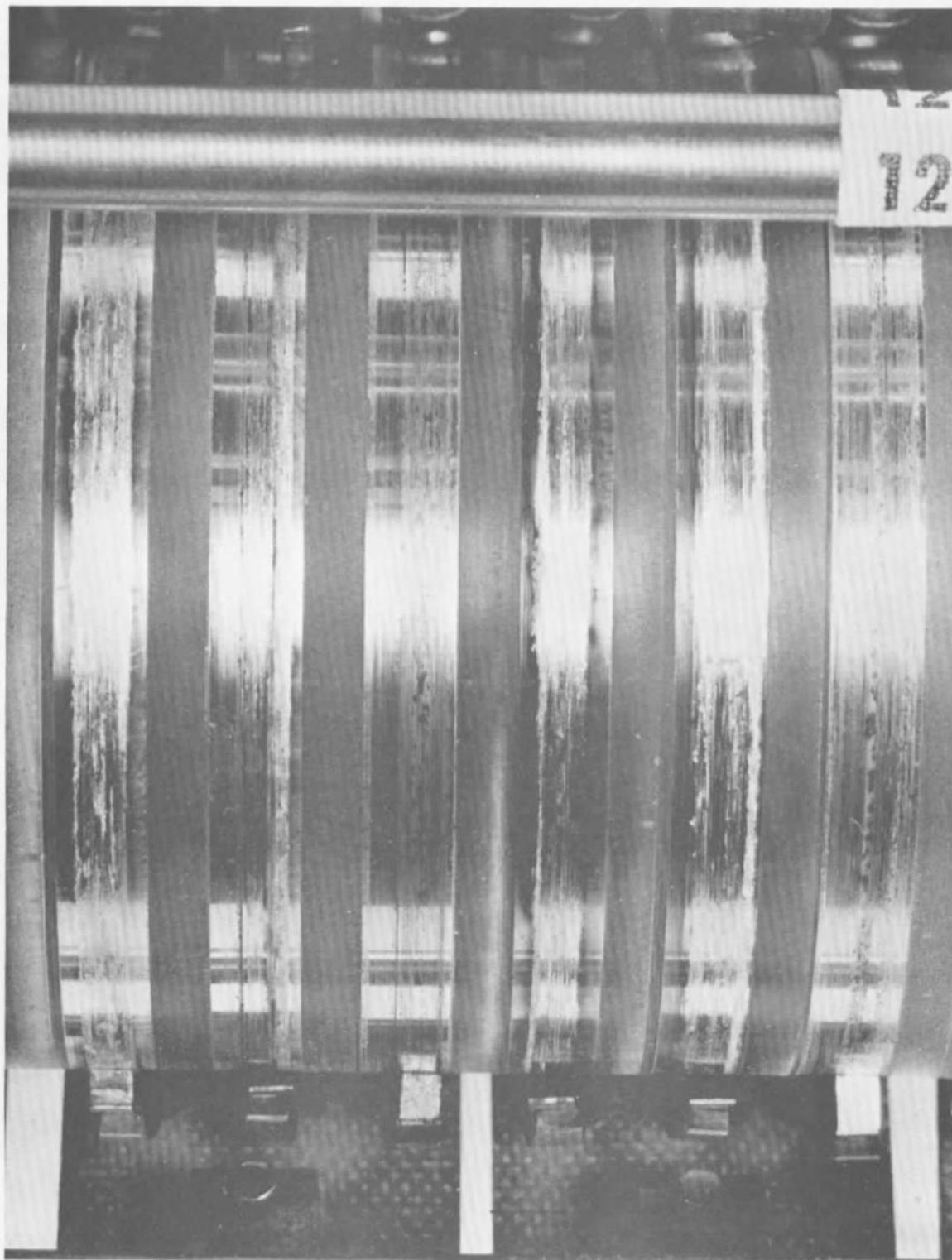Fig. 28 Detail at Positions 1 Through 6 of Assembly 2 After Testing

Fig. 29 Detail at Positions 7 Through 12 of Assembly 2 After Testing
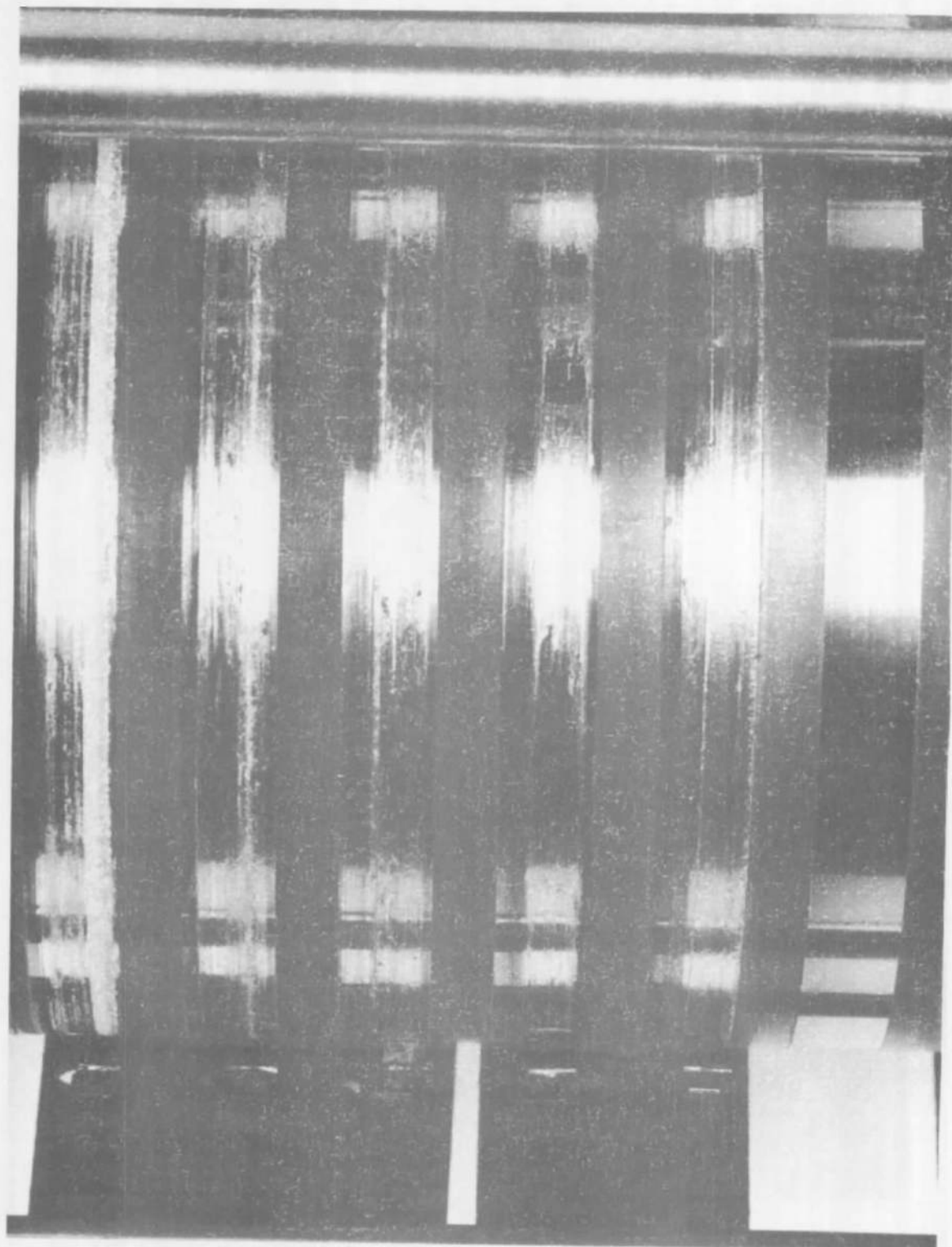
Fig. 30 Detail at Positions 13 Through 17 and Unnumbered Position of Assembly 2 After Testing
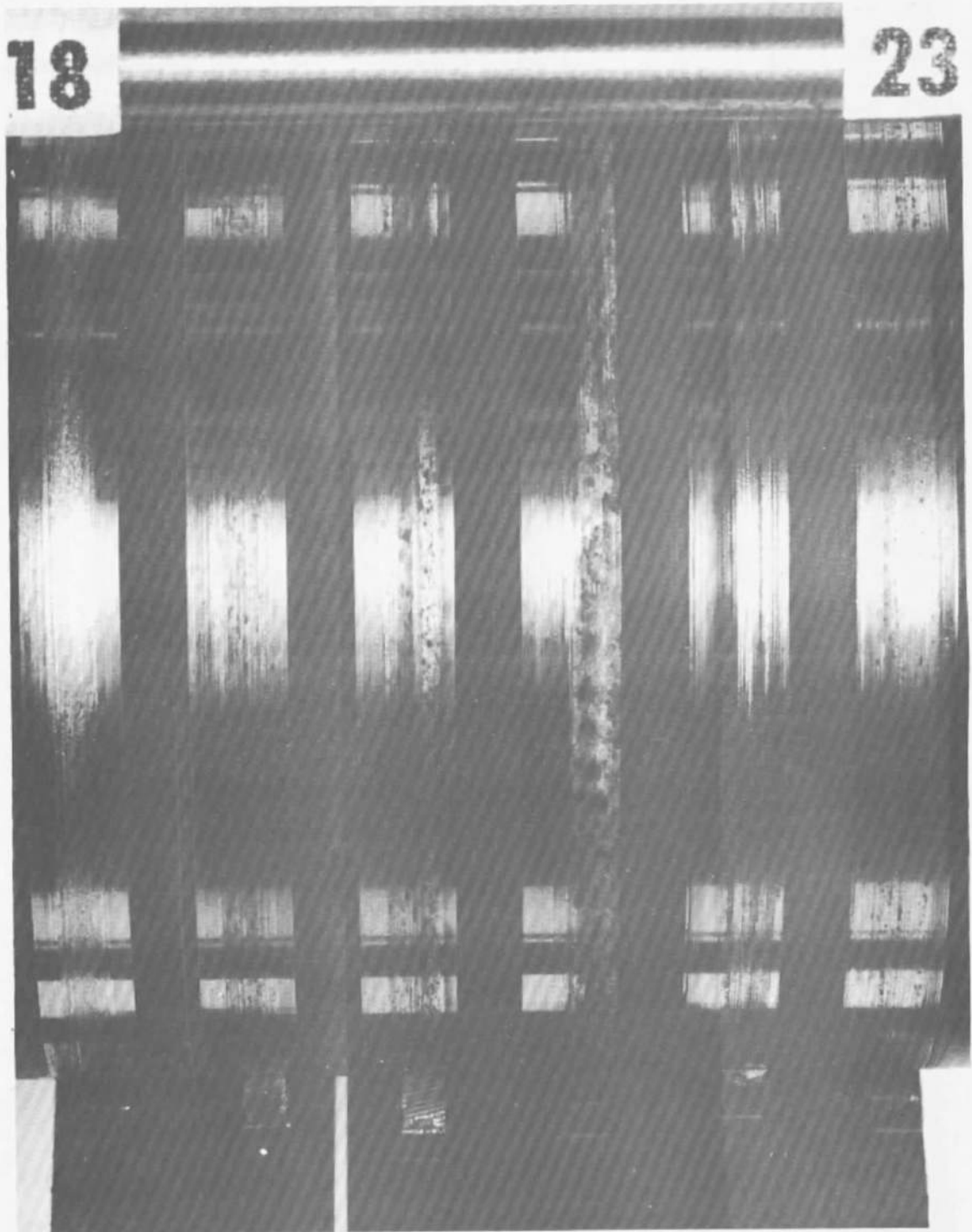
Fig. 31 Detail at Positions 18 Through 23 of Assembly 2 After Testing

One can note that the following brushes have failed and are broken off the supporting leaf springs at the bottom of the assembly: 1, 3, 4, 6, 8, 10, 11, 13, 14, 16, 17, 18, and 21. Additional brushes were broken off on the opposite side (not visible in Fig. 27) at Positions 1, 2, 5, 9, 15, and 23. Only at Positions 7, 12, 19, and 20 did both brushes operate for the full 500 hr of testing. The following brushes are seen to have suffered heavy wear (see Figs. 28, 29, and 30): 15, 22, and 23. Brush compositions were as follows:

Position	Composition (% wt)			
	Ag	Mo	MoS_2	Graphite
1	70	15	15	0
2	80	10	10	0
3	83	15	2	0
4	80	15	5	0
5	55	40	5	0
6	60	40	0	0
7	75	15	10	0
8	50	40	10	0
9	45	40	15	0
10	60	25	15	0
11	75	25	0	0
12	85	15	0	0
13	73	25	2	0
14	70	25	5	0
15	65	25	10	0
16	95	5	0	0
17	93	5	2	0
Unnumbered	No Brushes			
18	90	5	5	0
19	85	5	10	0
20	58	40	2	0
21	80	5	15	0
22	90	0	0	10
23	80	0	0	20

Figure 28 shows in detail the conditions at Positions 1 through 6. Both brushes broke off at Position 1, and ring wear was nil. One brush broke off at Position 2, and ring wear was nil. One brush was lost from Positions 3, 4, and 5 within 100 hr of operation, so that the brushes were not carrying current during the major part of the 500-hr run in vacuum; nevertheless, all four rings are worn, particularly 3, 4, and 6. It is significant that these four brush compositions had 15% or more of Mo and 5% or less of MoS_2, whereas Brush 2 had 10% Mo and 10% MoS_2.

Figure 29 shows the conditions at Positions 7 through 12. Both brushes at Positions 7 and 12 operated for the full 500 hr of testing; one brush from each of the four other positions failed at various times during testing. The four brushes that failed represented high Mo contents (25 and 40%), whereas the brush compositions that completed the test had 15% Mo. All of the rings were worn to some degree.

Figure 30 shows the conditions at Positions 13 through 17 and the unnumbered position (no brushes). At all of these positions, rings and brushes were worn to some degree. These brush compositions represented low MoS_2 contents and/or high Mo contents.

Figure 31 shows the conditions at Positions 18 through 23. Brushes of two silver-graphite compositions at Positions 22 and 23 were badly worn, and their rings were also worn. Brush 18 is a low MoS_2 content (5%), and both brush and ring at this position were worn. Brush 19 is 5% Mo, 10% MoS_2, and as expected from its composition, showed good performance; both brushes ran the full 500 hr of testing, and both brushes and ring showed relatively small amounts of wear. Brush 20 is an anomaly; it has a high Mo, low MoS_2 content (40% Mo, 2% MoS_2), yet showed good performance, with both brushes running the full 500 hr of testing and both brushes and ring showing relatively small wear. Position 21 experienced some arcing and an early failure (less than 0.5 hr of operation) of one brush. It appears that this brush might have been improperly mounted and was not riding properly on the ring. The ring was damaged by the arcing, as can be seen in Fig. 31. The second brush at Position 21 suffered only slight wear. The composition of

Brush 21 (5% Mo, 15% MoS_2) should have given good performance, based on trends noted with the other brush compositions, and the early failure may in fact have been due to improper installation rather than to the material itself.

Because of the comparatively poor performance of the Ag-Mo-MoS_2 composites and the good performance of Ag-Cu-MoS_2 composites, no further tests were performed with Ag-Mo-MoS_2 composites. Subsequent tests were directed toward optimizing the Ag-Cu-MoS_2 composites, verifying their performance, establishing their reproducibility, and exploring the effects of other operating conditions.

Test Run 3 (LMSC)

Test Run 3 contained 24 pairs of brushes of Ag-Cu-MoS_2 composites; no Ag-graphite brushes were tested. The copper content was maintained at 0, 2.5, and 5%; the MoS_2 content, at 7.5, 10, 12.5, and 15%. These compositions cover the range in which best results had been obtained in Test Run 1, and the compositional changes were made in smaller steps in order to define the optimum composition more exactly. Brushes were prepared from two batches of material; Batch 1 had been prepared at the same time the composites for brushes tested in Run 1 were prepared, and Batch 2 was prepared several months later. The two batches of material were tested at the same time in order to check the reproducibility of preparation. Also, testing material from Batch 1 a second time provided a check on the reproducibility of testing. Although most of the brushes operated against silver rings, eight pairs of brushes operated against gold rings so that the effect of ring material could be evaluated.

Assembly 3 was run-in for 20 hr in air and then operated for 630 hr in vacuum (7×10^{-6} Torr initially, dropping to 1×10^{-6} Torr at the end of the test). All brushes on this unit completed the full time of testing without a single failure. Ring and brush wear was low on practically all circuits. All brushes operated at nearly 70°F throughout the entire test. For one period of approximately 10 hr (after approximately 10 hr of operation in vacuum), the slip rings were not rotated and current was conducted through the circuits; no evidence of welding or burning from this condition of operation was observed.

Table 8 and Figs. 32 through 36 summarize the pertinent data and observations on brush and ring wear. Within the range of scatter, brushes from Batch 1 gave the same performance in both Assembly 1 and 3. Brushes with 10% MoS_2 from the two batches of material gave good reproducibility, whereas those with 15% MoS_2 from Batch 2 suffered greater wear than those from Batch 1.

Gold rings and silver rings wore about equally, but gold rings usually caused greater brush wear than silver rings.

At each copper level, increasing the MoS_2 content from 7.5 to 15% tended to increase brush wear, as illustrated in Fig. 37. This effect was most pronounced with no copper. Although brushes containing only 7.5 or 10% MoS_2 consistently suffered low wear (i.e., 0.010 in., or less), they caused greater ring wear, and the higher MoS_2 contents (i.e., 12.5 and 15%) are therefore preferable.

Brushes containing 12.5 and 15% MoS_2 and no copper showed extreme variability in brush wear. It was also observed that these brush materials, as well as the one containing 10% MoS_2 and no copper, were also the most difficult to machine properly, tending to crumble. These observations indicate that some copper is desirable, and it appears from the other data that 2.5% is adequate.

Noise level showed a general trend to increase during operation, but in all cases except one, the peak noise was held at 1.0 mV or lower, as measured on the oscilloscope. The sole exception was near the end of the run with 90 Ag − 2.5 Cu − 7.5 MoS_2 brushes (Ring 17), for which peak readings up to 4 mV were observed. This particular brush-ring combination also showed the worst ring wear. Figure 38 shows peak and average noise measurements for Ag-Cu-MoS_2 brushes from Batch 2 operated against silver rings after 50 and 604 hr of operation. These data illustrate the general trend for the noise to increase with the time of operation, as noted above. The relatively high noise after 604 hr for the 90 Ag − 2.5 Cu − 7.5 MoS_2 and 87.5 Ag − 5 Cu − 7.5 MoS_2 brushes indicate that 7.5% MoS_2 is less than desirable, although this is not confirmed by the noise measurements on the 92.5 Ag − 0 Cu − 7.5 MoS_2. Generally, MoS_2 contents of 10, 12.5, and 15% gave noise levels on the order of 0.5 mV with no significant variation with the content of either MoS_2 or Cu.

TABLE 8

BRUSH AND RING WEAR ON SLIP RING ASSEMBLY 3

Brush Position	Composition (% wt)			Batch	Ring Material	Wear (in.)			Ring Wear
	Ag	Cu	MoS$_2$			Brush 1	Brush 2	Average	
13	92.5	0	7.5	2	Ag	0.004	0.006	0.005	Severe
1	90	0	10	1	Ag	0.008	0.0065	0.007	Good
14	90	0	10	2	Ag	0.010	0.009	0.0095	Intermediate
5	90	0	10	1	Au	0.0025	0.0075	0.005	Good
9	90	0	10	2	Au	0	0.0115	0.0058	Good
15	87.5	0	12.5	2	Ag	0.002	0.011	0.0065	Good
2	85	0	15	1	Ag	0.007	0.0025	0.005	Good
16	85	0	15	2	Ag	0.0215	0.011	0.0162	Intermediate
6	85	0	15	1	Au	0.0185	0.010	0.014	Good
10	85	0	15	2	Au	0.025	0.025	0.025	Good
17	90	2.5	7.5	2	Ag	0.005	0.005	0.005	Worst
18	87.5	2.5	10	2	Ag	0.005	0.010	0.0075	Intermediate
19	85	2.5	12.5	2	Ag	0.0095	0.007	0.0082	Good
20	82.5	2.5	15	2	Ag	0.007	0.0075	0.007	Good
21	87.5	5	7.5	2	Ag	0.010	0.005	0.0075	Intermediate
3	85	5	10	1	Ag	0.005	0.006	0.0055	Intermediate
22	85	5	10	2	Ag	0.0085	0.0065	0.0075	Good
7	85	5	10	1	Au	0.0105	0.011	0.011	Good
11	85	5	10	2	Au	0.0135	0.014	0.0138	Good
23	82.5	5	12.5	2	Ag	0.0095	0.010	0.010	Good
4	80	5	15	1	Ag	0.002	0.005	0.0035	Intermediate
24	80	5	15	2	Ag	0.0135	0.0105	0.012	Good
8	80	5	15	1	Au	0.009	0.012	0.0105	Good
12	80	5	15	2	Au	0.0275	0.019	0.0232	Good

Fig. 32 Slip Ring Assembly 3 After Testing

Fig. 33 Detail at Ring 1 Through 6 of Assembly After Testing
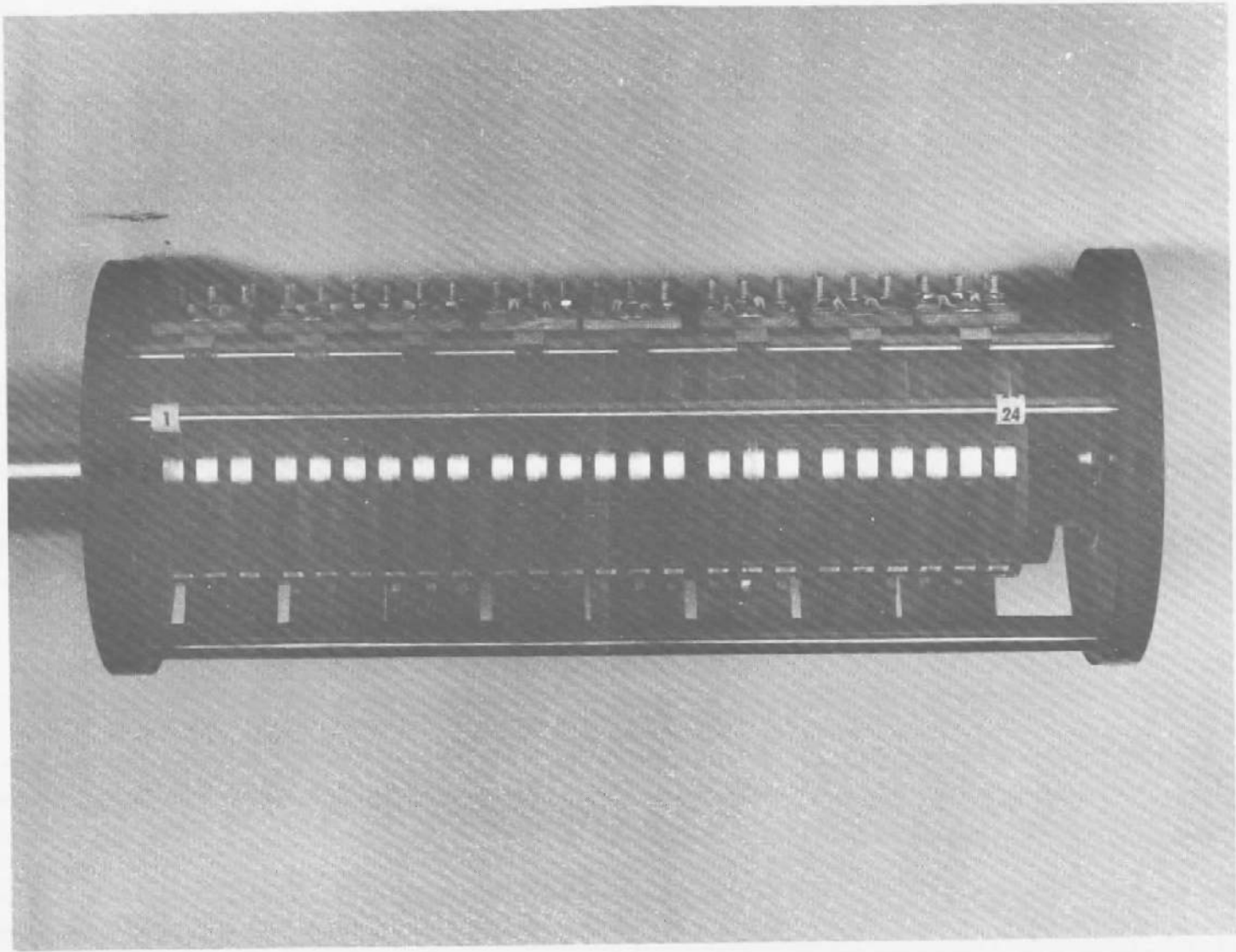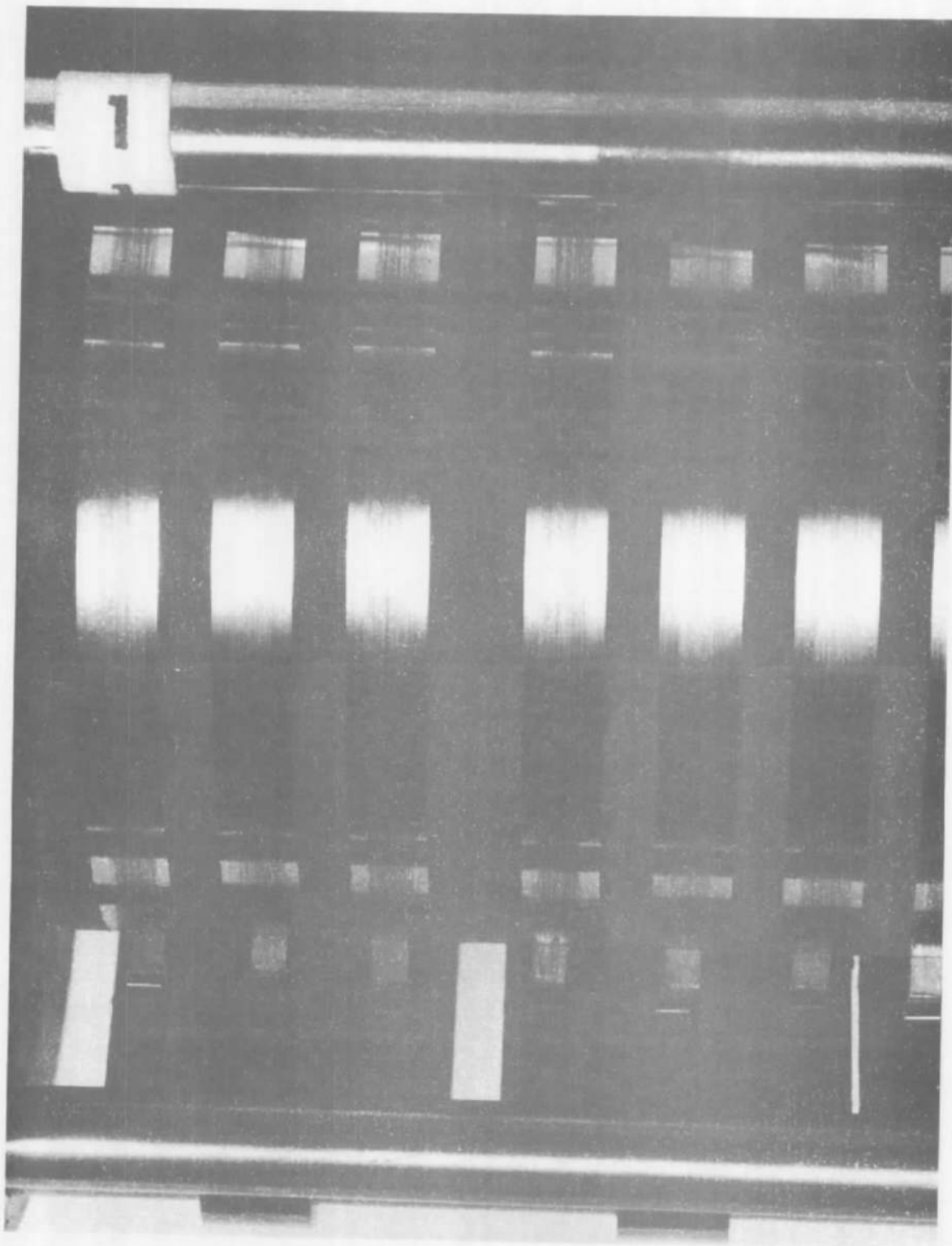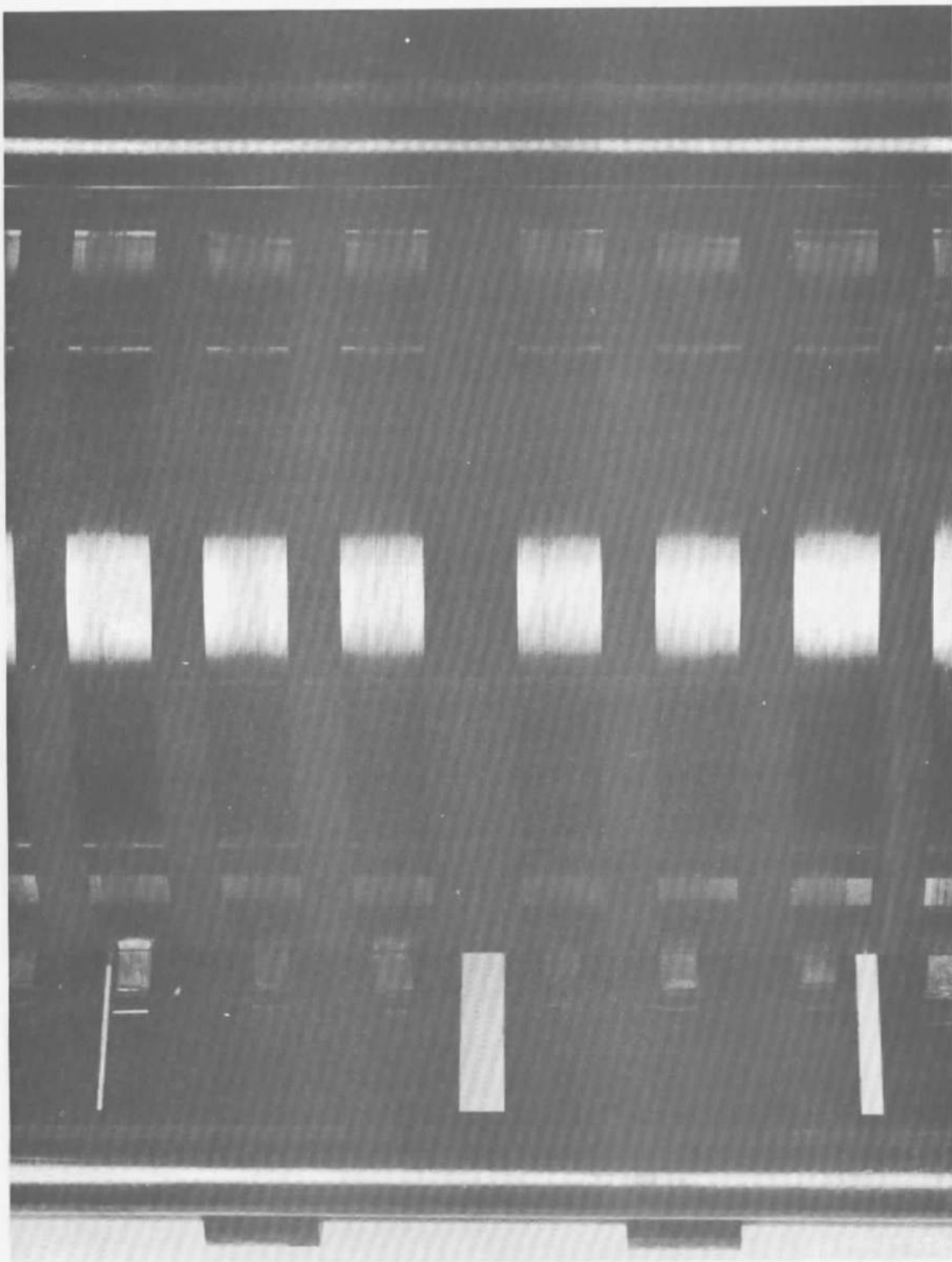
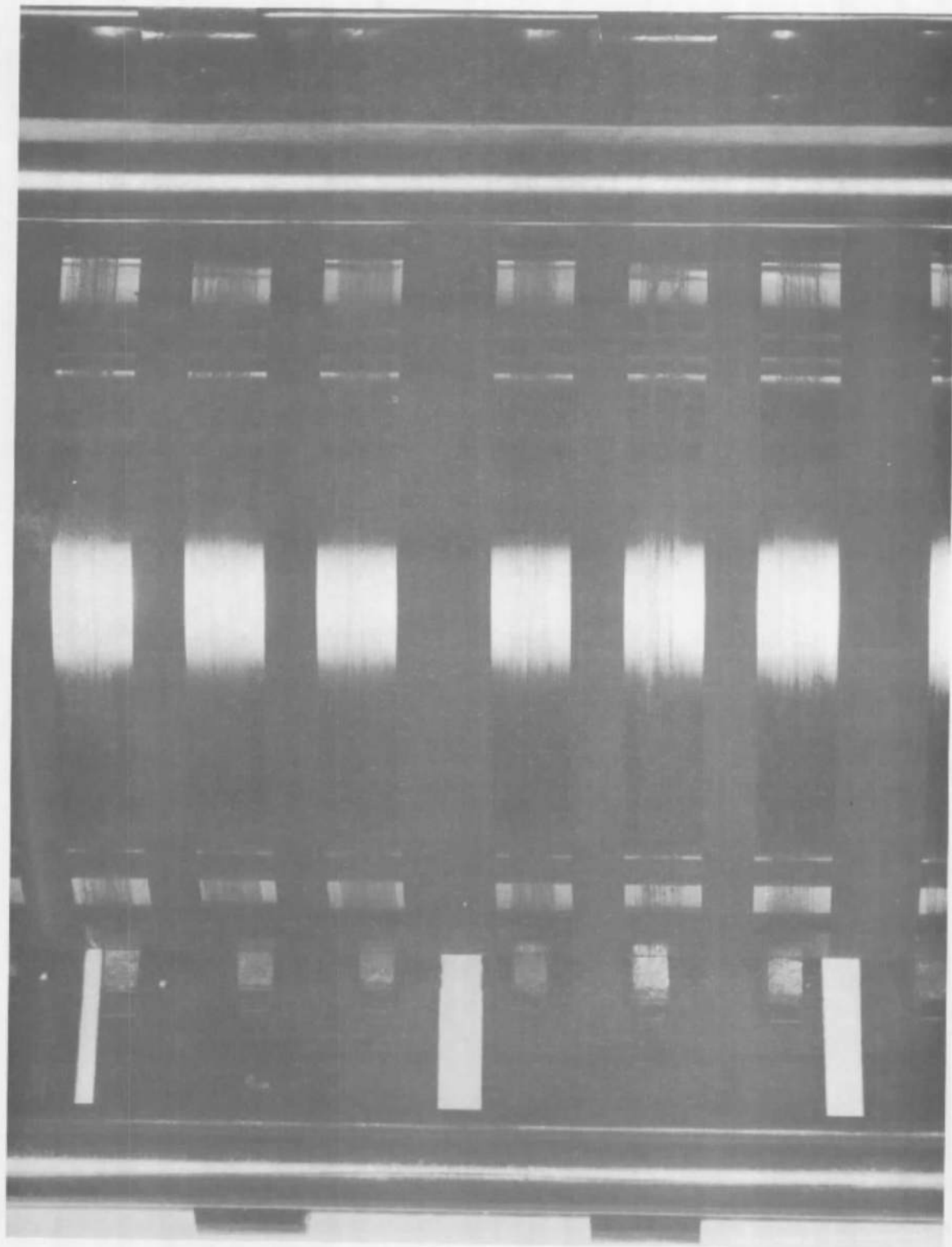Fig. 34 Detail at Ring 7 Through 12 of Assembly 3 After Testing

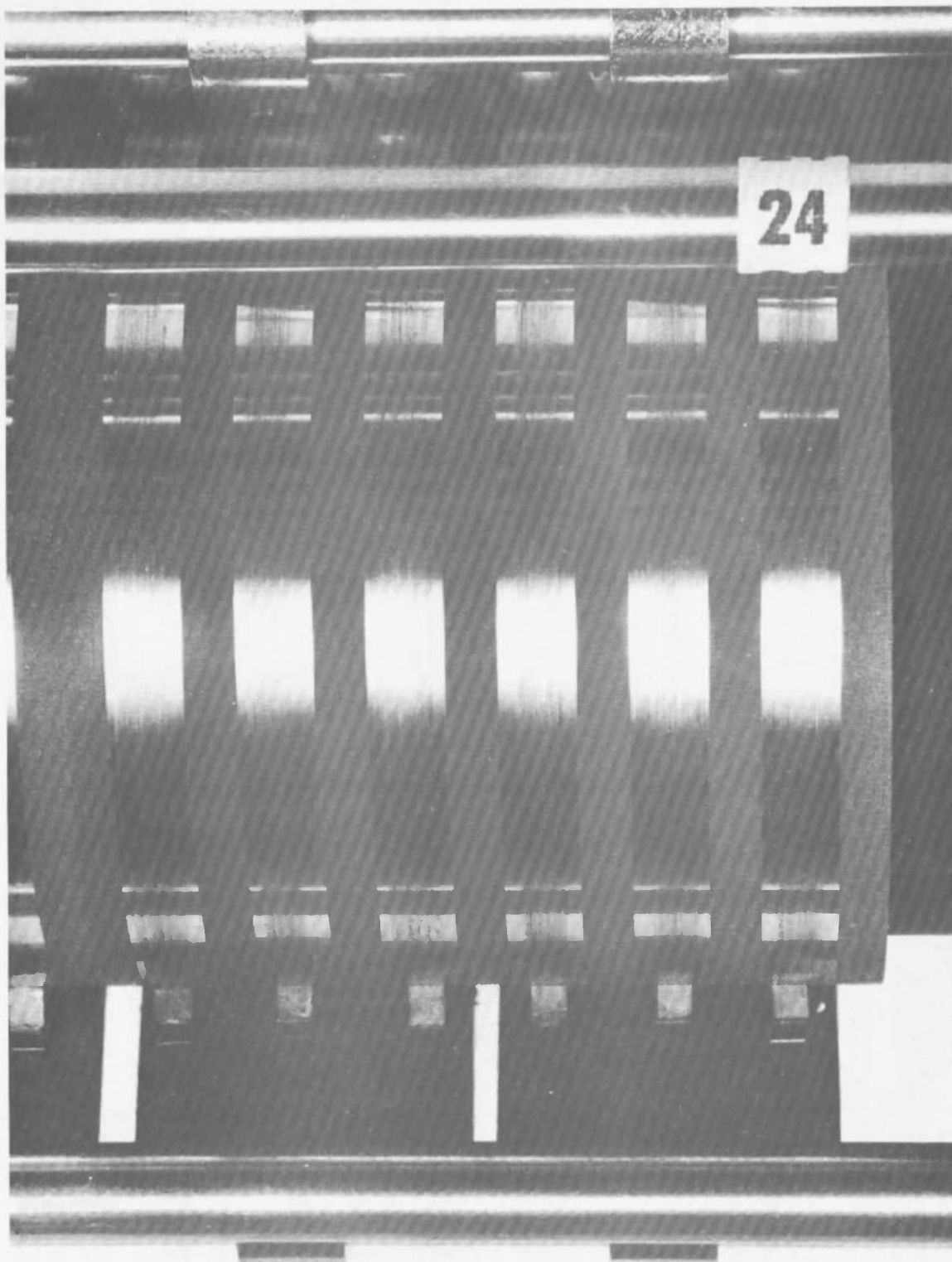Fig. 35 Detail at Ring 13 Through 18 of Assembly 3 After Testing

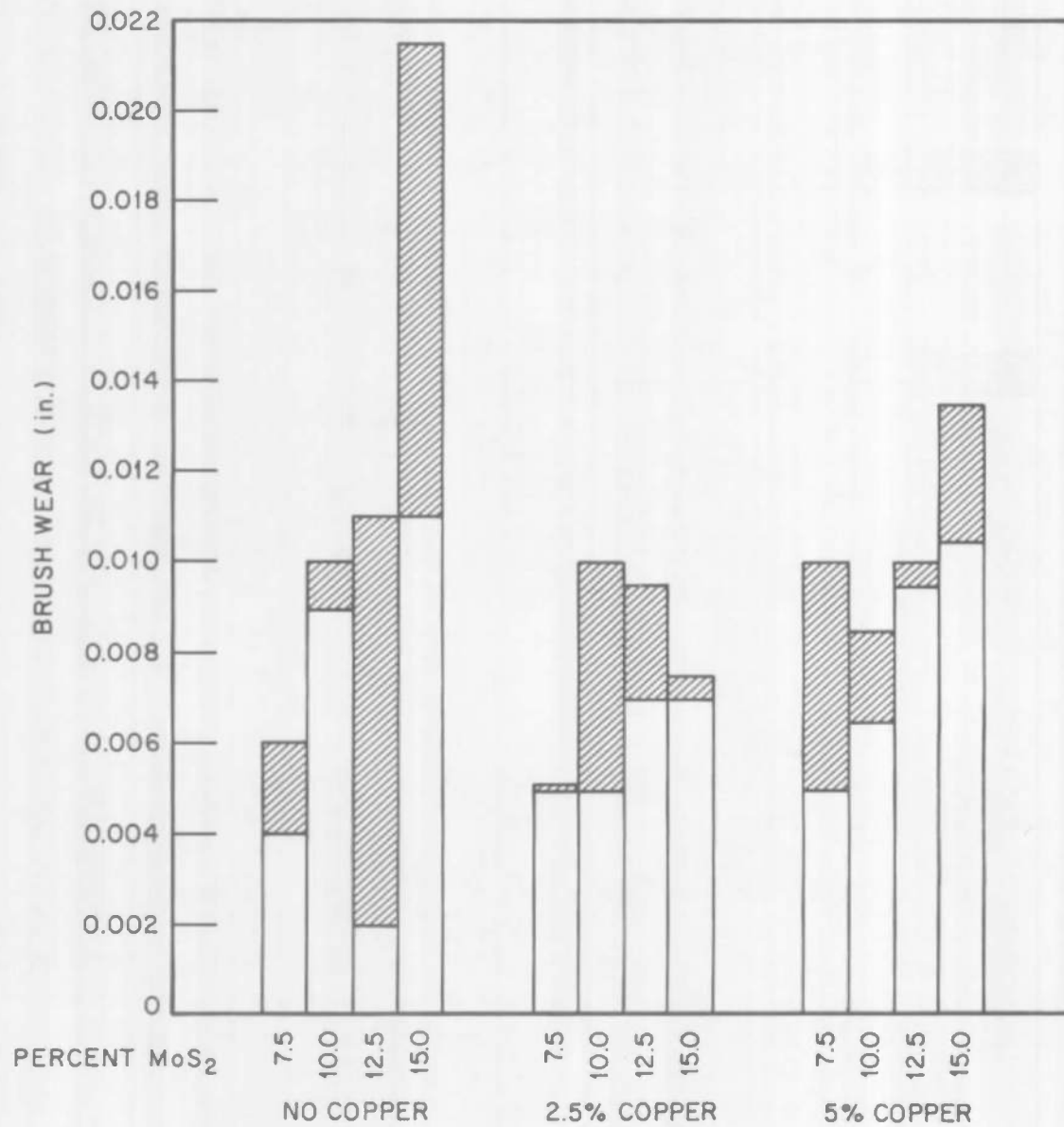Fig. 36 Detail at Ring 19 Through 24 of Assembly 3 After Testing

Fig. 37 Brush Wear of Ag-Cu-MoS$_2$ Composites From Botch 2 Against Silver Rings in Assembly 3

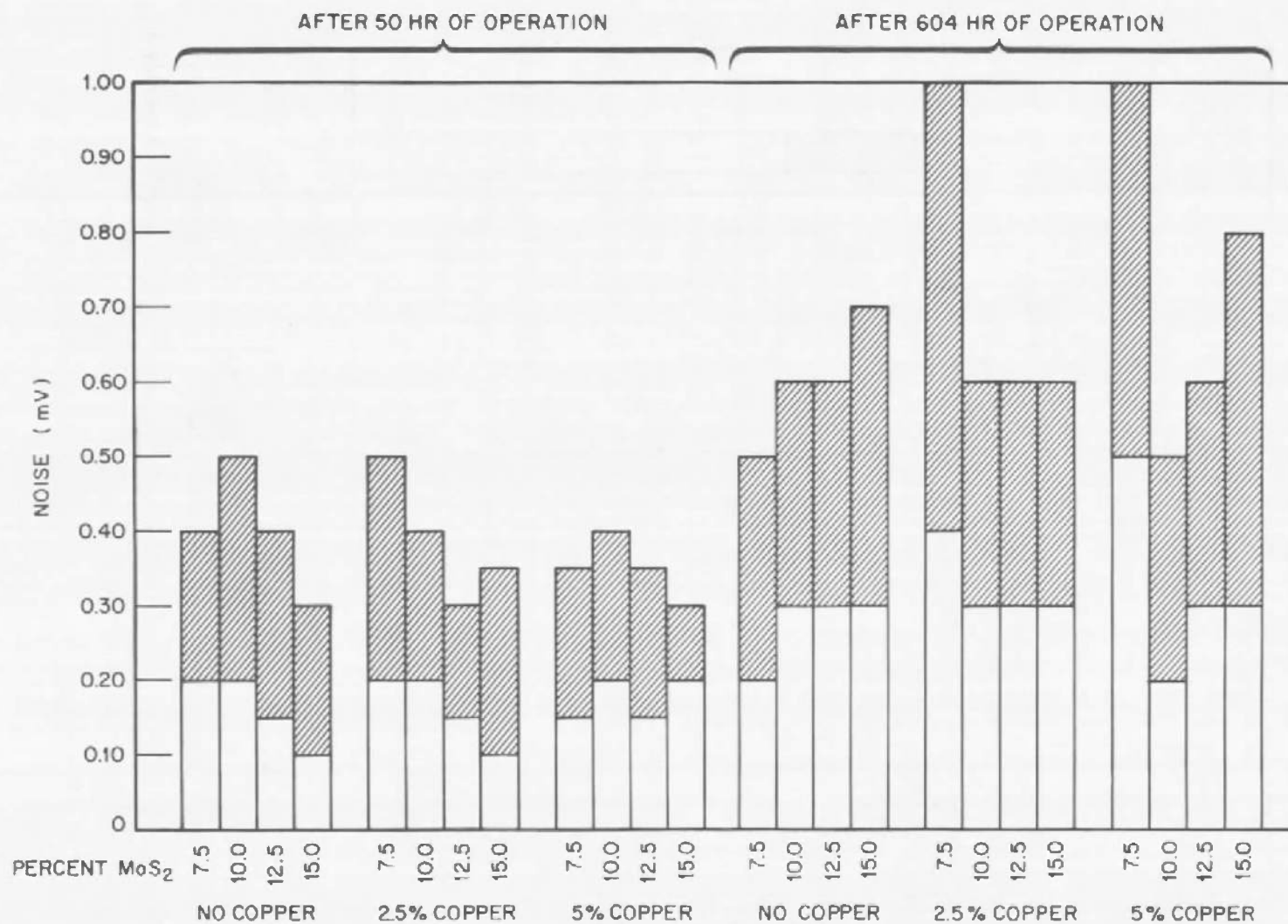Fig. 38 Noise Measurements for Ag-Cu-MoS₂ Brushes From Batch 2 Against Silver Rings in Assembly 3

Test Run 4 (LMSC).

Test Run 4 contained 24 pairs of brushes with $Ag\text{-}Cu\text{-}MoS_2$ composites; no Ag-graphite brushes were tested. All brushes were operated against silver rings, since results from Test Run 3 had indicated no benefits from gold rings. Most of the brushes contained 2.5% Cu and either 12.5 or 15% MoS_2, in accordance with earlier observations that these compositions were about optimum. Two pairs of brushes with no copper and six pairs with 5% copper were also tested to verify this conclusion. Brushes were operated at contact pressures of 6 and 10 psi to see how this affected performance. Half of the brushes were mounted on the same type holder as was used in the three previous runs, whereas the other half of the brushes were mounted on a special type of holder intended to provide a more accurate setting of the brush pressure and a more nearly constant brush pressure during operation. Figure 39 shows the modified brush assembly.

Assembly 4 was run-in for 20 hr in air and then operated for 847 hr in vacuum. Outgassing loads from the modified brush assembly caused some difficulty in reaching the low vacuum level for testing. The pressure during the first 50 hr of vacuum testing was above 1×10^{-5} Torr, and it then gradually improved to 2×10^{-6} Torr at the end of 847 hr.

Performance of Slip Ring Assembly 4 was generally excellent, with relatively low wear on the rings and brushes and low electrical noise. Rings were lightly worn, with Rings 19 and 20 being the only two rings on which wear was bad. One brush on each of three rings was broken off during the test (Rings 10, 13, and 22); both brushes on one ring (Ring 24) were broken off.

Table 9 summarizes measurements on the wear of brushes and rings for Slip Ring Assembly 4. Results indicate that a composition of 82.5 to 85% silver, 2.5% copper, and 15.0% molybdenum disulfide is about the optimum brush composition. Reducing the amount of molybdenum disulfide from 15 to 12.5% (and correspondingly increasing the silver content from 82.5 to 85.0%) did not significantly alter the wear characteristics of the brushes. Copper contents as high as 5% with molybdenum disulfide contents at 10% were not as good as the above compositions
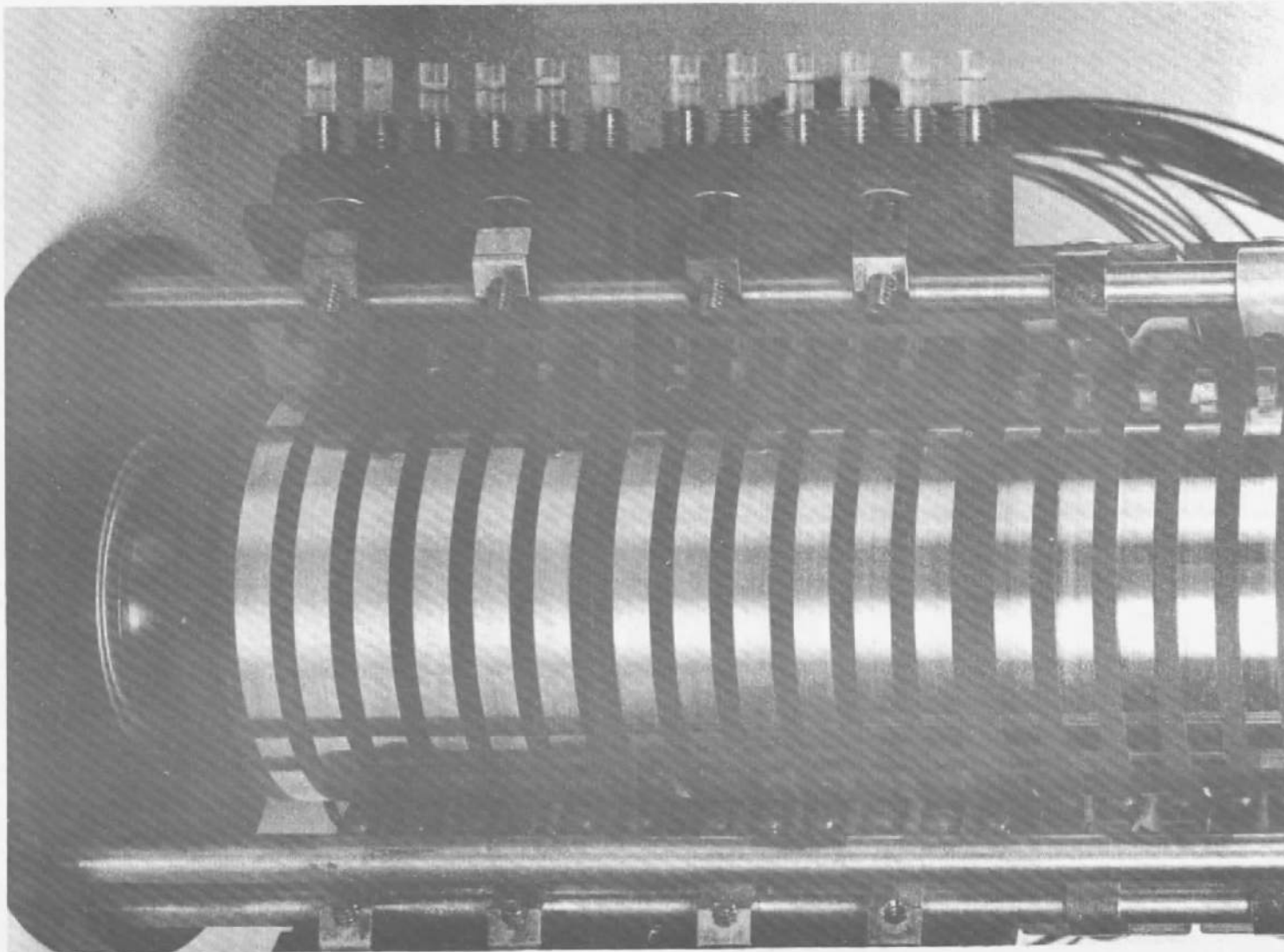
Fig. 39 Slip Ring Assembly 4 Before Testing, Showing Detail of Modified Brush Holder

TABLE 9

BRUSH AND RING WEAR ON SLIP RING ASSEMBLY 4

Brush Position	Composition (% wt)			Type of Brush Holder	Brush Pressure (psi)	Thickness (in.)				Wear (in.)			Ring Wear
						Initial		Final					
	Ag	Cu	MoS$_2$			Brush 1[a]	Brush 2[b]	Brush 1	Brush 2	Brush 1	Brush 2	Average	
1	82.5	2.5	15.0	1	10	0.088	0.087	0.074	0.078	0.014	0.014	0.0115	Light
2	82.5	2.5	15.0	1	10	0.088	0.065	0.079	0.076	0.009	0.009	0.0090	Light
3	82.5	2.5	15.0	1	6	0.107	0.090	0.096	0.093	0.011	0.006	0.0085	Light
4	82.5	2.5	15.0	1	6	0.087	0.099	0.076	0.087	0.011	0.012	0.0115	Light
5	85.0	2.5	12.5	1	10	0.090	0.097	0.080	0.087	0.010	0.010	0.0100	Light
6	85.0	2.5	12.5	1	10	0.096	0.092	0.088	0.087	0.008	0.005	0.0065	Light
7	85.0	2.5	12.5	1	10	0.082	0.108	0.070	0.098	0.012	0.010	0.0110	Light
8	85.0	5.0	10.0	1	10	0.066	0.094	0.082	0.087	0.004	0.007	0.0055	Light
9	82.5	2.5	15.0	1	10	0.097	0.092	0.083	0.085	0.014	0.007	0.0105	Light
10	80.0	5.0	15.0	1	10	0.076	0.070	M[c]	0.052		0.018	0.018	Light
11	85.0	0.0	15.0	1	10	0.072	0.053	0.0625	0.045	0.0095	0.008	0.0088	Light
12	85.0	0.0	15.0	1	10	0.063	0.063	0.0575	0.053	0.0055	0.010	0.0078	Light
13	82.5	2.5	15.0	2	10	0.113	0.098	M	0.086		0.012	0.012	Light
14	82.5	2.5	15.0	2	10	0.109	0.120	0.084	0.100	0.025	0.020	0.0225	Light
15	82.5	2.5	15.0	2	6	0.112	0.095	0.094	0.084	0.018	0.011	0.0145	Light
16	82.5	2.5	15.0	2	6	0.115	0.114	0.094	0.093	0.021	0.021	0.0210	Light
17	85.0	2.5	12.5	2	10	0.113	0.120	0.090	0.092	0.023	0.028	0.0255	Light
18	85.0	2.5	12.5	2	10	0.107	0.097	0.102	0.088	0.005	0.009	0.0070	Light
19	85.0	5.0	10.0	2	6	0.120	0.096	0.108	0.098	0.012	0.007	0.0095	Bad
20	85.0	5.0	10.0	2	6	0.085	0.078	0.080	0.076	0.005	0.002	0.0035	Bad
21	80.0	5.0	15.0	2	6	0.085	0.087	0.068	0.077	0.017	0.010	0.0135	Light
22	80.0	5.0	15.0	2	6	0.089	0.093	M	0.076		0.015	0.0150	Light
23	85.0	2.5	12.5	2	6	0.117	0.110	0.104	0.090	0.013	0.020	0.0165	Light
24	85.0	2.5	12.5	2	6	0.115	0.097	M	M				Light

(a) Brush 1 – brush without thermocouple
(b) Brush 2 – brush with thermocouple
(c) M – missing (broke off during test; no final measurement obtained)

because of increased ring wear, although brush wear was good. It may be possible to reduce the copper content below 2.5% without significantly lessening the resistance of the brushes to wear. Reproducibility from one batch of material to the next appears good. Reducing the brush pressure from 10 to 6 psi has had no effect on the brush wear within the limit of experimental scatter. If average values are taken, brush wear appears about 25% greater at 6 psi than at 10 psi, but this difference does not appear statistically significant.

Table 10 summarizes data on the contact resistance and noise level at the end of the test run (i.e., after 847 hr of operation in vacuum). Contact resistance was on the order of 10 mΩ, and noise level was on the order of 0.10 mV average and 0.20 mV peak. Brushes 19 and 20 had higher resistances and noise levels than the others and, as indicated in Table 9, also caused the worst ring wear; these brushes had higher contents of copper and lower contents of molybdenum disulfide, and their performance verifies earlier observations and conclusions that copper content should be kept below 5% and MoS_2 above 10%. Brush noise remained fairly constant on all brushes throughout the test, with a reduction by a factor of 4 in average noise and a factor of 6 in peak noise in a few cases during the test. Figure 40, for example, shows noise spectrum traces on Brush 1 at various times of operation and illustrates one of the cases where there was a significant improvement with the time of operation.

All brushes operated at temperatures between 76 and 90°F, with no significant variation with material, contact pressure, or time of operation. Final brush temperature after 847 hr of operation in vacuum was 88°F on most of the brushes.

The modified brush holder operated satsifactorily, and some if its design features were incorporated into the brush holders for Test Run 5.

Test Run 5 (AEDC).

Test Run 5 was a test of the scaled-up slip ring assembly in the 7-ft Aero-Space Simulation Chamber at AEDC. This assembly contained seven sets of brushes of Ag-Cu-MoS_2 and one set of brushes of Ag-graphite. The Ag-Cu-MoS_2 brushes included the two compositions (85 Ag — 2.5 Cu — 12.5 MoS_2 and 82.5 Ag — 2.5 Cu — 15 MoS_2) that were judged to be optimum, based on the results of the preceding

TABLE 10

CONTACT RESISTANCE AND NOISE LEVEL IN VACUUM AT END OF TEST RUN 4

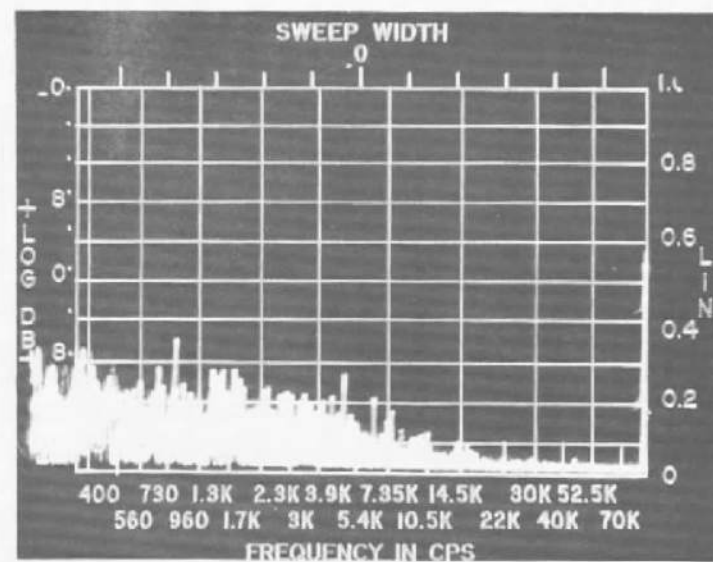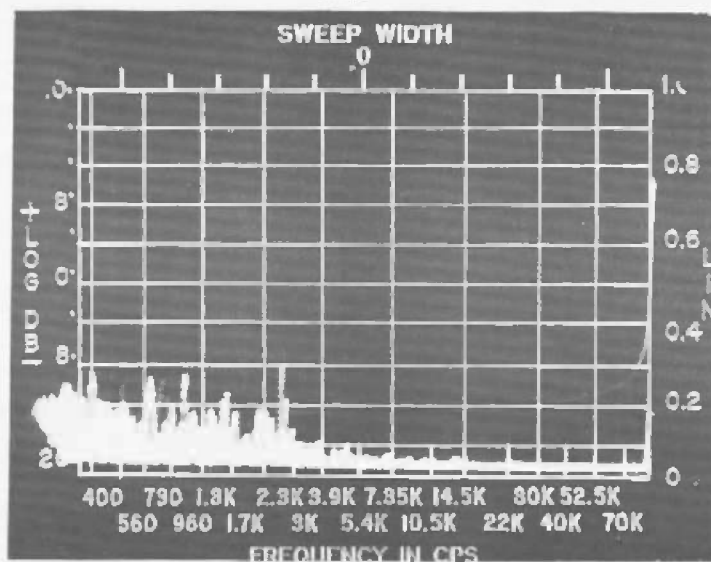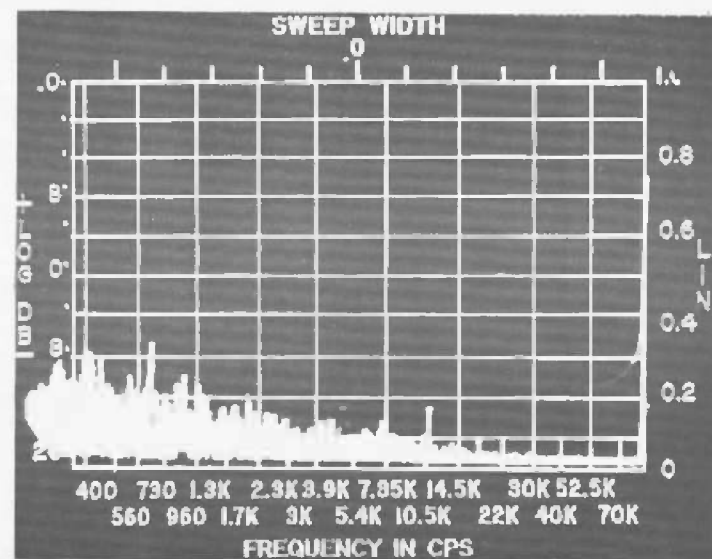| Brush Position	(Composition (% wt)			Brush Pressure (psi)	Contact Resistance (mΩ)		Noise (mV)	
	Ag	Cu	MoS$_2$		Static	Dynamic	Average	Peak
1	82.5	2.5	15.0	10	6.5	7.5	0.10	0.10
2	82.5	2.5	15.0	10	5.8	5.8	0.10	0.15
3	82.5	2.5	15.0	6	9.5	11.2	0.10	0.15
4	82.5	2.5	15.0	6				
5	85.0	2.5	12.5	10	14.0	15.0	0.10	0.15
6	85.0	2.5	12.5	10	8.5	9.8	0.10	0.15
7	85.0	2.5	12.5	10	12.2	15.2	0.15	0.25
8	85.0	5.0	10.0	10	16.5	17.5	0.15	0.20
9	82.5	2.5	15.0	10	19.5	20.0	0.15	0.25
10	80.0	5.0	15.0	10				
11	85.0	0.0	15.0	10	20.8	22.0	0.15	0.25
12	85.0	0.0	15.0	10	19.0	20.2	0.15	0.25
13	82.5	2.5	15.0	10	10.5	11.0	0.10	0.10
14	82.5	2.5	15.0	10	38.2	39.5	0.10	0.20
15	82.5	2.5	15.0	6	3.8	4.2	0.10	0.15
16	82.5	2.5	15.0	6	21.0	22.0	0.10	0.15
17	85.0	2.5	12.5	10	7.2	8.5	0.10	0.10
18	85.0	2.5	12.5	10	17.0	19.5	0.20	0.40
19	85.0	5.0	10.0	6	29.2	32.2	0.30	0.50
20	85.0	5.0	10.0	6	41.8	44.2	0.20	0.40
21	80.0	5.0	15.0	6	20.2	21.5	0.20	0.40
22	80.0	5.0	15.0	6				
23	85.0	2.5	12.5	6	23.0	25.0	0.15	0.40
24	85.0	2.5	12.5	6				
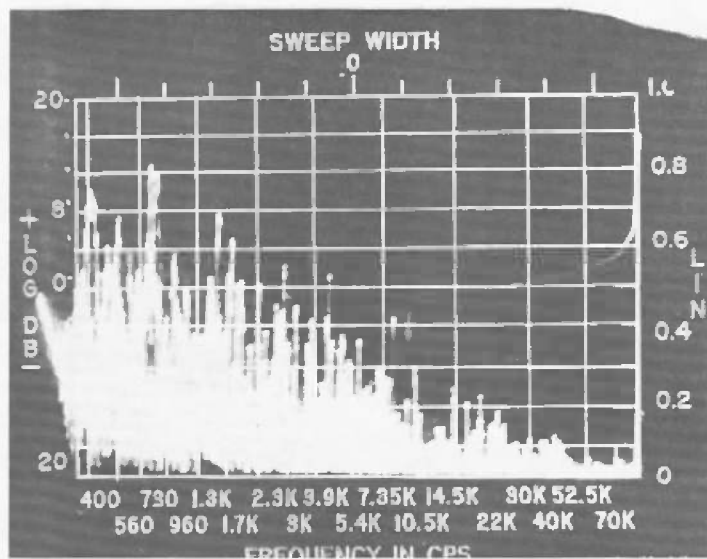
5 hr

307 hr

700 hr

848 hr

Fig. 40 Noise Spectrum Traces on Ring 1 After Various Periods of Operation in Vacuum

TABLE 11

BRUSH AND RING WEAR ON SLIP RING ASSEMBLY 5

Ring	Brush Composition (% wt)			Brush Processing	Ring Material	Contact Pressure (psi)	Current (A)	Brush Wear (in.)
	Ag	Cu	MoS$_2$					
1	85	2.5	12.5	Pressed and Sintered	Ag	10	75	0.017 0.011 0.011 0.014 0.013 avg
2	85	2.5	12.5	Pressed and Sintered	Ag	10	40	0.013 0.022 0.017 0.007 0.015 avg
3	85	2.5	12.5	Pressed and Sintered	Ag	6	75	0.012 0.021 0.003 0.014 0.012 avg
4	85	2.5	12.5	Pressed and Sintered	Au	10	75	0.008 0.009 0.005 0.005 0.007 avg

TABLE 11 (Continued)

5	85	2.5	12.5	Coined and Resintered	Ag	10	75	0.020 0.025 0.022 0.011 0.020 avg
6	82.5	2.5	15	Pressed and Sintered	Ag	10	75	0.020 0.015 0.009 0.013 0.014 avg
7	82.5	2.5	15	Coined and Resintered	Ag	10	75	0.021 0.014 0.014 0.013 0.016 avg
8	90 Ag — 10 graphite			Standard, commercially available	Au	10	75	0.150 0.255 0.195 0.244 0.206 avg

runs. Each of these two compositions were prepared in two ways; some were pressed and sintered only once, while others were pressed and sintered in the same manner and then repressed (coined) and resintered. Other independent variables studied in this test were brush contact pressure (6 and 10 psi), ring material (Ag and Au), and current (40 and 75 A). The purpose of this test was primarily to study the performance of the optimum brush-and-ring material combinations under conditions that duplicated those at which they would operate in supplying power to a secondary radiation simulator.

The torque to drive Assembly 5 was 119 in.-lb, measured by the vendor before shipment. The unit was shipped with a light coating of MIL-L-6085 oil to aid in running in. The unit was run-in at 15 rpm for 30 min in air with no current flowing. It was then cleaned with distilled solvent and dried with a stream of warm air to drive off the residual volatile matter before placing it into the vacuum chamber.

Assembly 5 was operated for 700 hr in vacuum. The chamber reached a vacuum on the 10^{-7} Torr scale in less than 2 hr from the start of evacuation, reached 1×10^{-8} Torr in 50 hr, and operated at around 5×10^{-9} Torr for the balance of the 700-hr test run. Table 11 summarizes the brush wear measured at the conclusion of this test, and Fig. 41 is a photograph that shows the conditions for the various brushes and rings. The Ag-Cu-MoS$_2$ brushes all wore on the order of 0.015 in. (range from 0.005 to 0.025 in.), whereas the Ag-graphite brushes wore an average of 0.206 in. (range from 0.150 to 0.255 in.), or a factor of almost 20 times as much. Rings 1 through 7 all showed relatively light wear, whereas Ring 8, which was contacted by the Ag-graphite brushes, was severely worn. Both brush and ring wear were lightest on Ring 4, which was the gold ring.

All of the Ag-Cu-MoS$_2$ composites operated with low noise levels, on the order of 4 mV. Initial noise levels were sometimes slightly higher, due probably to poor brush seating, but as the test proceeded, the noise levels dropped and leveled off at a fairly constant value after about 400 to 500 hr. The Ag-graphite brushes, on the other hand, had higher noise levels and the noise level tended to increase with time, reaching a peak value of about 200 mV after 700 hr of operation.
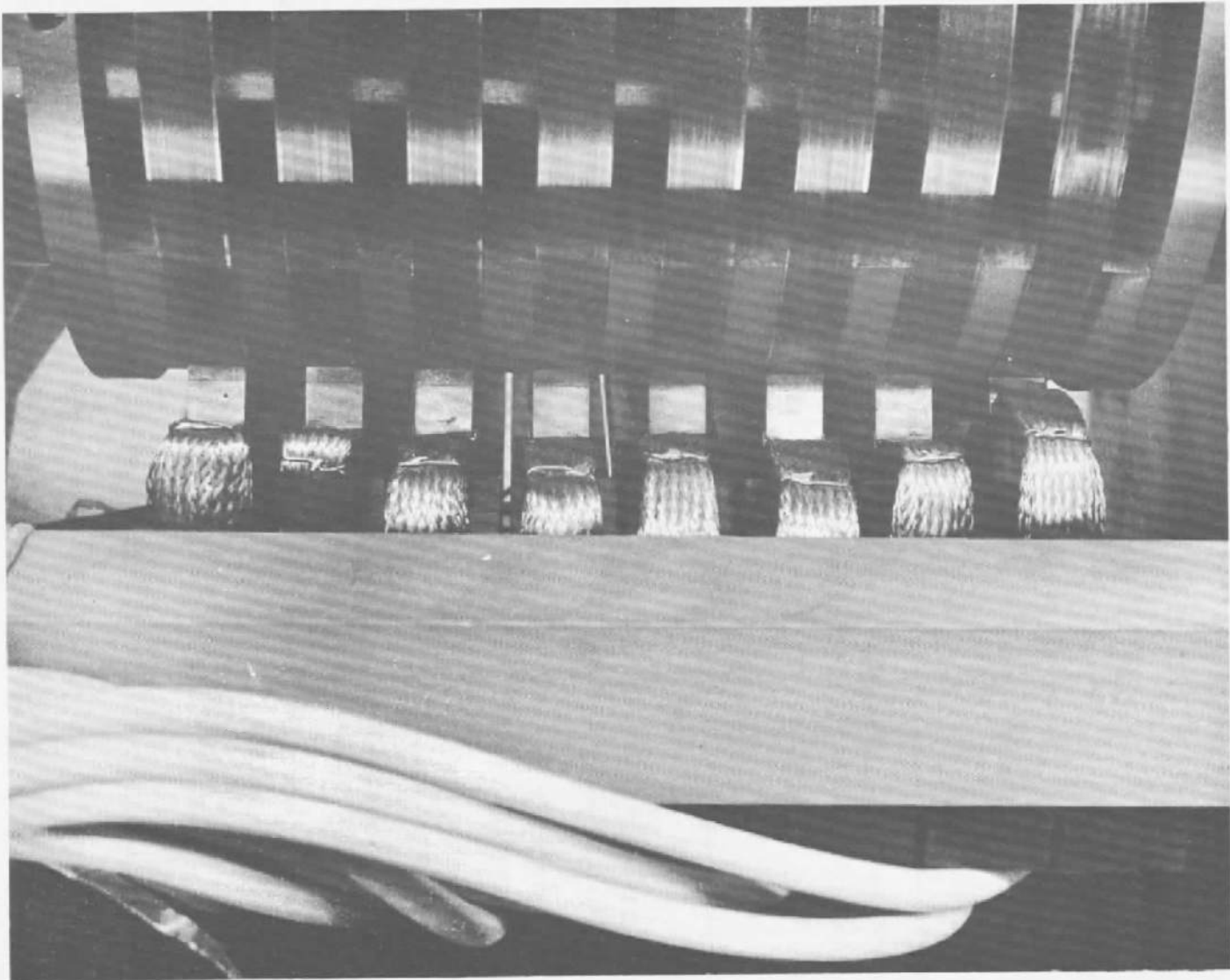
Fig. 41 Slip Ring Assembly 5 After Testing

Figure 42 compares the noise behavior of brushes of 90 Ag − 10 graphite and 85 Ag − 2.5 Cu − 12.5 MoS$_2$ operating at 75 A. Although there was a significant difference in peak noise between Ag-graphite and Ag-Cu-MoS$_2$ brushes, all four sets of the Ag-Cu-MoS$_2$ brushes operated at about the same noise levels despite differences in brush contact pressure, ring material, and processing. Neither gold rings (Ring 4) nor coining and resintering (Ring 5) appear to have any benefits compared to silver rings and pressing and sintering alone (Ring 1), so that their additional costs cannot be justified. Peak noise appears lower at 6 psi contact pressure than at 10 psi (Ring 3 vs. Ring 1), although the difference is small and probably not significant. There was no discernible difference between the peak noise from 82.5 Ag − 2.5 Cu − 15 MoS$_2$ and 85 Ag − 2.5 Cu − 12.5 MoS$_2$ brushes.

Rotational speeds from 0 to 15 rpm had no apparent effect on the noise level.

The dynamic brush resistance values were relatively high at the start of the 20-hr run-in in air, but were reduced to fairly constant levels at the end of the air run-in or during the first 10 hr of operation in vacuum. Resistance across brush-ring interfaces was less than the resistance of the electrical leads and was less than 1 mΩ in all cases.

Ag-Cu-MoS$_2$ brushes reached maximum temperatures of 125 to 135°F after about 16 hr of operation in air; their temperatures decreased below these values when they were put into operation in vacuum, and generally were in the range from 100 to 120°F after 700 hr of operation in vacuum. Ag-graphite brushes, on the other hand, operated at about 115°F after 16 hr in air, then increased to 124°F when operated initially in vacuum and were running generally between 107 and 115°F during the last 200 hr of the test. There was no noticeable increase in temperature even when rotation was stopped and the current was conducted across stationary points of contact on the rings. There were no indications of welding or hot spots during such times. In all cases, temperatures were reasonable and no cause for concern. It is probable that all of the Ag-Cu-MoS$_2$ brushes could have carried substantially higher currents without difficulty.
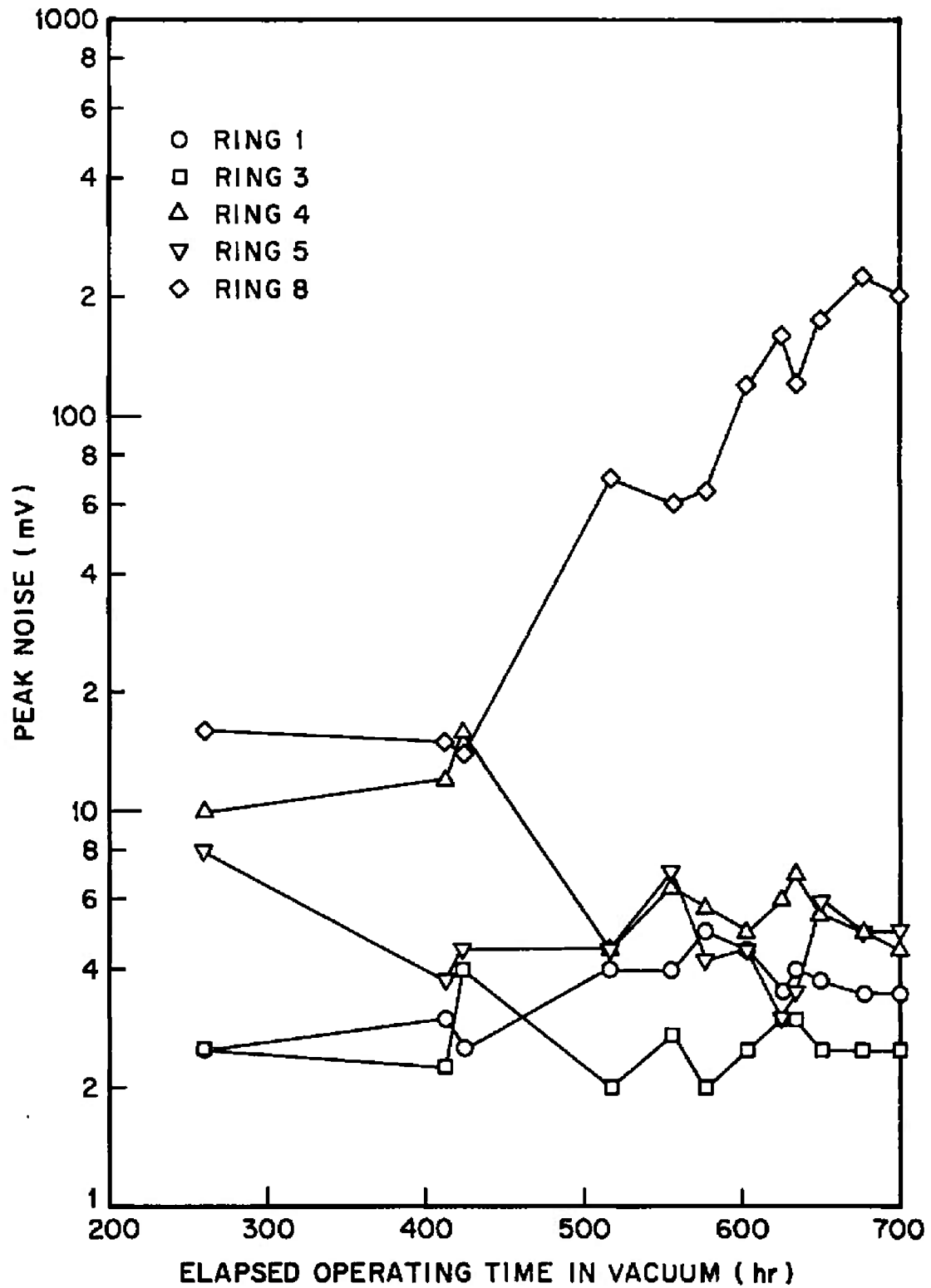
Fig. 42 Noise Levels on Slip Ring Assembly 5

SECTION 5

CONCLUSIONS

Tungsten filament lamps mounted on a cage that surrounds the test vehicle provide satisfactory simulation of secondary radiation for large aerospace systems environmental chambers.

Sliding contacts are preferable to other techniques for transmitting electrical power across sliding interfaces to the secondary radiation simulator.

Sliding contacts of silver-copper-molybdenum disulfide against rings of electro-deposited silver or gold provide satisfactory performance for use in transmitting electrical power to a secondary radiation simulator operating in ultrahigh vacuum. Optimum composition is from 82.5 to 85% silver, 2.5% copper, and 12.5 to 15% molybdenum disulfide. Such materials can be produced by powder metallurgy techniques. They have demonstrated satisfactory performance under the following conditions:

- Vacuum of 10^{-9} Torr
- Sliding velocities up to 424 in./min
- Lifetimes up to 847 hr of operation
- Contact pressures of 6 and 10 psi
- Current densities up to 300 A/in.^{2}

Wear and noise under such conditions are on the order of 0.015 in. and a few millivolts. These brushes do not show any tendency to weld to silver rings when conducting 300 A/in.^{2} or alter the subsequent performance even when the rings are stationary.

SECTION 6

REFERENCES

1. Space Materials Handbook, edited by C. G. Goetzel, J. B. Rittenhouse, and J. B. Singletary, 2nd edition, Lockheed Missiles & Space Company, Sunnyvale, California, 1964

2. C. D. Fitz, S. J. Lukasik, E. A. Mayer, and D. R. Simon, "Albedo and Planet Radiation Intercepted by an Earth Satellite," AEDC-TDR-63-92, May 1963

3. C. D. Fitz, E. A. Mayer, "Evaluation of Methods for Simulating the Earth's Albedo and Planet Radiation," Technical Note 4, Vitro Laboratories, Contract AF 40(600)-951, March 1963

4. W. H. McAdams, Heat Transmission, McGraw-Hill Book Co., New York, 1942

5. E. Pauls, "Solar Radiant Heat Simulation Modular Unit Vacuum Environment Tests" Research Inc., January 1964

6. W. W. Stickney, "Solar Spectrum Simulator," WADD Technical Report 60-847, November 1960

7. T. M. McCoy, "Hyperenvironment Simulation – Part II Development and Design of Simulation Facilities for Space Vehicle Environment," WADD Technical Report 60-785, December 1960

8. J. J. Lamb and R. A. Ditavanto, "Preliminary Investigation of Hyperenvironments and Methods of Simulation – Part II Simulation Methods," WADC Technical Report 57-456, November 1957

9. D. D. Carlson and R. H. Underwood, "Design of an Aerospace Systems Environmental Chamber," AEDC-TR-61-10, July 1961

10. F. G. Sherrell, "Investigation of the Contamination of Reflector Surfaces of Infrared Radiators to be Used in Space Simulators," AEDC-TDR-62-233, December 1962

11. W. A. Jaatinen and D. L. Rothackev, "Solar Radiation Simulation Studies, Part I and II," AEDC-TDR-63-90 and AEDC-TDR-63-91, May 1963

12. Gall and Feryers, "An Investigation of Two Infrared Radiation Lamp Configurations at Near Vacuum Conditions," AEDC-TDR-62-119, June 1962

13. D. F. Widgeon, "Radiant Heat Investigation," LMSC 800776, June 1961

14. Alfred Still and Charles E. Siskind, Elements of Electrical Machine Design, McGraw-Hill Book Co., New York, 3rd edition, 1954

15. C. G. Veinott, "Electrical Machinery Design by Digital Computers — After 9 Years," Electrical Engineering, p. 275, April 1963

16. "The Computer as a Design Tool — Design of Electrical Machinery," Conceicao & Parton; Electro-Technology, p. 50, July 1963

17. Francis J. Clauss, "Lubrication Under Space/Vacuum Conditions," Scientific Lubrication, Vol. 15, No. 4, pp. 180−199, March 1963

DOCUMENT CONTROL DATA - R&D
(Security classification of title, body of abstract and indexing annotation must be entered when the overall report is classified)

1. ORIGINATING ACTIVITY (Corporate author)	2a. REPORT SECURITY CLASSIFICATION
Materials Sciences Laboratory Lockheed Missiles and Space Company Palo Alto, California	UNCLASSIFIED
	2b. GROUP N/A

3. REPORT TITLE

ELECTRICAL TRANSMISSION COMPONENTS FOR A LARGE AEROSPACE ENVIRONMENTAL CHAMBER

4. DESCRIPTIVE NOTES (Type of report and inclusive dates)

N/A

This document has been approved for public release and its distribution is unlimited. *Per DDC TR 715 AD AG 4 700 dtd July 1965*

5. AUTHOR(S) (Last name, first name, initial)

FRANCIS J. CLAUSS, LMSC

6. REPORT DATE	7a. TOTAL NO. OF PAGES	7b. NO. OF REFS
February 1965	120	17

8a. CONTRACT OR GRANT NO.	9a. ORIGINATOR'S REPORT NUMBER(S)
AF 40(600)-1070	
b. PROJECT NO. 8952	AEDC-TR-65-40
c. Program Element 62405334	9b. OTHER REPORT NO(S) (Any other numbers that may be assigned this report) LMSC Report No. 2-68-64-1
d.	

10. AVAILABILITY/LIMITATION NOTICES

Qualified requesters may obtain copies of this report from DDC.

11. SUPPLEMENTARY NOTES	12. SPONSORING MILITARY ACTIVITY
N/A	Arnold Engineering Development Center, Air Force Systems Command, Arnold AF Station, Tennessee

13. ABSTRACT Secondary radiation in a large aerospace systems environmental chamber can be adequately simulated by an array of tungsten filament lamps mounted on a cage that surrounds the test vehicle. A total of 2528 lamps are required, arranged on 68 circuits that are individually controlled for the purpose of simulating orbital fluctuations. Peak input to each of the circuits is approximately 75A at 430V, and peak total input is 0.818MW. The simulator should be mounted so that it can tumble with the vehicle about the vehicle's pitch axis. Variations in intensity of secondary radiation around the circumference of the vehicle can be programmed electrically so that the simulator need not rotate about the roll axis of the test vehicle. Sliding electrical contacts are preferred to flexible cables or rotary transformers for transmitting power to the simulator, and separate slip rings can be provided for each of the circuits. Self-lubricating powder metallurgy composites of silver, copper, and molybdenum disulfide have demonstrated satisfactory performance in ultrahigh vacuum for use on slip rings providing power to the secondary radiation simulator. Experimental measurements indicate that brushes of such materials can be operated against silver or gold rings in ultrahigh vacuum with negligible wear and low noise over a period of 700 to 850 hr at sliding velocities up to 424 in./min while carrying densities up to 300 A/in.^{2}.

DD FORM 1473 1 JAN 64

14. KEY WORDS	LINK A		LINK B		LINK C	
	ROLE	WT	ROLE	WT	ROLE	WT
aerospace systems simulation chambers secondary radiation self-lubricating composites slip rings brushes silver copper molybdenum disulfide ultrahigh vacuum						

INSTRUCTIONS

1. ORIGINATING ACTIVITY: Enter the name and address of the contractor, subcontractor, grantee, Department of Defense activity or other organization (corporate author) issuing the report.

2a. REPORT SECURITY CLASSIFICATION: Enter the overall security classification of the report. Indicate whether "Restricted Data" is included. Marking is to be in accordance with appropriate security regulations.

2b. GROUP: Automatic downgrading is specified in DoD Directive 5200.10 and Armed Forces Industrial Manual. Enter the group number. Also, when applicable, show that optional markings have been used for Group 3 and Group 4 as authorized.

3. REPORT TITLE: Enter the complete report title in all capital letters. Titles in all cases should be unclassified. If a meaningful title cannot be selected without classification, show title classification in all capitals in parenthesis immediately following the title.

4. DESCRIPTIVE NOTES: If appropriate, enter the type of report, e.g., interim, progress, summary, annual, or final. Give the inclusive dates when a specific reporting period is covered.

5. AUTHOR(S): Enter the name(s) of author(s) as shown on or in the report. Enter last name, first name, middle initial. If military, show rank and branch of service. The name of the principal author is an absolute minimum requirement.

6. REPORT DATE: Enter the date of the report as day, month, year; or month, year. If more than one date appears on the report, use date of publication.

7a. TOTAL NUMBER OF PAGES: The total page count should follow normal pagination procedures, i.e., enter the number of pages containing information.

7b. NUMBER OF REFERENCES: Enter the total number of references cited in the report.

8a. CONTRACT OR GRANT NUMBER: If appropriate, enter the applicable number of the contract or grant under which the report was written.

8b, 8c, & 8d. PROJECT NUMBER: Enter the appropriate military department identification, such as project number, subproject number, system numbers, task number, etc.

9a. ORIGINATOR'S REPORT NUMBER(S): Enter the official report number by which the document will be identified and controlled by the originating activity. This number must be unique to this report.

9b. OTHER REPORT NUMBER(S): If the report has been assigned any other report numbers (either by the originator or by the sponsor), also enter this number(s).

10. AVAILABILITY/LIMITATION NOTICES: Enter any limitations on further dissemination of the report, other than those imposed by security classification, using standard statements such as:

(1) "Qualified requesters may obtain copies of this report from DDC."

(2) "Foreign announcement and dissemination of this report by DDC is not authorized."

(3) "U. S. Government agencies may obtain copies of this report directly from DDC. Other qualified DDC users shall request through

_____ ."

(4) "U. S. military agencies may obtain copies of this report directly from DDC. Other qualified users shall request through

_____ ."

(5) "All distribution of this report is controlled. Qualified DDC users shall request through

_____ ."

If the report has been furnished to the Office of Technical Services, Department of Commerce, for sale to the public, indicate this fact and enter the price, if known.

11. SUPPLEMENTARY NOTES: Use for additional explanatory notes.

12. SPONSORING MILITARY ACTIVITY: Enter the name of the departmental project office or laboratory sponsoring (paying for) the research and development. Include address.

13. ABSTRACT: Enter an abstract giving a brief and factual summary of the document indicative of the report, even though it may also appear elsewhere in the body of the technical report. If additional space is required, a continuation sheet shall be attached.

It is highly desirable that the abstract of classified reports be unclassified. Each paragraph of the abstract shall end with an indication of the military security classification of the information in the paragraph, represented as (TS), (S), (C), or (U).

There is no limitation on the length of the abstract. However, the suggested length is from 150 to 225 words.

14. KEY WORDS: Key words are technically meaningful terms or short phrases that characterize a report and may be used as index entries for cataloging the report. Key words must be selected so that no security classification is required. Identifiers, such as equipment model designation, trade name, military project code name, geographic location, may be used as key words but will be followed by an indication of technical context. The assignment of links, rules, and weights is optional.